2017

# Investigation of lupane triterpene as a novel PTP1B allosteric inhibitor for the improvement of neurite outgrowth and synaptogenesis

Tiantian Jin
*University of Wollongong*

UNIVERSITY
OF WOLLONGONG
AUSTRALIA

# Investigation of lupane triterpene as a novel PTP1B allosteric inhibitor for the improvement of neurite outgrowth and synaptogenesis

A Thesis submitted in fulfilment of the
requirements for the award of the degree

DOCTOR OF PHILOSOPHY

From

School of Medicine
University of Wollongong

By

TIANTIAN JIN

2016

# Certification

I, Tiantian Jin, declare that this thesis, submitted in fulfilment of the requirements for the award of Doctor of Philosophy, in the School of Medicine, University of Wollongong, is entirely my own work unless otherwise referenced or acknowledged. This manuscript has not been submitted for qualification at any other academic institution.

Tiantian Jin

2016

# Statements

In accordance with the University of Wollongong thesis committee 'Guidelines for Preparation, Submission and examination of HDR Theses (02-12-2015), this PhD thesis is presented in 'Journal Article Style'. It is comprised of a series of original studies published in peer-reviewed journals, of which I am the first author. I hereby declare that I am the primary designer of these studies, have carried out experimental procedures, data analysis and manuscript preparation.

Tiantian Jin

2016

I consent to the presentation of this PhD in 'Journal Article Style' and I acknowledge the above statement pertaining to student contribution to be correct.

Prof. Xu-Feng Huang, Principal Supervisor

2016

Dr. Yinghua Yu, Supervisor

Dr Haibo Yu, Supervisor

2016

`

# Publications

The following publications and presentations have arisen directly from work contained within this thesis.

**Publications in Refereed Journals:**

- **JIN, T.**, YU, H. & HUANG, X.-F*. Selective binding modes and allosteric inhibitory effects of lupane triterpenes on protein tyrosine phosphatase 1B. *Scientific reports*, 6, 20766, 2016.
- **JIN, T.**, YU, Y. & HUANG, X.-F*. Protein Tyrosine Phosphatase 1B mediates Phencyclidine-induced BDNF reduction and neurogenesis impairment in hypothalamic neurons, *PNAS* (Under review)
- **JIN, T.**, YAN, S., ZHANG, J., YUAN, D., HUANG, X.-F*. & LI, W*. A label-free and high-throughput separation of neuron and glial cells using an inertial microfluidic platform. *Biomicrofluidics*, 10, 034104, 2016

**Publications in Conference Proceedings:**

- **JIN, T.**, YU, Y. & HUANG, X.-F*. "Protein Tyrosine Phosphatase 1B inhibition is a new strategy for schizophrenia treatment", Neuroscience R&D technology conference, Barcelona, Spain, 2015.
- **JIN, T.**, YU, H. & HUANG, X.-F*. "Selective binding modes and allosteric inhibitory effects of lupane triterpenes on protein tyrosine phosphatase 1B", International Union for Pure and Applied Biophysics, Brisbane, Australia, 2014.
- **JIN, T.**, YU, H. & HUANG, X.-F*. "Computational modelling of PTP1B allosteric inhibition", Molecular Modelling, Brisbane, Australia, 2014.
- **JIN, T.**, YU, H. & HUANG, X.-F*. "Virtual Screening Identifies Lupane Triterpenes as Allosteric Inhibitors of Protein Tyrosine Phosphatase 1B", Australasian Neuroscience Society, Melbourne, Australia, 2013.

`

# Table of Contents


Certification ..... i
Statements ..... ii
Publications ..... iii
Table of Contents ..... iv
List of Figures ..... vi
List of Abbreviations ..... vii
Abstract ..... ix
Acknowledgements ..... xii
Chapter One ..... 1
1.1 Introduction ..... 1
1.2 Literature Review ..... 2
1.2.1 PTP1B is a recognized drug target for leptin resistance ..... 2
1.2.2 New aspect of PTP1B: a BDNF signalling blocker in neurological disorders ..... 5
1.2.3 Phencyclidine models show BDNF reduction and dysfunction in schizophrenia ..... 6
1.2.4 Neuregulin-1 (NRG1) and susceptibility to schizophrenia ..... 8
1.2.5 Challenges in discovering PTP1B traditional inhibitors: disadvantages of targeting PTP1B active site ..... 9
1.2.6 Developing PTP1B allosteric inhibitors is an alternative strategy ..... 13
1.2.7 Lupane triterpenes are candidates as PTP1B allosteric inhibitors ..... 16
1.2.8 Application of computational modelling to determine lupane triterpenes as PTP1B allosteric inhibitors ..... 18
1.2.9 Application of inertial microfluidic platform to separate and collect neurons and glial cells ..... 19
1.3 Aims ..... 22
1.4 Hypothesis ..... 23
1.5 Significance ..... 24
1.6 Methods and Materials ..... 26
1.6.1 Homology modelling of PTP1B ..... 26
1.6.2 Molecular docking ..... 26
1.6.3 Molecular dynamics simulations ..... 27
1.6.4 Binding free energy calculation ..... 28
1.6.5 Trajectory analysis ..... 29

`

1.6.6 PTP1B and TCPTP inhibition assay of lupane triterpenes by *p*NPP phosphatase assay ..... 29
1.6.7 PTP1B inhibition kinetics assay of lupane triterpenes by *p*NPP phosphatase assay ..... 30
1.6.8 Immunoprecipitation assay of PTP1B ..... 30
1.6.9 Ethics statement ..... 31
1.6.10 Primary cell culture of wide type and Nrg1 -/+ mouse hypothalamic neurons ..... 31
1.6.11 Mouse hypothalamic cell line culture ..... 32
1.6.12 Immunofluorescence and image analysis ..... 33
1.6.13 Quantitative real-time PCR ..... 34
1.6.14 Western blot analysis ..... 34
1.6.15 Neuron Neuropeptide Y (NPY) detection ..... 36
1.6.16 Design and fabrication of inertial microfluidic device ..... 36
1.6.17 Inertial microfluidic separation of neurons and glia ..... 36
1.6.18 Statistical analysis ..... 37
1.7 Summary ..... 38
Chapter Two ..... 40
Selective binding modes and allosteric inhibitory effects of lupane triterpenes on protein tyrosine phosphatase 1B ..... 40
Statement from co-authors ..... 41
Chapter Three ..... 72
Protein Tyrosine Phosphatase 1B mediates phencyclidine-induced BDNF reduction and neurogenesis impairment in hypothalamic neurons ..... 72
Statement from co-authors ..... 73
Chapter Four ..... 112
A label-free and high-throughput separation of neuron and glial cells using an inertial microfluidic platform ..... 112
Statement from co-authors ..... 113
Chapter Five ..... 126
5.1 Overall Discussion ..... 126
5.2 Conclusion ..... 133
5.3 Recommendations for Future Research ..... 134
References ..... 137
Appendix ..... 148

`

# List of Figures

Figure 1.1: The mechanism of PTP1B regulating leptin signalling and BDNF-mediated signalling……..…..4

Figure 1.2: High similarity of structure in the catalytic domain between TCPTP and PTP1B.....12

Figure 1.3: PTP1B active site, allosteric site and WPD loop conformational change in the PTP2B crystallography structure…….……..15

Figure 1.4: The formula of allosteric ligands used in this study including compound 2, compound 3 and lupane triterpenes…….17

Figure 1.5: The inertial microfluidic device applied in this work…..…….21

`

# List of Abbreviations

| | |
|---|---|
| AgRP | Agouti-related protein |
| Akt | Protein kinase B (PKB), also known as Akt |
| BDNF | Brain-derived neurotrophic factor |
| BSA | Bovine serum albumin |
| CHARMM | Chemistry at HARvard Macromolecular Mechanics |
| CNS | Central nervous system |
| DEP | Dielectrophoresis |
| DIO | Diet-induced obese |
| DMEM | Dulbecco's modified Eagle medium |
| DMSO | Dimethyl sulfoxide |
| DOPE energy | Discrete Optimized Protein Energy |
| ER | Endoplasmic reticulum |
| ErbB4 | v-erb-a erythroblastic leukemia viral oncogene homolog 4 |
| FACS | Fluorescence-activated cell sorting |
| FBS | Foetal bovine serum |
| FDU | 5-Fluoro-2′-deoxyuridine |
| FEP | Free Energy Perturbation |
| GAFF | General Amber force field |
| GFAP | Glial Fibrillary Acidic Protein |
| GFP | Green fluorescent protein |
| GSK3β | Glycogen Synthase Kinase 3β |
| JAK1 | Janus Kinase 1 |
| JAK2 | Janus Kinase 2 |
| JAK3 | Janus Kinase 3 |
| KO | Knock-out |
| MACS | Magnetically-activated cell sorting |
| MAP2 | Microtubule-associated protein 2 |
| MD | Molecular dynamics |
| NAMD | Nanoscale Molecular Dynamics |
| NeuN | Neuronal nucleus marker |
| NF-κB | Nuclear factor-κB |
| NMDA | N-methyl-D-aspartate |
| NMR | Nuclear magnetic resonance spectroscopy |
| NPY | Neuropeptide Y |
| NPY | Neuropeptide Y |
| NR2A | NMDA receptor subunit 2A |
| NR2B | NMDA receptor subunit 2B |
| NRG1 | Neuregulin-1 |
| PBS | Phosphate buffered saline |
| PCP | Phencyclidine |
| PDMS | Polydimethylsiloxane |
| PME | Particle Mesh Ewald |
| PMSF | Phenylmethanesulfonyl fluoride |
| POMC | Pro-opiomelanocortin |
| PROPKA | Program to predict pKa |

`

| | |
|---|---|
| PSD-95 | Postsynaptic density protein 95 |
| PTP1B | Protein Tyrosine Phosphatase 1B |
| PTPs | Protein Tyrosine Phosphatases |
| qRT-PCR | Quantitative real-time PCR |
| REMD | Replica-Exchange Molecular Dynamics |
| SGAs | Second generation antipsychotics |
| SNPs | Single nucleotide polymorphisms |
| STAT3 | Signal transducer and activator of transcription 3 |
| SYN | Synaptophysin |
| TCPTP | T-cell protein tyrosine phosphatase |
| TNF-α | Tumor necrosis factor α |
| TrkB | Tropomyosin-related kinase B |
| VMD | Visual molecular dynamics |
| WPD | PTP1B rsidues 179-181, Trp-Pro-Asp |
| WT | Wild-type |

`

# Abstract

An impaired synaptogenesis is known to be a common neuropathology in a number of severe mental disorders including schizophrenia, Parkinson disease, bipolar and dementia. Protein tyrosine phosphatase 1B (PTP1B) has been reported to impair neurite outgrowth and synaptic formation via attenuating Brain-derived neurotrophic factor (BDNF)-mediated signalling. Leptin signalling also facilitates BDNF and promotes synaptogenesis which is inhibited by PTP1B. Therefore PTP1B is a potential drug target to reverse BDNF-mediated neurogenesis. In this study, lupane triterpenes, a cluster of natural products, are determined as novel PTP1B allosteric inhibitors which inhibit PTP1B with strong potency and selectivity. Lupane triterpenes inhibit psychotomimetic drug-induced PTP1B and reverse PTP1B-caused BDNF reduction and neurogenesis impairment, indicating that lupane triterpenes are potential drug candidates for PTP1B inhibition and PTP1B-related neurological disorders.

Firstly, lupane triterpenes were identified as novel PTP1B allosteric inhibitors which strongly and specifically inhibited PTP1B. In Chapter 2, through computational studies including molecular docking and molecular dynamics simulations, lupane triterpenes were confirmed to bind to PTP1B allosteric site. Following binding free energy calculations were established to characterise the interactions between lupane triterpenes structures and PTP1B allosteric binding site, providing evidence for future chemical modifications. Moreover, pro-inflammatory factor TNFα stimulated PTP1B level in neurons which was, however, inhibited by lupane triterpenes treatments. Considering that PTP1B overexpression has been reported to impair BDNF-mediated neurogenesis in neurons, it is of interest to investigate whether lupane triterpenes are able to reverse PTP1B-mediated BDNF reduction and neurite outgrowth impairment in neurons.

`

Secondly, PTP1B was found to be significantly increased in phencyclidine (PCP)-treated neurons and caused downstream BDNF reduction and neurogenesis impairment. In Chapter 3, the psychotomimetic drug PCP induced PTP1B through blockage of NMDA receptor subunit 2B (NR2B). Enhanced PTP1B attenuated BDNF-mediated Akt/GSK3β signalling, leading to reduced synaptogenesis. Furthermore, leptin increases BDNF expression and promotes synaptogenesis which was also impaired by PCP-induced PTP1B. PTP1B directly inhibited JAK2 phosphorylation and thus attenuated leptin signalling and pSTAT3, leading to reduced BDNF. Importantly, the study showed that lupeol, one of the lupane triterpenes, significantly reduced PTP1B expression and stimulated BDNF level, restored leptin signalling, BDNF-mediated signalling and synaptogenesis. Lupeol also improved the treatment effects of current antipsychotic drugs on reversing PCP-induced BDNF alterations, implicating PTP1B inhibition as a potential treatment strategy.

Furthermore, I developed a label-free and high-throughput microfluidic platform based on the inertial microfluidic technique to separate neurons and glial cells from dissected brain tissue rapidly and continuously (see Chapter 4). The collected neurons and glia were confirmed healthy with significantly improved purity. Moreover, PCP reduced BDNF level in both separated and unseparated neurons with no significant difference, indicating that the device did not change the cell biological properties responding to drug treatment. Increasing evidence has shown that neurons and glia both play significant roles in the development of neurite outgrowth and synaptic formation. Therefore, it will be necessary to investigate the protein alterations, such as PTP1B, in both cell types contributing to disease-induced impairment in neurogenesis and synaptogenesis. However, it is difficult to differentiate the roles of neurons and glia because the methods used to separate and collect neurons and glial cells from brain

`

tissues are ineffective and inefficient. This microfluidic microchip can enrich and purify both neurons and glia with unaltered morphology and biological function. We therefore anticipate that this microfluidic device will be an outstanding platform for future cell culture studies to investigate disease mechanism and perform drug screening.

`

# Acknowledgements

I would like to thank the School of Medicine (as well as the former School of Health) and the Illawarra Health and Medical Research Institute (IHMRI), University of Wollongong (UOW) for their academic support through my PhD studies. I also appreciate financial support from the China Scholarship Council (CSC) and IPTA scholarship from University of Wollongong to allow me to continue my higher degree study.

To my supervisors Professor Xu-Feng Huang, Dr Yinghua Yu and Dr Haibo Yu, I would like to express my heartfelt thank you for your inspiration, guidance, encouragements and great supports through the whole periods of my candidature, especially in those difficult times to revise and publish paper. Your great knowledge and timely guidance since the development of ideas through to the completion of my papers and thesis was greatly appreciated and will never be forgotten. I feel fortunate and honoured to have all of you to be my supervisors.

I would like to express my deep gratitude to Professor Weihua Li and his talent group members Ms Dan Yuan, Dr Jun Zhang and Mr Sheng Yan and in School of Mechanical, Materials and Mechatronic Engineering in University of Wollongong, for their helpful discussions about inertial microfluidics. I am also thankful to Mr Thomas Griffiths and Mr Zorik Chilingaryan in School of Chemistry in University of Wollongong, for their suggestions and help to establish the computational modelling. Then I would like to show great appreciation to Associate Professor Karen Charlton in School of Medicine and Associate Professor Aaron Oakley in School of Chemistry for their time and patience examining the proposal of this project and appreciate their inspiring comments.

`

Deep gratitude to my colleagues from the Centre of Translational Neuroscience, UOW, for your advices, technical supports, and encouragements for my laboratory experiments and academic writing. In particular, my special appreciation to our lab manager Ms Hongqin Wang as well as Dr Kiefer Zhang and Ms Yizhen Wu, for your great supports and company through my cell culture studies and most of my biological experiments during my candidature. I also expend my gratitude to Dr Tracey Maddocks for your advice and help through my animal maintenance and care; Dr Alex Szabo, Dr Danielle Camer, Dr Jessica Andrew, Dr Meng He, Dr Martin Engle, Ms Hoang Lan Chi Dinh, Ms Licai Cheng, and Mr Jeremy Lum for your great advices for my laboratory experiments; Dr Elisabeth Frank, Dr Francesca Fernandez, Dr Katrina Weston-Green, Dr Kelly Newell and Dr Natalie Matosin for your advice for my conference presentations and thesis; special thanks to Ms Linda Cohen for your professional editing for my published papers and our technical officers in the IHMRI for their extraordinary work of equipment maintenance.

Finally, I wish to express my love and gratitude to my family. Thanks to my mother Xingjing and my father Weiguo, for their support, encouragement, love and sacrifice in these years. They make this work more meaningful than it is.

`

# Chapter One

## 1.1 Introduction

Protein Tyrosine Phosphatase 1B (PTP1B) is an intracellular protein which is widely expressed in the human body including the brain, liver, muscles, and adipose tissue. PTP1B has been found up-regulated in obesity, type 2 diabetes and breast cancer, indicating PTP1B is a potential drug target in these diseases (Ukkola and Santaniemi, 2002, Zabolotny et al., 2008, Yip et al., 2010). Recent studies have revealed a new aspect of PTP1B which inhibits BDNF/TrkB signalling and leads to impaired neurite outgrowth and synaptic formation, implicating PTP1B as a therapeutic target in neurological disorders (Ozek et al., 2014, Krishnan et al., 2015). It is therefore necessary to develop PTP1B inhibitors. PTP1B traditional inhibitor is designed to target PTP1B active site. It is difficult to achieve inhibition selectivity against PTB1B, however, due to the fact that PTP1B active site and surrounding catalytic domains are highly similar to other members of the Protein Tyrosine Phosphatase (PTP) family (Julien et al., 2011, St-Pierre and Tremblay, 2012). PTP1B allosteric inhibitor was then discovered and proposed as an alternative drug design strategy to specifically inhibit PTP1B (Wiesmann et al., 2004, Zhang and Zhang, 2007). Therefore it is of interest to develop novel PTP1B allosteric inhibitors and investigate their treatment efficacy.

`

## 1.2 Literature Review

### 1.2.1 PTP1B is a recognized drug target for leptin resistance

Protein tyrosine phosphatase 1B is encoded by gene *PTPN1* which is located on human chromosome 20q13 (Brown-Shimer et al., 1990), a region identified as closely related to obesity (Lembertas et al., 1997, Lee et al., 1999). Numerous epidemiological studies have reported *PTPN1* single nucleotide polymorphisms (SNPs) associated with development of obesity in the worldwide population (Tsou and Bence, 2012). PTP1B is ubiquitously expressed in the central nervous system (CNS) (Bence et al., 2006) which is known to induce obesity via attenuating leptin signalling (Zabolotny et al., 2002).

Leptin is a hormonal signal which acts in the brain and controls food intake and energy expenditure (Schwartz and Porte, 2005, Morton and Schwartz, 2011). The leptin signalling pathway is initialized by the tyrosine phosphorylation of Janus Kinase 2 (JAK2) which subsequently modulates downstream signals such as the signal transducer and activator of transcription 3 (STAT3) (Morris and Rui, 2009) (Fig.1.1). The JAK2/STAT3 pathway is strongly linked to significant weight loss and feeding inhibitions (Coppari et al., 2009). Phosphorylated STAT3 transports into cell nucleus and affects regulation of appetite by affecting the transcription of hypothalamic neuropeptides such as neuropeptide Y (NPY), agouti-related protein (AgRP) and precursor pro-opiomelanocortin (POMC). NPY and AgRP stimulate food intake and decrease energy expenditure as orexigenic factors which are opposite to anorexigenic neuropeptide POMC (Schwartz et al., 2000) (Fig.1.1).

Leptin resistance in the CNS is one of the factors causing obesity. One of the contributors to leptin resistance is PTP1B which dephosphorylates JAK2 and thus attenuates central leptin signalling (Cheng et al., 2002) (Fig.1.1). Previous studies have

`

revealed that pro-inflammatory factor TNF-α stimulates PTP1B via activating Nuclear factor-κB (NF-κB), leading to leptin resistance (Picardi et al., 2010, Yu et al., 2013a) (Fig.1.1). Inhibition of neuronal PTP1B is essential to maintain leptin sensitivity as well as prevent obesity development (Bence et al., 2006). Neuron-specific deletion of PTP1B in mice has shown lower adiposity, enhanced leptin sensitivity, improved energy expenditure and has prevented weight gain in animals fed a high-fat diet (Bence et al., 2006). Moreover, central administration of PTP1B antisense oligonucleotides also displays reduced hypothalamic PTP1B expression in a diet-induced obese (DIO) rat model, resulting in restored leptin signalling and control of energy balance (Picardi et al., 2010). Therefore PTP1B is a drug target for obesity treatment.

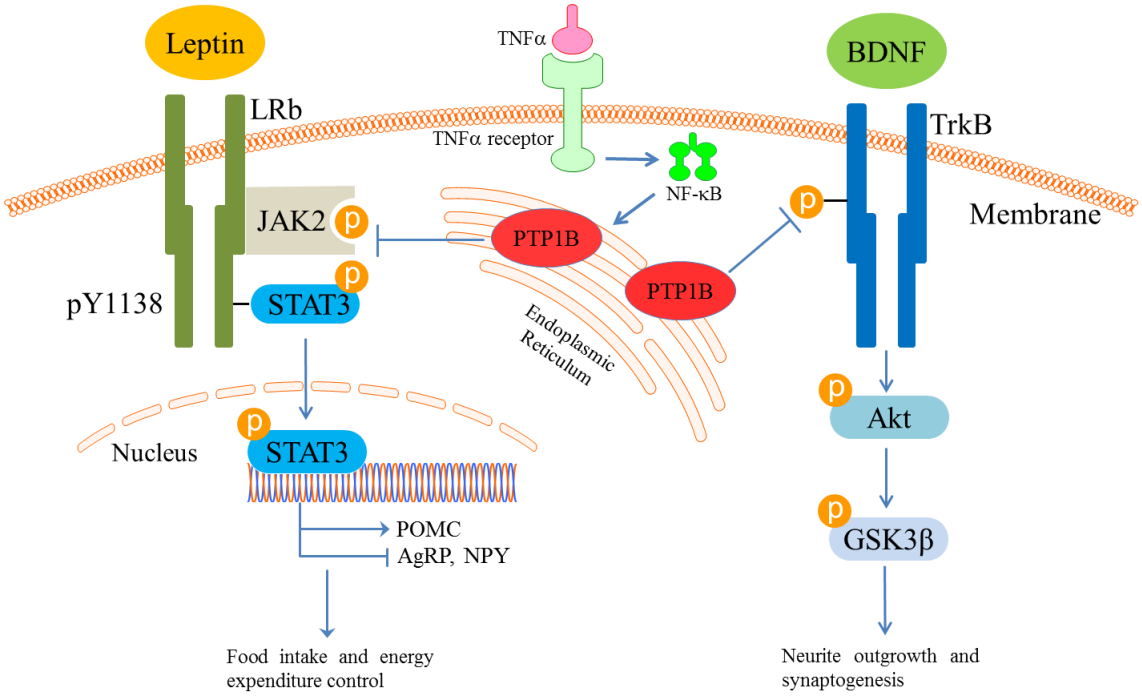


Figure. 1.1: PTP1B attenuates leptin signalling via blocking the JAK2/STAT3 pathway and leads to development of obesity. Leptin signalling is activated via JAK2 phosphorylation which further regulates pSTAT3 and downstream gene transcription including POMC, AgRP and NPY to modulate energy homeostasis. Furthermore, PTP1B inhibits BDNF receptor TrkB phosphorylation and therefore attenuates BDNF-mediated Akt/GSK3β signalling, leading to impaired neurite outgrowth and synaptogenesis. TNF-α is a critical pro-inflammatory cytokine activation of NF-κB which results in over expression of PTP1B.

`

### 1.2.2 New aspect of PTP1B: a BDNF signalling blocker in neurological disorders

As already mentioned, PTP1B has been demonstrated to attenuate leptin signalling (Zabolotny et al., 2002). Leptin is not only beneficial to energy homeostasis but also plays an important role in promoting synaptogenesis and neurite outgrowth to facilitate learning and memory (Bariohay et al., 2005, Komori et al., 2006, Yamada et al., 2011). One of previous study has reported that leptin stimulation improves neurite outgrowth and synaptogenesis markers in mouse neural cell lines, as well as increasing cell proliferation and differentiation to promote hippocampal neurogenesis (Moon et al., 2013). In *in vivo* studies, memory deficits and decreased synapse density have been observed in leptin or leptin receptor deficient rodents (Li et al., 2002, Bouret et al., 2004, Pinto et al., 2004, Farr et al., 2006), such as *ob/ob* mice, *db/db* mice and *fa/fa* rats. Importantly, leptin administration increases brain-derived neurotrophic factor (BDNF) mRNA in the hypothalamic nucleus and facilitates BDNF expression in hypothalamic STAT3-positive neurons (Komori et al., 2006). Numerous studies have revealed that BDNF plays an important role in regulating neurite outgrowth, synaptic plasticity and cognitive function (Huang and Reichardt, 2001).

BDNF and its receptor, tropomyosin-related kinase B (TrkB) are highly expressed in a number of brain regions. BDNF has a high affinity to bind TrkB receptor on either side of the synapse, facilitating both presynaptic release of excitatory neurotransmitters and postsynaptic receptor insertion, as well as spine maintenance (Noble et al., 2011). Recently, Ozek et al. reported that PTP1B overexpression inhibited BDNF/TrkB signalling while inhibition of PTP1B or genetic PTP1B deficiency restored BDNF/TrkB signalling and BDNF-mediated neurite outgrowth and BDNF-induced metabolic effects (Ozek et al., 2014). Krishnan et al. further demonstrated that PTP1B inhibited tyrosine phosphorylation of TrkB to attenuate BDNF signalling in the neurological disorder Rett

`

syndrome model which presents autistic features (Fig.1.1). Pharmacological inhibition of PTP1B ameliorated the behaviour test and improved survival in mice models (Krishnan et al., 2015). Increasingly, studies have disclosed the influence of PTP1B on neuronal development. Fuentes et al. revealed that PTP1B participated in neuronal plasticity formation and reduction of PTP1B level improved dendritic filopodia, learning and memory (Fuentes et al., 2012). It is important to note that the reduction of BDNF has been reported in a number of mental disorders including schizophrenia (Angelucci et al., 2005, Favalli et al., 2012). Therefore it is of great interest to investigate the role of PTP1B in modulating BDNF-mediated neurite outgrowth and synaptogenesis in schizophrenia-like models.

### 1.2.3 Phencyclidine models show BDNF reduction and dysfunction in schizophrenia

Phencyclidine (PCP) is a recognized psychotomimetic drug. PCP is a non-competitive and dosage-dependent blocker of the N-methyl-D-aspartate (NMDA)-type glutamate receptors, binds equally to NMDA receptor subunit 2A (NR2A) and NMDA receptor subunit 2B (NR2B) (Paoletti and Neyton, 2007) and induces psychotic symptoms that are similar to schizophrenia in humans and rodents (Javitt and Zukin, 1991, Morris et al., 2005). Apart from other recognized psychotomimetic drugs including amphetamine, PCP is capable of mimicking negative symptoms such as alogia, anhedonia, and social withdrawal, as well as cognitive deficits in addition to positive symptoms including delusions, hallucinations, and thought disorder in schizophrenia (Andreasen, 1995, Jentsch and Roth, 1999). PCP has been reported to induce reduction of neurite outgrowth and synaptogenesis. The effects of PCP on reducing dendritic spine density and neurite outgrowth have been reported in both *in vitro* and *in vivo* studies (Hajszan et al., 2006, Adachi et al., 2013). A decreased number of spines in the prefrontal cortex of

`

rats has been confirmed using sub-chronic PCP treatment (Hajszan et al., 2006), suggesting that PCP treatment contributes to abnormal synaptic function in schizophrenia-related behaviours (Frankle et al., 2003).

BDNF alteration is widely observed in schizophrenia pathophysiology (Favalli et al., 2012). Durany et al. observed reduced concentration of BDNF in post-mortem tissue collected from patients with schizophrenia, compared to control (Durany et al., 2001). Increasing evidence also shows the alteration of BDNF transcriptional level. Weickert et al. found a significant decrease of BDNF mRNA, TrkB mRNA and BDNF level in schizophrenia patients (Weickert et al., 2003, Weickert et al., 2005). The majority of studies have found the reduction of BDNF serum level in first-episode and medication naive schizophrenia patients compared to healthy control (Buckley et al., 2007, Chen et al., 2009).

Previous studies have reported that PCP treatment is associated with alteration of BDNF protein level and mRNA level. Sub-chronic PCP administration induced severe disruption of cognitive performance with reduction of BDNF in various regions of rat brains (Snigdha et al., 2011). Other researchers have administered PCP in cultured cortical neurons and disclosed decreased BDNF mRNA level (Katanuma et al., 2014). A recent study found that PCP treatment for 48 hours reduced the amount of BDNF, decreased secretion of BDNF and inactivated Trk receptors in cultured neurons. The number of synaptic sites and expression of synaptic proteins were also suppressed, together with diminished glutamatergic neurotransmission (Adachi et al., 2013). Moreover, PCP suppressed the BDNF-mediated signalling Akt/GSK3β pathway (Adachi et al., 2013), which has been shown to regulate synaptogenesis and neurite outgrowth (Kitagishi et al., 2012, Smillie et al., 2013) (Fig.1.1). For example, Akt

`

facilitated dendritic spine protein and Akt phosphorylation involved in working memory formation (Emamian et al., 2004). GSK3β was expressed abundantly in neurons in the developing rat brain to regulate dendrite extension and synapse formation (Leroy and Brion, 1999). Therefore, BDNF reduction and dysfunction are responsible for the loss of synaptic connections caused by PCP. Since PTP1B inhibits BDNF-mediated signalling, it is interesting to investigate the role of PTP1B in PCP models and develop potent PTP1B inhibitors to reverse PCP induced alterations.

### 1.2.4 Neuregulin-1 (NRG1) and susceptibility to schizophrenia

A genome-wide scan of diverse schizophrenia populations has provided insight into mechanisms of this disorder and revealed several genes, such as neuregulin-1(NRG1), to be closely associated with schizophrenia (Stefansson et al., 2002, Harrison and Weinberger, 2004). Research on NRG1 and its receptor ErbB4 (v-erb-a erythroblastic leukaemia viral oncogene homolog 4) improved our understanding of schizophrenia-induced impairment of neurodevelopment, neurotransmission and synaptic plasticity (Mei and Xiong, 2008). It has been reported that mutant mice, heterozygous for either NRG1 or ErbB4, displayed behaviour abnormality, cognitive deficit and reduced functional NMDA receptors compared to wild-type mice, which however overlapped with mouse models for schizophrenia (Stefansson et al., 2002). Therefore models based on NRG1 mutation have been established to explore the implications for the pathophysiology of schizophrenia and potential treatments.

Recent studies have used NRG1-/+ mutant mice to investigate the interactions between NRG1 and NMDA receptor (Bjarnadottir et al., 2007, Zhang et al., 2016). NRG1 signalling has been confirmed to stimulate phosphorylation of Y1472 on the NR2B subunit of the NMDA receptor which played a key role regulating channel properties. The reduction of NR2B Y1472 phosphorylation was associated with the behavioural

`

abnormalities and altered synaptic plasticity in NRG1 -/+ mutant mice. These results indicated that attenuated NRG1/ErbB4 signalling contributed to the psychopathology of schizophrenia through the impairment of NMDAR modulation, NR2B in particular.

### 1.2.5 Challenges in discovering PTP1B traditional inhibitors: disadvantages of targeting PTP1B active site

Full-length PTP1B (encoded by PTPN1) is 435 amino acids (about 50 kDa) (Chernoff et al., 1990), including an N-terminal catalytic domain (the so-called PTP domain) and a C-terminal domain which localizes the PTP1B to the endoplasmic reticulum (Frangioni et al., 1992) (Fig.1.2a). PTP1B belongs to the Protein Tyrosine Phosphatases (PTPs) family, which contains more than 100 members. Most members display a consensus catalytic loop signature $(H/V)C(X)_5R(S/T)$, the so-called PTP loop or catalytic loop, which is normally composed of 8 amino acids from His214 to Arg221 (Barford et al., 1994), including the active site Cys215 which is conserved and essential for enzyme catalysis (Julien et al., 2011, St-Pierre and Tremblay, 2012). PTP1B also contains a PTP loop located in a catalytic cleft formed by four other loops. The depth of the catalytic cleft contributes to specifically recognizing tyrosine as the substrate (Johnson et al., 2002).

As previously mentioned, the PTPs family has many members. One of them is T-cell protein tyrosine phosphatase (TCPTP) which is similar in structure to PTP1B. TCPTP (encoded by PTPN2) is cloned from a peripheral human T-cell cDNA library (Cool et al., 1989). The alternative splicing gives rise to two variants of TCPTP (Fig.1.2a): a 45 kDa form (TC45) which lacks the hydrophobic C-terminus and targets the nucleus, and a 48kDa form (TC48) which localizes to the Endoplasmic reticulum (ER) by the C-terminus (Tiganis et al., 1999, Tiganis and Bennett, 2007). The amino acid sequence

`

identity between the PTP domains of TCPTP and PTP1B is 74% (Fig.1.2a) with a minor difference in four clusters of amino acid residues, and TCPTP shares a strong similarity with PTP1B in 3D structure (Fig.1.2b). Additionally, TCPTP has a catalytic cleft containing the active site Cys216 and the catalytic efficiencies between TCPTP and PTP1B are almost identical based on their catalytic constant ($K_{cat}$) and Michaelis constant ($K_m$) (Iversen et al., 2002). However TCPTP regulates different biological functions despite high structural similarity to PTP1B. PTP1B has been confirmed to dephosphorylate JAK2 to attenuate leptin signalling while TCPTP dephosphorylated JAK1 and JAK3 to regulate the immune system (Simoncic et al., 2002), suggesting that TCPTP may have little influence on mediating central leptin signalling. In an addition, entirely TCPTP knock-out mice showed damage in their immune system such as haematopoiesis defects (You-Ten et al., 1997).

The active site plays as an essential role in PTP1B catalysis which processes as a two-step mechanism. In the first step, the sulphur atom of Cys215 begins a nucleophilic attack on the phosphate on the tyrosine, and then Asp181 acts as a general acid to protonate the tyrosyl-leaving group of the substrate. An intermediate cysteinyl-phosphate is therefore formed (Tonks, 2003). In the second step, the phosphate is released from the intermediate by hydrolysis, mediated by Gln262 and Asp181. Traditional PTP1B inhibitor design targets the active site Cys215 and most active-site targeted inhibitors are non-hydrolyzable pTyr mimetics (Zhang and Zhang, 2007). The traditional inhibitors target both active site residues and neighbouring residues, so called subpockets which are adjacent to the PTP active site to increase the inhibition selectivity (Zhang, 2002). However considering PTP1B and TCPTP share a very similar active site loop and surrounding loops (Iversen et al., 2002), it is doubtful whether the selectivity of active-site targeted drugs, PTP1B traditional inhibitors in other words,

`

inhibit PTP1B over TCPTP. On the other hand, PTP1B traditional inhibitors are pTyr mimetics which generally display high charge density, making it difficult to penetrate cell membranes, leading to poor bioavailability. Therefore, the novel drug discovery is targeting the allosteric site of PTP1B which inhibits PTP1B activity by affecting the movement of WPD (Residues 179-181, Trp-Pro-Asp) loop in PTP1B (Wiesmann et al., 2004).

`

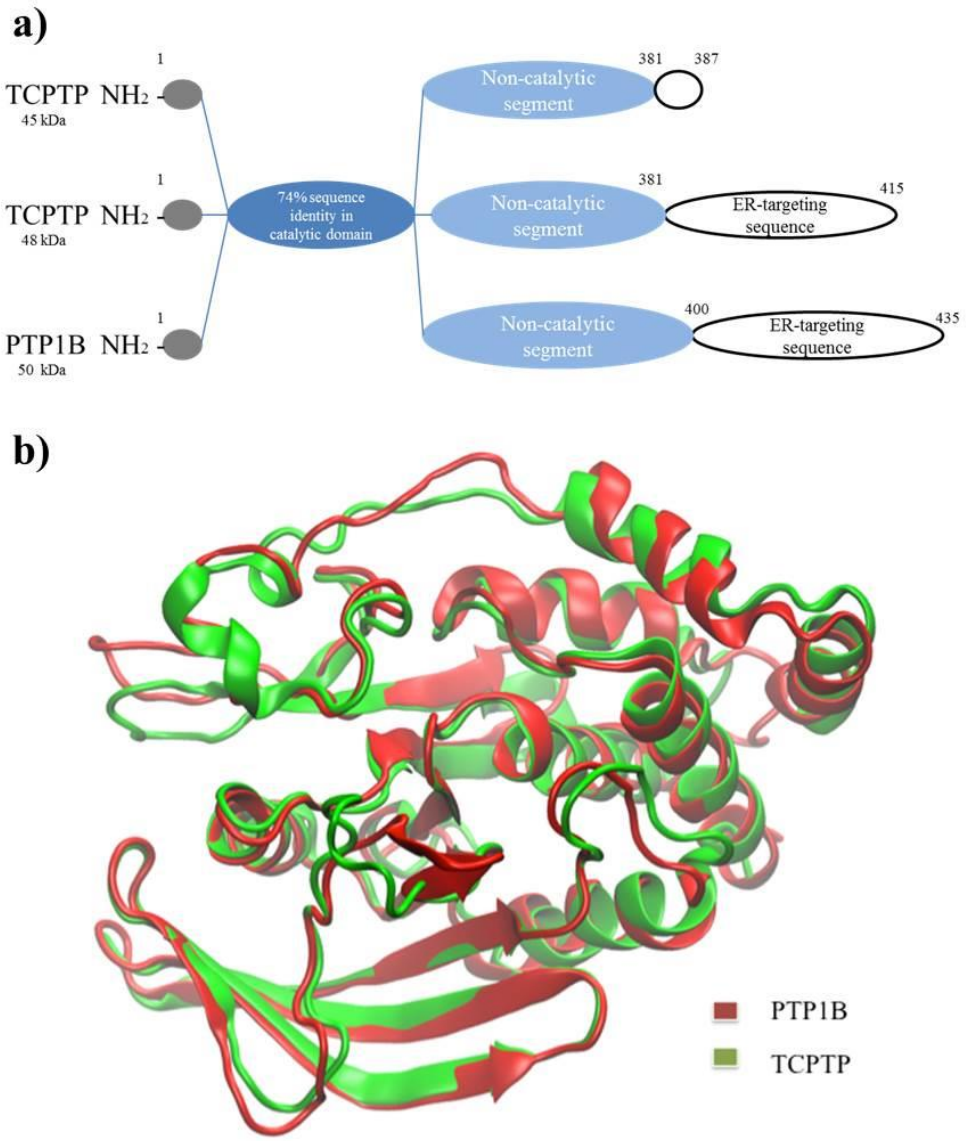


Figure. 1.2: This picture represents the strong similarity of structure in the PTP domain between TCPTP and PTP1B. They have 74% identity in sequence (a) and strong similarity in the 3D structure (b). Due to the conservative catalytic domains, it is difficult to develop selective PTP1B inhibitors which specifically target PTP1B (PDB code: 1PTY) over TCPTP (PDB code: 1L8K).

`

### 1.2.6 Developing PTP1B allosteric inhibitors is an alternative strategy

The WPD (Residues 179-181, Trp-Pro-Asp) loop is an important feature in the catalysis of PTP1B (Barr, 2010). Under physiological conditions, protein can exhibit multiple conformations and sometimes involve large-scale conformational transitions (so-called allosteric transition) in contrast to the usual static view brought by a single structure. This is nicely illustrated by the movement of the WPD loop in PTP1B captured by X-ray crystallography. During the transition of the WPD loop in catalysis, PTP1B expresses two different conformations, open and closed (Fig.1.3c). In the open model (PDB Entry 2HNP), the WPD loop forms an open binding crevice which allows active site access to reach the tyrosine substrate and in the closed conformation (PDB Entry 1SUG), the WPD loop closes over the cleft where the active site forms an intermediate with the phosphate, sequestering the cysteinyl-phosphate intermediate and one nucleophilic water molecule (Pannifer et al., 1998), finally, phosphoryl transfer from the intermediate to the buried water molecular occurs and the WPD loop re-opens the cleft to continue catalysis. The conformation difference provides a new design of PTP1B inhibitors called PTP1B allosteric inhibitors. Allosteric inhibition aims to prevent WPD movement from open mode to closed mode and results in the inactivity of PTP1B. In 2004, the PTP1B allosteric site was identified, sited 20 Å away from the catalytic pocket (Wiesmann et al., 2004) (Fig.1.3a). The high-resolution crystal structures of PTP1B in complex with allosteric inhibitors including compound 2 and compound 3 (Fig.1.4), revealed that instead of targeting the enzymatic active site, these inhibitors bond to an allosteric site composed by $\alpha$3, $\alpha$6 and $\alpha$7 (Wiesmann et al., 2004) (Fig.1.3b). It has been proposed that through long-range coupling these allosteric inhibitors can prevent the closure of the WPD loop and thus the formation of the active state of the enzyme. In this way, the inhibitors locked PTP1B in a catalytically incompetent state. It is

`

encouraging that the allosteric inhibitors showed high potency in inhibiting PTP1B while at the same time having significant selectivity over TCPTP. Allosteric inhibitors have advantage over other inhibitors, which target the active site, since key residues involved in the allosteric binding are not conserved in most PTPs (Zhang and Zhang, 2007). Interestingly, this allosteric inhibition strategy has also been applied to target SHP2, which is another member of the PTPs family, showing a potent, selective and orally efficacious inhibition (Chen et al., 2016, Garcia Fortanet et al., 2016). Therefore, allosteric inhibition is an ideal treatment strategy in PTPs inhibition including PTP1B. Considering only a few selective PTP1B inhibitors with acceptable pharmacological properties are under clinical trials, such as TransTech Pharma Inc TTP814, and Ohr Pharmaceutical Inc Trodusquemine (MSI-1436) (Krishnan et al., 2014), which are in Phase II and Phase I testing, respectively (Osherovich, 2011), it is necessary to develop novel PTP1B allosteric inhibitors.

`

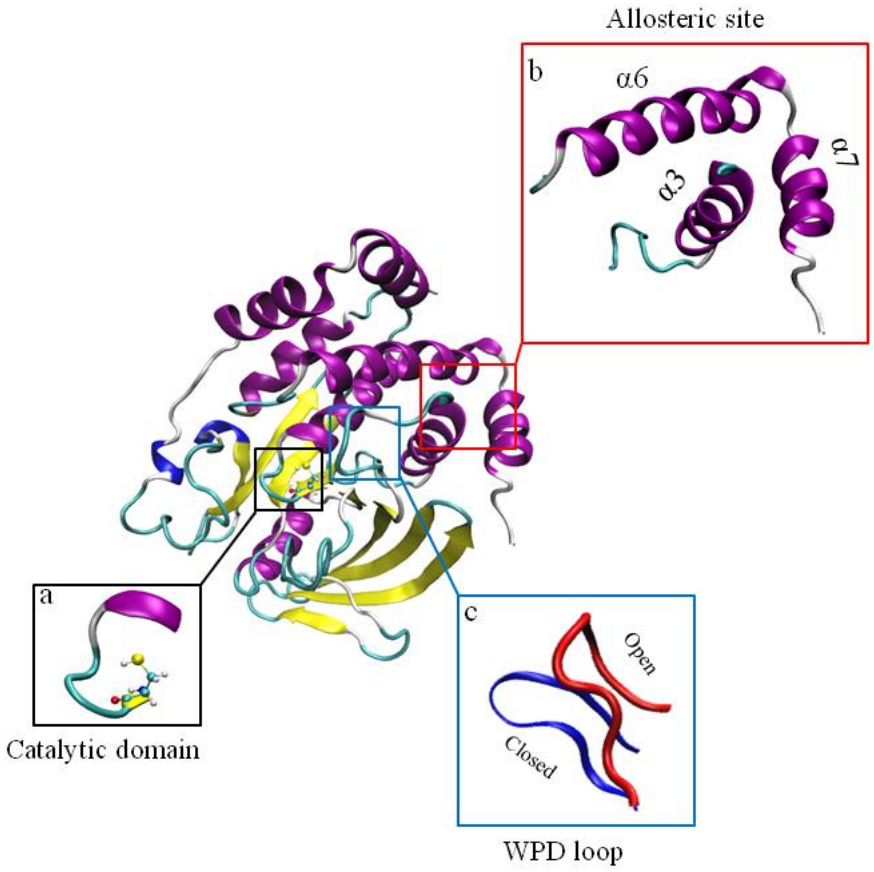


Figure. 1.3: The crystallography structure of PTP1B. PTP1B has an active site Cysteine 215 with surrounding catalytic loop (a) and an identified allosteric site (b) which is surrounded by the α3 helix, α6 helix and α7 helix. During PTP1B activation, the WPD loop (c) moves from the open position to the closed position. Allosteric inhibition aims to prevent the WPD loop to keep PTP1B in an inactive state and lose activity.

`

### 1.2.7 Lupane triterpenes are candidates as PTP1B allosteric inhibitors

Triterpenes are pentacyclic chemical compounds which are major natural components of human diets, isolated from vegetable oils, cereals and fruits (Moreau et al., 2002). Previous studies have mentioned the enormous utility of triterpenes as anti-cancer drugs, anti-inflammation drugs and anti-diabetes drugs (Ovesna et al., 2004, Liby et al., 2007). As one family of triterpenes, lupane triterpenes have been studied for decades. Lupane triterpenes are major natural components of vegetables, fruits and medical plants including white cabbage, pepper, carrot, pea, birch bark, rosemary leaves and mistletoe shoots (Laszczyk, 2009). Previous studies have established lupane triterpenes as anti-cancer drugs, anti-inflammation drugs, anti-diabetes drugs and anti-viral drugs (Baltina et al., 2003, Tolstikova et al., 2006). Lupane triterpenes have four members including lupeol, lupenone, betulin and betulinic acid (Fig.1.4). All four members of lupane triterpenes have shown potent PTP1B inhibition activity *in vitro* (Na et al., 2009, Choi et al., 2009, Xu et al., 2009). One previous study has shown that lupeol could inhibit PTP1B with a high potency (IC50=5.6μM) (Na et al., 2009) and the extra kinetic assay indicates that lupeol acts as a non-competitive inhibitor of PTP1B which means lupeol is a potential PTP1B allosteric inhibitor. This is because when a compound inhibits the enzyme, it could target on either active site as a competitive inhibitor or bind to allosteric site as a non-competitive inhibitor. Lupeol fits in non-competitive inhibition mode. Therefore lupeol is a potential PTP1B allosteric inhibitor. However, the molecular mechanism and the location of the binding site of lupeol and other lupane triterpenes targeting PTP1B remains speculative. Considering the promising results for the allosteric PTP1B inhibitors, my work aims at characterising the selectivity and binding mode of lupane triterpenes targeting PTP1B including lupeol, lupenone, betulin and betulinic acid in *silico* and *in vitro*, as well as validating their biological and

`

physiological functions in various cellular models, in order to develop ideal potential PTP1B allosteric inhibitors in the future.

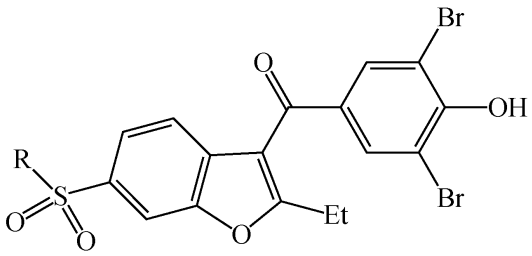


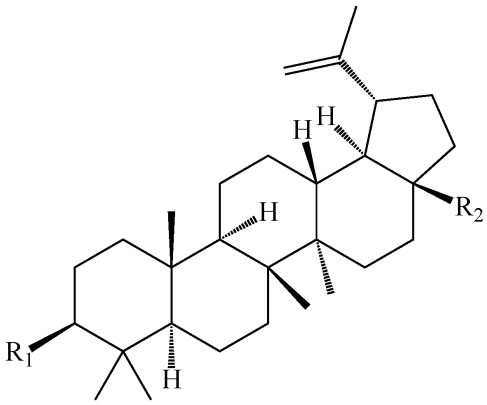


Compound 2: R = 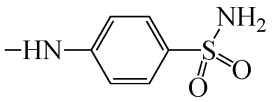


Compound 3: R = 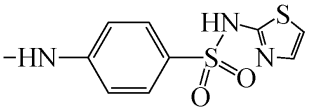


| | | |
|---|---|---|
| Lupeol: | $R_1$ = -OH | $R_2$ = -$CH_3$ |
| Lupenone: | $R_1$ = =O | $R_2$ = -$CH_3$ |
| Betulin: | $R_1$ = -OH | $R_2$ = -OH |
| Betulinic acid: | $R_1$ = -OH | $R_2$ = -COOH |

Figure .1.4: The formula of allosteric ligands used in this study. Compound 2 and 3 have been reported to be allosteric inhibitors by Wiesmann et al (Wiesmann et al., 2004). Four members of lupane triterpenes were selected. It appears that lupeol, lupenone, betulin and betulinic acid share a pentacyclic hydrophobic main structure with distinctions of functional groups in the $R_1$ and $R_2$ positions.

`

### 1.2.8 Application of computational modelling to determine lupane triterpenes as PTP1B allosteric inhibitors

The present PhD project applies computational modelling as a method to characterise the structural interactions between PTP1B and lupane triterpenes, to demonstrate lupane triterpenes as PTP1B allosteric inhibitors. Computer-aided drug discovery plays a critical role in the investigation of therapeutically small molecules to develop drug candidates (Kubinyi, 2006). As a well-established computational technique, molecular docking is applied to predict the preferred orientation of one molecular bond to another (Kitchen et al., 2004), such as lupane triterpene to PTP1B. The interactions between two molecules are mainly forces including electrostatic forces, van der Waal interactions and solvent-related forces. All the types of energy will be detected by a search algorithm and then converted into numerical values via a statistical scoring function. Docking scores will be provided after the calculation which could help to evaluate the most possible binding site of the molecule targeting the protein (Warren et al., 2006). The relation between biological molecules always plays an important role in signal transduction. By using docking to mimic the interaction between two molecules such as lupane triterpene and PTP1B, could provide the information including affinity and activity of the lupane triterpenes. However, docking only provides a rigid structure of protein-ligand complex which is flexible in nature solvent environment (Kitchen et al., 2004). Instead, molecular dynamics (MD) simulation is then applied to determine the motion of atoms and resulting conformational change of lupane triterpenes upon binding to PTP1B. MD calculates a time-dependent trajectory concerning the movements of individual particles in a protein-ligand complex, to investigate the stability and flexibility of the formed complex, and implicate the important structural feature of the ligand and protein binding site involved in forming the bound complex

`

(van Gunsteren et al., 2006). Overall, application of computational modelling aims to disclose the binding mode of lupane triterpenes targeting PTP1B allosteric site, and reveal the potential drug design strategy to improve efficacy.

### 1.2.9 Application of inertial microfluidic platform to separate and collect neurons and glial cells

A cell culture model will be broadly applied in this project including primary neuron culture, which is a widely used experimental method, closely mimicking the physiological status of neurons *in vivo* and provides a convincing and convenient platform to perform drug treatments. However one major challenge is to separate neurons from complex cell mixtures dissected from brain tissues with high purity and efficiency. For example, glial cell is the major component in brain tissue which normally outnumbers neurons in mammalian brain regions (Bear MF, 2006). Medium-based procedure is a conventional method for pure neuron and pure glial cell cultures where NeuroBasal medium with FDU (5-Fluoro-2′-deoxyuridine) is used to inhibit glial cells proliferation (Brewer, 1997, Hilgenberg and Smith, 2007, Medicine, 2015). However, such a method requires long-term incubation with chemical treatment, wasting both time and experimental materials. Apart from this medium-based separation method, immune-specific separation is broadly applied in neuron-related research. Fluorescence-activated cell sorting (FACS) and magnetically-activated cell sorting (MACS) have been widely used for separating cells (Radbruch and Recktenwald, 1995). However, labelling target cells with antibodies may disturb the immunochemistry analysis on targets of interest. Therefore, a label-free and high-throughput technique is required to continuously separate neurons and glial cells to bridge this gap for neuroscience research. On the other hand, there is increasing evidence of glia, in particular astrocyte abnormality, modulating synaptic dysfunction in several brain

`

disorders including schizophrenia (Seifert et al., 2006, Allen, 2014). A recent study observed that astrocyte loss in the prefrontal cortex triggered neuronal damage causing cognitive impairment in the animal model (Lima et al., 2014). Therefore it is of great interest to investigate the specific role of neurons and glia in *in vitro* schizophrenia-like models in future studies. Furthermore, PTP1B has been recently found expressed in microglial cells (Song et al., 2016), indicating the need for investigation of glial PTP1B contributing to BDNF reduction in the future.

In the present study, I collaborated with a research group in the department of engineering in University of Wollongong, to develop an inertial microfluidic device to separate neurons and glial cells. This inertial microfluidic platform has a built-in serpentine micro-channel made by Polydimethylsiloxane (PDMS), a bio-compatible material, utilizing hydrodynamic forces to continuously separate particles of different sizes with high performance (Zhang et al., 2014b) (Fig.1.5). Inertial microfluidics is a very promising candidate due to its high throughput and simple structure, it has been widely used to extract blood plasma (Lee et al., 2011, Zhang et al., 2014a), isolate circulating tumour cells (CTCs) (Mach et al., 2011, Hou et al., 2013, Ozkumur et al., 2013), and separate leukocytes from blood, (Wu et al., 2012) etc. As a label-free technique without the use of antibody affinity, filter or centrifugation, inertial microfluidics is highly desirable to ensure minimal damage and alteration to neurons. This microfluidic device will be very useful to separate and collect both neurons and glia spontaneously from the brain section of interest, and establish a platform to characterise the specific role of neuron and glia in neurological disorders.

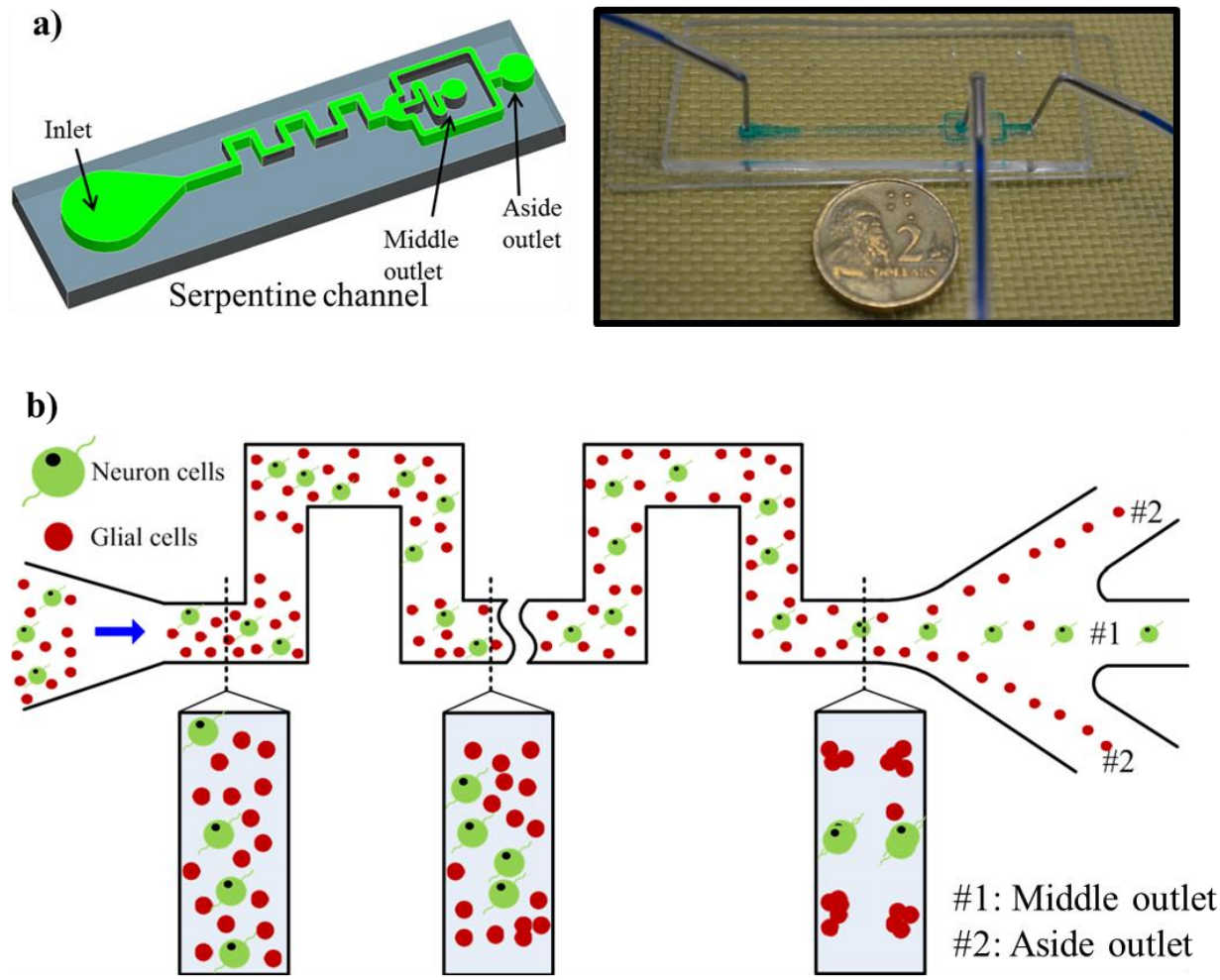


Figure. 1.5: a): The inertial microfluidic device applied in this work. B): Schematic illustration of the micro-channel structure used for cell separation. A filter upstream of the serpentine channel prevents the channel from being blocked by large debris. A trifurcation outlet system was used with middle outlet #1 for neuron collection, two symmetrical side branches merged together as outlet #2 for glial cell collection.

`

## 1.3 Aims

The aims of this research were to:

1. Determine lupeol and other lupane triterpenes as PTP1B allosteric inhibitors using computational modelling and biological assay, to confirm these compounds specifically bind to PTP1B allosteric site and selectively and potently inhibit PTP1B.

2. Investigate the role of PTP1B regulating BDNF level, BDNF-mediated signalling, leptin signalling, synaptogenesis and neurite outgrowth in the PCP-mimicked schizophrenia model and Neureglin-1 knockout animal model.

3. Demonstrate that lupane triterpene treatment is an effective treatment to alter PCP-induced BDNF reduction and neurogenesis impairment, indicating that PTP1B inhibition is a potential therapeutic strategy to be combined with current antipsychotic olanzapine to enhance treatment efficacy.

4. Develop an innovative microfluidic device to separate neurons and glial cells with purity and viability, in order to provide a reliable platform to investigate the specific role of neurons and glia in neurological diseases such as schizophrenia and associated metabolic disorders.

`

## 1.4 Hypothesis

1. Lupeol and other lupane triterpenes are PTP1B allosteric inhibitors which target PTP1B allosteric site and form a stable protein-ligand complex. The structure of lupane triterpenes will be characterised to provide advice for future chemical modifications. Lupane triterpenes are able to specifically inhibit PTP1B over TCPTP, which will be examined in this part of study.

2. PTP1B is significantly altered in Phencyclidine-treated and Neureglin-1 knockout model, and thus negatively regulated synaptogenesis and neurite outgrowth through the reduction of BDNF, attenuation of BDNF-mediated signalling and impairment of leptin signalling.

3. Lupeol treatment is able to significantly inhibit PTP1B and reverse PCP-induced psychopathological alterations to increase BDNF, restore BDNF-mediated signalling and leptin signalling, as well as enhance the treatment efficacy and prevent side effects of current antipsychotic such as olanzapine.

4. An innovative microfluidic device is able to separate neurons and glial cells with efficacy and efficiency. Collected neurons and glial cells are healthy and functional to perform downstream experiments.

`

## 1.5 Significance

1. One challenge in PTP1B inhibition is that most PTP1B inhibitors target the PTP1B active site. The PTP1B active site and nearby catalytic domains are highly conservative in the PTP family. For example, PTP1B is highly similar to TCPTP in amino acid sequence and 3D structure. To inhibit PTP1B with enhanced selectivity, PTP1B allosteric site has been discovered as a novel drug target. PTP1B allosteric inhibition is able to prevent the conformational change of the WPD loop during catalysis, thus keeping PTP1B in an inactivated state. In the present project, I aim to identify lupane triterpenes (lupeol, lupenone, betulin and betulinic acid) as novel PTP1B allosteric inhibitors.

2. Reduction of BDNF and attenuation of BDNF-mediated signalling lead to impaired neurogenesis which has been recognized in mental disorders including schizophrenia. PTP1B has been reported to attenuate BDNF-mediated signalling. PTP1B has also been revealed to inhibit leptin signalling which is a crucial factor stimulating BDNF expression. Therefore, it is important to investigate the role of PTP1B in the impairment of BDNF-mediated signalling and whether PTP1B directly regulates BDNF expression through leptin signalling in schizophrenia-mimicked models.

3. In the present study, lupane triterpene treatment is applied to the PCP treated model to reverse PCP-induced alterations including BDNF reduction, BDNF-mediated signalling attenuation and synaptogenesis impairment. Furthermore, lupane triterpene treatment is applied combined with antipsychotic (olanzapine) treatment to confirm the improved efficacy of co-treatment due to PTP1B inhibition.

4. Neurons are of particular interest in investigating the psychopathology of mental illness including schizophrenia. Primary neuron culture is broadly used to collect and

`

analyse neurons in mammalian brain tissue. However, it is difficult to isolate purified neurons from cell mixture in brain tissue culture. In the present study, a microfluidic device is introduced to separate and collect neurons and glial cells with high purity and viability. Moreover, such application will be useful in future studies to differentiate the role of neurons and glia in disease development and will be established as drug screening platform.

`

## 1.6 Methods and Materials

### 1.6.1 Homology modelling of PTP1B

In this study, a published PTP1B crystal structure (PDB id: 1T49) was applied. This PTP1B structure was an open and inactive conformation which contains 282 amino acids, and the α7 (17 amino acids) was not resolved (labelled as PTP1B282). Helix α7 plays a crucial role in PTP1B allosteric inhibition. However there is no PTP1B crystal structure with α7 in the inactive state. Here, homology modelling with Modeller 9v8 was performed in order to construct the missing helix α7 based on the active conformation of PTP1B (PDB id: 1PTY) (labelled as PTP1B299) (Sali and Blundell, 1993). The best PTP1B299 model based on the DOPE energy was chosen from total 100 models generated, and then subjected to equilibrium molecular dynamics simulations for 40 ns to reach equilibrium and optimize the modelled structure.

### 1.6.2 Molecular docking

Autodock Vina (version 1.1.2) was used to carry out docking studies (Trott and Olson, 2010). The docking process was established via re-docking previous demonstrated PTP1B allosteric inhibitor, compound 2 to PTP1B282 as in the co-crystal structure (Wiesmann et al., 2004). The protonation states of the PTP1B titratable groups were assigned at pH 7.0 using PROPKA3.1 (Olsson et al., 2011). Docking study was then performed sequentially in two steps. Firstly, blind docking was performed in which a cube large enough to cover the whole PTP1B protein (75 Å × 60 Å × 60 Å) was established to detect potential binding pockets. Then, focused docking which involved localized docking with a smaller cube (22.5 Å × 22.5 Å × 22.5 Å) was set up, targeting the potential binding site of interest (e.g. active site, allosteric site, or other sites of interest identified from the previous blind docking procedure). In each focused docking

`

study of lupane triterpenes binding to PTP1B282 and PTP1B299, total 20 conformations of the PTP1B-ligand complexes which showed lowest binding affinities were listed for further analysis. The best binding mode from docking study was selected as the initial structure for the following molecular dynamics simulations. Multiple dockings based on different snapshots collected from equilibrium molecular dynamics simulations (PTP1B282 and PTP1B299), were also performed. Qualitatively, the identified populated binding poses are similar. In addition, blind docking of lupane triterpenes targeting TCPTP (1L8K) was performed.

### 1.6.3 Molecular dynamics simulations

Molecular dynamics simulations were established to characterise the stability and flexibility of the PTP1B-lupane triterpenes complexes. In this study, total 9 different systems were set up (PTP1B282, PTP1B282 with Compound2, PTP1B282 with Lupeol, PTP1B299, PTP1B299 with Compound2, PTP1B299 with Lupeol, PTP1B299 with Lupenone, PTP1B299 with Betulin, PTP1B299 with Betulinic acid). All of the systems were solvated in a box full of TIP3P water molecules, which extended about 12 Å from the surface of the protein. Then counter ions of $Na^+$ were applied to neutralize the systems. The salt (NaCl) concentration was set to 0.15 mol/L. Molecular dynamics simulations were carried out using NAMD 2.9 (Phillips et al., 2005). The protein and the ligands were represented with the GAFF force field (Wang et al., 2004) and the non-polarizable CHARMM PARAM27 force field (MacKerell et al., 1998), respectively. Langevin algorithm was applied to set up periodic boundary conditions for all of the systems, maintaining the temperature at 298.15 K, and the Langevin Piston Nose-Hoover method was used to keep the pressure constant at 1.0 bar. Particle Mesh Ewald (PME) method (Darden et al., 1993) was performed to calculate the electrostatic interactions. The van der Waal forces were treated with a cut-off at 12 Å. All of the

`

covalent bonds which involved hydrogen were kept rigid applying the Rattle algorithm and the time step was set to 1.0 fs. In the equilibrium simulations of PTP1B homology modelling, a harmonic restraint on the backbone atoms except α7 was established with a decreasing force constant from 64.0 to 1.0 kcal/mol/$Å^2$ for 10 ns. The simulations continued for 30 ns without any restraints. For the molecular dynamics simulations of the docked complexes, a harmonic restraint on the backbone atoms was setup with a decreasing force constant from 32.0 to 1.0 kcal/mol/$Å^2$ for 3 ns followed by 20 or 100 ns equilibrium simulations.

**1.6.4 Binding free energy calculation**

Free energy perturbation distributed replica-exchange molecular dynamics (FEP/λ-REMD) (Woods et al., 2003, Jiang et al., 2009) was carried out to calculate binding free energy of lupeol and betulinic acid binding to PTP1B. The reason to perform computationally intensive absolute binding free energies is because the binding modes for lupeol and betulinic acid revealed by docking and subsequently molecular dynamics simulations are rather different. Therefore it is difficult to apply relative binding free energy calculations, which assume that the available conformational spaces are strongly overlapped (Hansen and van Gunsteren, 2014). Based on previous literature, free energy difference was called between the unbound ligand in the aqueous solution and the bound ligand in the binding site of the target protein as the absolute binding free energies. The total free energy was divided into four terms, namely repulsive and dispersive components of the Lennard-Jones potential based on the Weeks-Chandler-Anderson scheme, the electrostatic contribution, and the restraining potential. Ligand was decoupled from the environment in four steps through four thermodynamic coupling parameters (λ). No corrections have been carried out to the potential electrostatic finite-size artefacts (Rocklin et al., 2013, Reif and Oostenbrink, 2014). In

`

order to accelerate the convergence, each λ-staging FEP window was treated as a replica and the λ-exchange occurred along the entire alchemical reaction path. This method has been successfully applied to study which investigated the interactions between glycoside hydrolases and polysaccharides (Payne et al., 2013). For both PTP1B-lupeol and the PTP1B-betulinic acid complex in this study, FEP/λ-REMD simulations started from a 100 ns equilibrated snapshot. Total set of 64 replicas including 36 repulsive, 12 dispersive, and 16 electrostatic, was carried out in the simulations with an exchange frequency of one every 1,000 steps (1 ps). In each replica, 1.0 ns simulations were performed in which the last 0.8 ns simulations were averaged to calculate the ligand binding free energies. The protein-ligand complexes contained a positional translational restraint with a force constant of 10.0 kcal/mol/$Å^2$. The error analyses were assigned using four sequential simulations of 0.2 ns each.

### 1.6.5 Trajectory analysis

Trajectory snapshots were saved every picosecond (i.e. every 1,000 steps). Either the molecular visualization program VMD 1.9 (Humphrey et al., 1996) or CHARMM (Brooks et al., 2009) was performed to analyse the trajectory data.

### 1.6.6 PTP1B and TCPTP inhibition assay of lupane triterpenes by *p*NPP phosphatase assay

EnzoLyte Colorimetric *p*NPP Protein Phosphatase Assay kit (AS-71105, Anaspec) was applied to determine the inhibitory effects of lupane triterpenes targeting PTP1B and TCPTP. The recombinant human PTP1B (ab42572, Abcam Inc), recombinant human TCPTP (ab42575, Abcam Inc), Lupeol (L5632, Sigma-Aldrich), lupenone (1617-70-5, Faces Biochemical Co.Ltd), betulin (B9757, Sigma-Aldrich), betulinic acid (B8936, Sigma-Aldrich) and compound 3 (765317-72-4, Merck Millipore) were dissolved in

`

Dimethyl sulfoxide (DMSO) or water. Experiment was processed based on manufacturer instructions. Briefly, 25 ng PTP1B or TCPTP was incubated in different concentrations of compounds (control drug compound 3, lupeol, lupenone, betulin, betulinic acid) for 10 min in assay buffer (assay kit supplied) at 25°C, and then the reaction was initiated by adding the 20 mM *p*NPP reagent and stopped by NaOH (assay kit supplied) after 30 min at 25°C. All readings were detected and recorded using a spectraMAX 384 microplate spectrophotometer. The absorbance was set up at 405 nm. Negative control wells without enzymes were calibrated. The PTP1B and TCPTP inhibition potency of the lupane triterpenes was determined by $IC_{50}$, calculated using the GraphPad Prism 5 program (GraphPad Software Inc).

### 1.6.7 PTP1B inhibition kinetics assay of lupane triterpenes by *p*NPP phosphatase assay

The kinetics assay of PTP1B-catalysed hydrolyses in the presence of betulin and betulinic acid were performed using the *p*NPP Protein Phosphatase Assay kit described above. The reaction mixture consisted of six different concentrations of *p*NPP (1.0, 2.0, 4.0, 8.0, 16.0, and 20.0 mM) as PTP1B substrate and different concentrations of lupeol, betulin, and betulinic acid. The Lupeol group was set up as a control group. The absorbance at 405 nm was detected by a spectraMAX 384 microplate spectrophotometer twice every minute for a total of 15 min. Michaelis-Menten constant ($K_m$) and maximum velocity ($V_{max}$) of PTP1B were determined via Lineweaver-Burk plots using the GraphPad Prism 5 program (GraphPad Software Inc).

### 1.6.8 Immunoprecipitation assay of PTP1B

Based on the instructions of the Pierce Classic IP Kit (26146, Thermo Fisher Scientific Inc) with minor modifications (Lorenz, 2011), PTP1B was detected using the 25 $\mu$g

`

PTP1B antibody (sc-1718, Santa-Cruz) for 12 h at 4℃ to form immune complexes. Immune complexes were then isolated by adding the protein G-agarose, washed three times in the phosphatase assay buffer from the EnzoLyte Colorimetric *p*NPP Protein Phosphatase Assay kit (AS-71105, Anaspec), and resuspended in the same buffer. Samples were analysed for the phosphatase activity using the same *p*NPP assay kit mentioned above.

### 1.6.9 Ethics statement

This study was approved by the Animal Ethics Committee, University of Wollongong (Application Approval #: AE15/13 and AE16/01), and complied with the 'Australian Code of Practice for the Care and Use of Animals for Scientific Purposes' (Australian Government National Health and Medical Research Council, 2004), in accordance with the International Guiding Principles for Biomedical Research Involving Animals. All efforts have been performed to minimize animal numbers, animal stress and prevent suffering.

### 1.6.10 Primary cell culture of wide type and Nrg1 -/+ mouse hypothalamic neurons

In chapter 3 and chapter 4, primary hypothalamic cell cultures from hypothalamic tissues of postnatal day 0 (PN0) wild-type (WT) and Neuregulin-1 (NRG1)-knockout (KO) C57BL/6 mice were prepared based on previous literature (Hilgenberg and Smith, 2007). The culture medium was adapted according to Johns Hopkins online protocol (Medicine, 2015), which was composed of 480 ml NeuroBasal medium (21103-049, Gbico) with additive 10 ml B27 (17504-044, Gbico), 5ml glutamine (25030081, Thermo Fisher Scientific Inc), 5 ml penicillin-streptomycin (15140122, Gbico) and 9 g glucose (G7021, Sigma-Aldrich). Neurons were plated at either a final density of $1.5 \times 10^5$ cells per $cm^2$ onto Poly-D-Lysine-coated coverslips for immunofluorescence

`

imaging (G400-13, ProSciTech) or a final density of $5 \times 10^5$ cells per $cm^2$ into Poly-D-Lysine-coated 12-well cell culture plate for collect protein or RNA, and maintained at 37°C with 5% $CO_2$. At DIV 10, 25 μM PCP (P3209, Sigma-Aldrich) was applied to neurons for 3h and 48h. To investigate effect of PCP on leptin signalling, 100 nM leptin (450-31-5000, PeproTech) was applied to neurons after PCP stimulations for 4 hours. To examine the influence of PTP1B inhibition on neurite synaptogenesis, 50 μM lupeol (L5632, Sigma-Aldrich) was administrated to primary hypothalamic neurons which have been treated by 25 μM PCP for 24 hrs, and then co-incubated for another 24 hrs. The DMSO concentration was controlled below 0.5%. Neurons were then collected for further experiments including immunofluorescence imaging, qRT-PCR and western blot.

### 1.6.11 Mouse hypothalamic cell line culture

The mouse hypothalamic A-59 neurons (mHypoA-49 neurons, CELLutions) and mouse hypothalamic E-46 neurons (mHypoE-46 neurons, CELLutions) were grown in monolayer in Dulbecco's modified Eagle medium (DMEM) (D5796, Sigma-Aldrich) with 10% foetal bovine serum (FBS) (SFBS-F, Bovogen Biologic.Pty.Ltd) and 1% penicillin/streptomycin. Hypothalamic cells were maintained at 37°C with 5% $CO_2$. In Chapter 2, to detect PTP1B inhibition of lupeol and betulinic acid, Murine TNFα (T7539, Sigma-Aldrich) was applied to induce PTP1B expression in cell, Lupeol and betulinic acid were dissolved in Dimethyl sulfoxide (DMSO), then diluted in sterile water, and mixed with serum free cell culture medium. The DMSO concentration was controlled below 0.5%. The final concentrations of lupeol and betulinic acid in the cell culture medium were 28 μM (5× of the $IC_{50}$ value) and 7.5 μM (5× of the $IC_{50}$ value), respectively. In chapter 3, to expose the role of PCP in hypothalamic cell line, administration of 1 μM PCP (low dosage) or 25 μM PCP (high dosage) (P3209, Sigma-

`

Aldrich) were applied to neurons for 3 and 48 hrs. To investigate the NMDA receptor subunit involved in PTP1B expression, both low dosage (5 µM) and high dosage (50 µM) of NR2A antagonist Peaqx (I2892, Sigma-Aldrich) and NR2B antagonist ifenprodil (P1999, Sigma-Aldrich) were administrated to cell line for 24 and 48 hrs. To reveal the signalling pathway involved in PCP induced leptin signalling dysfunction, 100 nM leptin (450-31-5000, PeproTech) was administrated to cells for 4 hrs after PCP 3 and 48 hrs. Prior to leptin treatment, the cell culture medium was replaced with serum free medium for 4 hrs. To investigate the effect of PTP1B inhibition in hypothalamic cells, 10 µM and 50 µM PTP1B inhibitor Lupeol and 5 µM atypical antipsychotic Olanzapine (O1141, Sigma-Aldrich) were dissolved in Dimethyl sulfoxide (DMSO), then diluted in sterile water, and mixed with serum free cell culture medium. Cells were exposed to 25 µM PCP for 48 hours and replaced with serum free cell culture medium, then lupeol treatment, olanzapine treatment and co-treatment were applied to cells for 24 hrs individually. The DMSO concentration was controlled below 0.5%.

### 1.6.12 Immunofluorescence and image analysis

For immunochemical staining, primary neurons and primary glial cells were washed by PBS and fixed with 4% paraformaldehyde in Dulbecco's PBS for 30 min at room temperature. The samples were further incubated with 100% methanol for 10 min in -20°C, and blocked with 5% donkey serum in phosphate buffered saline teween20 (PBST) for 1 hr at 37 °C. Then, anti-PTP1B antibody (SAB1306060, Sigma-Aldrich), anti-BDNF antibody (SC-20981, Santa-Cruz), anti-SYN antibody (701503, Life Technnology), anti-microtubule-associated protein 2 (MAP2) antibody (M9942, Sigma-Aldrich), anti-NeuN antibody (MAB377, Merck Millipore) and anti-Glial Fibrillary Acidic Protein (GFAP) antibody (G9269, Sigma-Aldrich) were applied overnight at 4°C. PTP1B, SYN, BDNF and GFAP were visualized with isotype-specific donkey anti-

`

rabbit IgG (H+L) secondary antibody conjugated with Alexa Fluor 488. MAP2 and NeuN were visualized by donkey anti-mouse IgG (H+L) secondary antibody conjugated to Alexa Fluor 594. The concentrations of antibodies were applied following manufacturer manuals. A confocal microscope (Leica TCS SP5 Advanced System, Leica Microsystem) was used to obtain images. Software Image J. 10 (http://rsbweb.nih.gov/ij/download.html) with plugin NeuriteQuant (Dehmelt et al., 2011) was applied to quantify the immunoreactivity based on from 5 independent culture wells.

### 1.6.13 Quantitative real-time PCR

Quantitative real-time PCR (qRT-PCR) was performed as previously described (Yu et al., 2013b). Neurons were collected for RNA extraction via Aurum™ Total RNA Mini Kit (7326820, Bio-Rad Laboratories) and reversed to cDNA by using Applied Biosystems™ High Capacity cDNA Reverse Transcription Kit (4368814, Life Technology). Real-time PCR was then performed via SensiFAST™ SYBR No-ROX Kit (BIO-98005, Bioline). The mRNA expression levels of PTP1B (Forward: TGGCCTGACTTTGGAGTCCC; Reverse: CTCCAGTGTGCGTTTGGGTG.), SYN (Forward: GAACAAGTACCGAGAGAACAACAA; Reverse: GGTCAGTGGCCATCTTCACA.), BDNF (Forward: GGGTCACAGCGGCAGATAAA; Reverse: GCCTTTGGATACCGGGACTT.) and TCPTP (Forward: AGAGTGGCCAAGTTTCCAG; Reverse: CACACCATGAGCCAGAAATG.) were normalized to γ-actin (Forward: GCTAACAGAGAGAAGATGACG; Reverse: CAGATGCATACAAGGACAGC), which served as the internal control. Experiments were performed in triplicate.

### 1.6.14 Western blot analysis

`

Detailed protocols were described in our previous study (Yu et al., 2013b), primary cultured hypothalamic neurons, mHypoA-59 cells and mHypoE-46 cells were washed with ice-cold phosphate buffered saline (PBS) and lysed in NP-40 lysis buffer (FNN0021, Invitrogen) containing a protease inhibitor cocktail, beta-glycerophosphate (Sigma-Aldrich) and phenylmethanesulfonyl fluoride (PMSF) (Sigma-Aldrich). Cell lysates were centrifuged at 14,000 rpm for 10 min at 4°C. The supernatants were collected and protein concentrations were determined using the DC$^{TM}$ Protein Assay kit (5000121, Bio-Rad Laboratories) was used according to the manufacturer instructions. Equal amounts of protein (15 $\mu$g) were separated on 4-20% Criterion$^{TM}$ TGX $^{TM}$ Precast Gels (567-1095, Bio-Rad Laboratories) using SDS-PAGE. Following electrophoresis (120 V for 1.5 h), the proteins were transferred to polyvinylidene difluoride membranes (100 V for 1 hr). Membranes were blocked in 5% bovine serum albumin (BSA) or 5% skim milk depending on the primary antibodies used, followed by incubation with the primary antibodies anti-PTP1B (SAB1306060, Sigma-Aldrich), anti-BDNF antibody (SC-20981, Santa-Cruz), pNR2B$^{Tyr1472}$ (4208S, Cell Signaling Technology), NR2B (4207S, Cell Signaling Technology), anti-pAkt$^{Ser473}$ (D9E, Cell Signaling Technology), anti-Akt (SC8312, Cell Signaling Technology), anti-pGSK3β$^{Ser9}$ (5B3, Cell Signaling Technology), GSK3β (D75D3, Cell Signaling Technology), pJAK2$^{Tyr1007/1008}$ (C80C3, Cell Signaling Technology), JAK2 (D2E12, Cell Signaling Technology), pSTAT3$^{Tyr705}$ (D3A7, Cell Signaling Technology), STAT3 (79D7, Cell Signaling Technology) and anti-actin (MAB1501, Merck Millipore) in 1% BSA or 1% skim milk overnight at 4°C. Following washes (3 x 5 min) in Tris Buffered Saline + 0.1% Tween 20, membranes were incubated with respective secondary antibodies for 1 hr at 25°C. Blots were visualized using Amersham$^{TM}$ ECL$^{TM}$ Detection Reagents (RPN2106, Ge Healthcare) and exposed in dark room. The bands corresponding to the proteins of interest were

`

scanned and analysed using the automatic imaging analysis system Quantity One (Bio-Rad Laboratories). All quantitative analyses were normalized to actin.

### 1.6.15 Neuron Neuropeptide Y (NPY) detection

The mouse hypothalamic NPY/GFP neurons (mHypoA-NPY/GFP neurons, CELLutions) were cultured in the 96-well plate in the same incubation condition as mHypoA-59 neurons. 5μM olanzapine, 50μM lupeol and co-treatment of olanzapine and lupeol were applied to neurons. After 6h treatment, discard culture medium and measure neuron NPY-bound GFP immunoactivity using FlexStation 3 (Molecular Devices). Wavelength of detection is set from 488 nm to 510 nm, cut-off at 495 nm.

### 1.6.16 Design and fabrication of inertial microfluidic device

The serpentine channel used in our experiments consists of 15 zigzag periods; the channel has a uniform 42 μm depth, and the length and width of each U-turn are 700 μm. The micro-channel is 200 μm wide. A trifurcating outlet at the end of the channel is implemented at the end of the serpentine channel. Two-sided symmetrical bifurcations are combined into a single outlet to simplify the collection of two-sided streams. The microfluidic device was fabricated by the standard photolithography and soft lithography techniques (Duffy et al., 1998) (provided by collaborator). Prior to these cell experiments, the device was rinsed with phosphate buffered saline (PBS) at 100 μl/min for 10 min using a syringe pump (Legato 100, Kd Scientific), after which the devices were sterilized through exposure to UV light for 30 min.

### 1.6.17 Inertial microfluidic separation of neurons and glia

Primary neurons and glia were prepared based on 1.6.10, Hypothalamic tissues were digested and triturated to suspend cells in 7 ml culture medium. 2 ml cell suspension was assigned as an Inlet group for comparison, while the other 5 ml suspension of

`

hypothalamic cell mixture was infused into the inertial microchip to perform separations under different flow rates (350 µl/min, 550 µl/min, 750 µl/min). Separated cells were collected from the Outlet Middle and Outlet Aside under three typical flow rates respectively. Separation efficacy was applied to determine the optimal flow rate. Cells separated from optimal flow rate were collected for further culture and tests. Purity of separation and enrichment ratio were measured to evaluate separation performance. Separation purity is defined as the ratio of target cells number to the total cells number, while enrichment is determined as the ratio of target cells concentration from the outlet to the target cells concentration from the inlet.

### 1.6.18 Statistical analysis

Data in the present study were analysed using the SPSS 19 statistical package (SPSS, Chicago, IL). T-test and One-way analysis of variance (ANOVA) followed by the *post-hoc* Tukey-Kramer honestly significant difference (HSD) test were carried out based on individual experiments. Data were expressed as mean ± SEM, and $P < 0.05$ was considered statistically significant.

`

## 1.7 Summary

Current challenge in PTP1B drug discovery was mentioned that PTP1B traditional inhibitors hardly inhibit PTP1B with potency, selectivity and lack of bioavailability. PTP1B traditional inhibitors target PTP1B active site, which is highly similar to other members of PTPs in both amino acid sequence and 3D structure. Therefore PTP1B allosteric inhibition was introduced which targets PTP1B unique allosteric site, making PTP1B allosteric inhibition as a promising strategy for drug discovery. Here I proposed lupane triterpenes as PTP1B allosteric inhibitors candidates based on the properties shown in previous literatures. Computational modelling combined with biological assays and cell culture will be applied to confirm lupane triterpenes as PTP1B allosteric inhibitors.

Furthermore, I reviewed the rising evidences which reported that PTP1B impaired neurite outgrowth and synaptogenesis via attenuating BDNF-mediated signalling. All these evidences indicated that PTP1B may have a crucial role modulating impaired neurogenesis in neurological disorders such as schizophrenia and PTP1B inhibition could be an alternative medication treatment. Phencyclidine (PCP)-treated model and neuregulin-1 knock-out model were introduced which have been broadly applied to mimic psychopathology of schizophrenia and testify treatment effects. Both models will be applied to investigate the role of PTP1B contributing to BDNF reduction and attenuation of BDNF-mediated signalling. Moreover, lupane triterpene will be applied to determine that PTP1B inhibition is a potential therapeutic strategy.

At last, the current issue in primary cell culture was discussed which is the difficulty to collect purified and enriched neurons and glia  without chemical reagent and antibody disturbance. In the present study, inertial microfluidic microchip will be introduced to

`

spontaneously separate and collect both neurons and glia. Importantly, interest in glial cell is rising due to increasing evidences revealed the glia dysfunction in several brain disorders including schizophrenia with significant cognitive impairments. Consequently, an effective and efficient platform is required to separate and collect neurons and glia from the same brain section of interest at the same time to establish co-culture system in the future study, Microfluidic-based technology will meet this requirement and broadly applied in the future study.

In conclusion, the present study will firstly apply computational modelling and biological assays to determine lupane triterpenes as novel PTP1B allosteric inhibitors in chapter 2. Then schizophrenia-mimicked models will be used to investigate the role of PTP1B in BDNF reduction and neurogenesis impairment, and determine PTP1B allosteric inhibition by lupane triterpenes is a potential therapeutic strategy in chapter 3. Inertial microfluidic separation to collect purified and functional neurons and glia will be performed and discussed in chapter 4.

`

# Chapter Two

---

Selective binding modes and allosteric inhibitory effects of lupane triterpenes on protein tyrosine phosphatase 1B

Reprinted from Scientific Report, Open-access

Available at: http://www.nature.com/articles/srep20766

Statement from co-authors

This is to attest that the PhD candidate, Tiantian Jin, contributed significantly to the investigation

**JIN, T.**, YU, H. & HUANG, X.-F*. Selective binding modes and allosteric inhibitory effects of lupane triterpenes on protein tyrosine phosphatase 1B. Scientific reports, 6, 20766.

Tiantian Jin designed and performed the experimental work, analysed the data, interpreted results, and wrote the manuscript. Two co-authors are his PhD supervisors, who have provided comments on experimental design, data analysis, results interpretation, and revision of manuscripts.

Tiantian Jin: 29/8/2016

Haibo Yu:

Xu-Feng Huang: 28/8/2016

SCIENTIFIC REPORTS

OPEN

# Selective binding modes and allosteric inhibitory effects of lupane triterpenes on protein tyrosine phosphatase 1B

Received: 01 October 2015
Accepted: 04 January 2016
Published: 11 February 2016

Tiantian Jin[1], Haibo Yu[2] & Xu-Feng Huang[1]

**Protein Tyrosine Phosphatase 1B (PTP1B) has been recognized as a promising therapeutic target for treating obesity, diabetes, and certain cancers for over a decade. Previous drug design has focused on inhibitors targeting the active site of PTP1B. However, this has not been successful because the active site is positively charged and conserved among the protein tyrosine phosphatases. Therefore, it is important to develop PTP1B inhibitors with alternative inhibitory strategies. Using computational studies including molecular docking, molecular dynamics simulations, and binding free energy calculations, we found that lupane triterpenes selectively inhibited PTP1B by targeting its more hydrophobic and less conserved allosteric site. These findings were verified using two enzymatic assays. Furthermore, the cell culture studies showed that lupeol and betulinic acid inhibited the PTP1B activity stimulated by TNFα in neurons. Our study indicates that lupane triterpenes are selective PTP1B allosteric inhibitors with significant potential for treating those diseases with elevated PTP1B activity.**

Protein Tyrosine Phosphatase 1B (PTP1B) is an intracellular protein which is widely expressed in the body including the brain, liver, muscles, and adipose tissue, and which is up-regulated in obesity, type 2 diabetes and breast cancer[1–3]. Obesity is a major health problem leading to various life-threatening diseases such as diabetes, cardiovascular disease and certain cancers[4]. An elevated PTP1B level contributes to the development of obesity and its related metabolic disorders[5,6]. Considerable efforts have been made towards new anti-obesity drug developments. PTP1B has been considered as a therapeutic target for treating obesity. Previous studies have shown that inhibiting neuronal PTP1B in obese mice reduces fat deposition, improves energy expenditure and prevents weight gain[7,8].

However, there are some outstanding challenges in PTP1B-based small-molecule therapeutics. First, it is difficult to achieve inhibition selectivity against PTP1B by targeting the active site. PTP1B is a member of the Protein Tyrosine Phosphatase (PTP) family, which contains more than 100 members. Most PTPs have a consensus active loop signature $(H/V)C(X)_5R(S/T)$, where the cysteine (C) is a conserved active site that is essential for enzyme catalysis[9]. Of particular interest, PTP1B shares a 74% identical sequence in its catalytic domain with T-cell protein tyrosine phosphatase (TCPTP)[10] and they have almost superimposable active sites. TCPTP has different biological functions and signalling pathways from PTP1B as demonstrated in mouse models[11]. Studies have shown the regulatory functions of TCPTP on the immune system[12]. Homozygous TCPTP-deficient mice died at 3–5 weeks of age due to the haematopoietic defect caused by immune system damage[11]. Therefore, an effective PTP1B inhibitor needs to have sufficient selectivity for PTP1B over TCPTP. Second, inhibitors targeting the intracellular target PTP1B need to have satisfactory cellular penetration. Current PTP1B inhibitors are designed to bind to the PTP1B active site, the phosphotyrosine (pTyr)-binding pocket, serving as competitive inhibitors to reduce PTP1B activity[13]. These PTP1B inhibitors mimic pTyr and are negatively charged at a physiological pH. Consequently, it is difficult for most PTP1B inhibitors to penetrate the cell membrane[14].

Due to the challenges of the active site targeted inhibitors mentioned above, an alternative drug design strategy has been proposed to develop inhibitors targeting the PTP1B allosteric site instead[13]. Recent X-ray

[1]Centre for Translational Neuroscience, School of Medicine, University of Wollongong, and Illawarra Health and Medical Research Institute (IHMRI), Wollongong, NSW 2522, Australia. [2]School of Chemistry, University of Wollongong, Wollongong, NSW 2522, Australia. Correspondence and requests for materials should be addressed to X.F.H. (email: xhuang@uow.edu.au) or H.Y. (email: hyu@uow.edu.au)

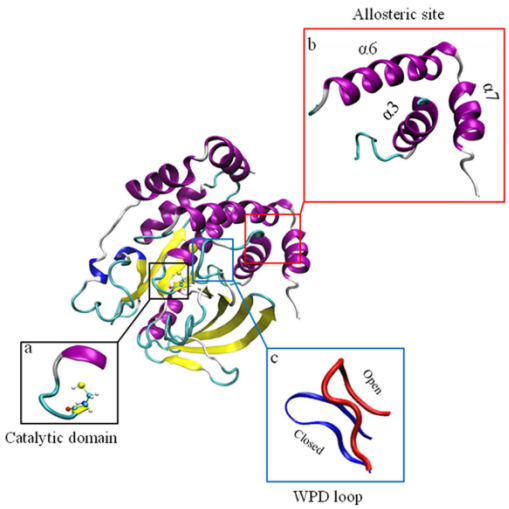


**Figure 1. The crystallography structure of PTP1B.** PTP1B has an active site Cysteine 215 with surrounding catalytic loop (**a**) and a previous identified allosteric site (**b**) which is surrounded by α3 helix, α6 helix and α7 helix. During PTP1B activation, WPD loop (**c**) moves from the open position to the closed position.

crystallographic studies have revealed an allosteric transition in PTP1B accompanying its catalysis, which is situated about 20 Å away from the catalytic domain including active site Cys215 and catalytic loop consisting His214, Ser216, Ala217, Gly218, Ile219, Gly220 and Arg221[15,16] (Fig. 1a,b). The catalytic WPD loop (Trp179, Pro180, and Asp181) and neighbouring residues can exist in two distinct conformations: "open" and "closed"[17] (Fig. 1c). In the open state, the WPD loop stands beside the active site to form an open binding site, which is accessible for substrates. In contrast, in the closed state, the WPD loop closes over the binding site, forming a catalytically competent state. Thus an allosteric inhibitor can be designed to prevent the movement of the WPD loop and maintain the WPD loop in an open (inactive state)[16]. Unlike the active site of PTP1B, the allosteric site is not well conserved among PTPs and is substantially less polar[15]. Thus targeting the allosteric site might offer a promising approach to developing PTP1B inhibitors with both improved selectivity and bioavailability. The high-resolution X-ray structures of PTP1B, in complex with three allosteric inhibitors, including compound 2 and compound 3 (Fig. 2), show that these inhibitors target the allosteric site formed by α3, α6 and α7[16]. Encouragingly, these allosteric inhibitors show high potency in inhibiting PTP1B with selectivity over other PTPs[16]. Considering the limited selective PTP1B inhibitors on trial[18], allosteric inhibition becomes a promising strategy to discover selective PTP1B inhibitors[19,20].

Recently, the lupane triterpenes, lupeol, lupenone, betulin and betulinic acid (Fig. 2), have been shown to be potent PTP1B inhibitors *in vitro*[21–23]. Na *et al.* showed that lupeol can inhibit PTP1B with a high potency ($IC_{50} = 5.6\mu M$), and acts as a non-competitive inhibitor of PTP1B[21]. Therefore lupeol might target a binding site other than the active site of PTP1B. We propose the lupane triterpenes as potential PTP1B allosteric inhibitors and aim to reveal their molecular inhibitory mechanisms. First, we performed molecular docking, molecular dynamics simulations and binding affinity calculations to predict the allosteric binding site targeted by lupane triterpenes and characterise the key interactions and residues involved in the binding. Second, we used enzymatic assays to determine the inhibition selectivity of lupane triterpenes against PTP1B over TCPTP. We carried out kinetic assays to confirm their allosteric binding modes. Finally, we examined the cellular activities of selected lupane triterpenes for their ability to inhibit PTP1B activity in hypothalamic neurons. This combination of molecular modelling, enzymatic assays and cell culture studies has established lupane triterpenes as potent and selective PTP1B inhibitors with significant potential for treating diseases with elevated PTP1B activity.

## Methods

**Homology modelling of PTP1B.** The PTP1B crystal structure (PDB id: 1T49) used in this study was the open, inactive conformation containing 282 amino acids, in which the α7 was not resolved (labelled as PTP1B282). Considering that there was no crystal structure of PTP1B with α7 available in the inactive state, and also the important role of α7 in allosteric inhibition, homology modelling with Modeller 9v8 was carried out to construct the missing helix based on the active conformation of PTP1B (PDB id: 1PTY) (labelled as PTP1B299)[24]. 100 models were generated and the best model based on the DOPE energy was chosen and subjected to equilibrium molecular dynamics simulations (40 ns) to equilibrate and optimise the modelled structure (see Molecular dynamics simulations).

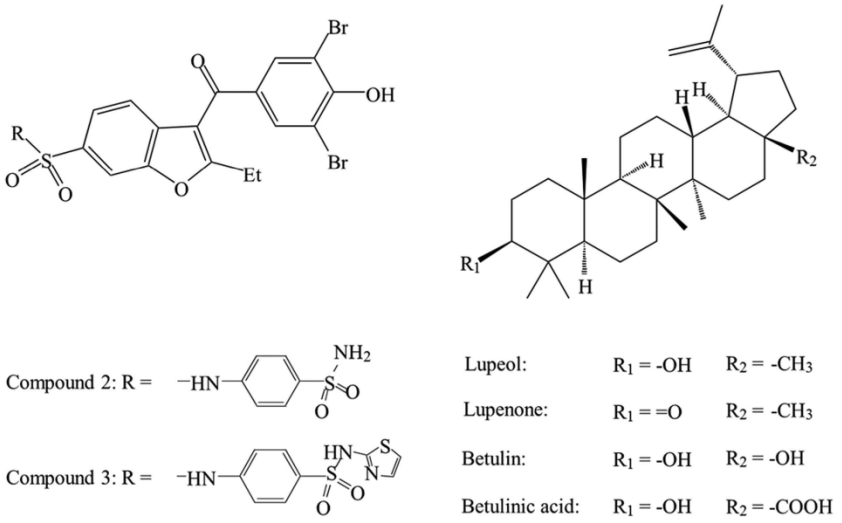


**Figure 2. The formula of allosteric ligands used.** Compounds 2 and 3 have been reported to be allosteric inhibitors by Wiesmann *et al.*[16]. Four members of the lupane triterpenes are selected for this work.

**Molecular docking.** Docking simulations were carried out with Autodock Vina (version 1.1.2)[25]. The docking protocol was established by re-docking compound 2 to PTP1B282 as in the co-crystal structure[16]. The protonation states of the titratable groups in PTP1B were assigned at pH 7.0 by PROPKA3.1[26]. Docking was performed sequentially in two steps. Initially, a box large enough to cover the whole protein (75 Å × 60 Å × 60 Å) was used to detect potential binding pockets. Then, the second step involved localised docking with a smaller box (22.5 Å × 22.5 Å × 22.5 Å) centred at the potential binding site of interest (e.g. the active site, the allosteric site, or other site of interest identified from the blind docking procedure). In each focused docking study of lupane triterpenes targeting PTP1B282 or PTP1B299, 20 conformations of the complexes with the lowest binding affinities were listed for further analysis and the best binding mode was selected to be the initial structure for the molecular dynamics simulations. Multiple dockings, based on different snapshots sampled from equilibrium molecular dynamics simulations (PTP1B282 and PTP1B299), were performed. Qualitatively, the identified populated binding poses are similar.

**Molecular dynamics simulations.** Molecular dynamics simulations were performed to study the stability and flexibility of the PTP1B-lupane triterpenes complexes. 9 different systems were set up (Table S1). All of the systems were solvated in a box of TIP3P water molecules, which extended about 12 Å from the surface of the protein, and the systems were neutralised with counter ions of $Na^+$. The salt (NaCl) concentration was set to 0.15 mol/L. Simulations were carried out using NAMD 2.9[27]. The protein and the ligands were represented with the non-polarisable CHARMM PARAM27 force field[28] and the GAFF force field[29], respectively. All of the systems were simulated in periodic boundary conditions using the Langevin algorithm to maintain the temperature at 298.15 K, and the Langevin Piston Nose-Hoover method to keep the pressure constant at 1.0 bar. The electrostatic interactions were calculated using the Particle Mesh Ewald (PME) method[30]. The van der Waal forces were treated with a cut-off of 12 Å. All of the covalent bonds involving hydrogen were kept rigid using the Rattle algorithm and time step set to 1.0 fs. In the equilibrium simulations of the homology modelling of PTP1B, a harmonic restraint on the backbone atoms except $\alpha 7$ was applied with a decreasing force constant from 64.0 to 1.0 kcal/mol/Å$^2$ over 10 ns. The simulations were continued for 30 ns without any restraints. For the molecular dynamics simulations of the docked complexes, a harmonic restraint on the backbone atoms was applied with a decreasing force constant from 32.0 to 1.0 kcal/mol/Å$^2$ over 3 ns followed by 20 or 100 ns equilibrium simulations (Table S1).

**Binding free energy calculation.** Free energy perturbation distributed replica-exchange molecular dynamics (FEP/$\lambda$-REMD) was applied to calculate binding free energy[31,32]. The motivation to carry out computationally intensive absolute binding free energies is because the binding modes for lupeol and betulinic acid predicted by docking and subsequently molecular dynamics simulations are rather different. This could be difficult for relative binding free energy calculations, which assume that their available conformational spaces are significantly overlapped[33]. To be consistent with previous literature, we call the free energy difference between the unbound ligand in the aqueous solution and the bound ligand in the binding pocket of the target protein as the absolute binding free energies. The total free energy was decomposed into four terms, namely repulsive and dispersive components of the Lennard-Jones potential according to the Weeks-Chandler-Anderson scheme, the

electrostatic contribution, and the restraining potential. The ligand was decoupled from the environment in four steps via four thermodynamic coupling parameters (λ). No corrections have been applied to the potential electrostatic finite-size artefacts[34,35]. In order to speed up the convergence, each λ-staging FEP window was treated as a replica and the λ-exchange occurred along the entire alchemical reaction path. This approach has been successfully used to study the interactions between glycoside hydrolases and polysaccharides[36]. Generally, for both PTP1B-lupeol and the PTP1B-betulinic acid complex, the FEP/λ-REMD simulations started from a 100 ns equilibrated snapshot. A set of 64 replicas (36 repulsive, 12 dispersive, and 16 electrostatic) was applied in the simulations with an exchange frequency of one every 1,000 steps (1 ps). For each replica, a total of 1.0 ns simulations were carried out in which the last 0.8 ns simulations were averaged to determine the ligand binding free energies. The protein-ligand complexes included a positional translational restraint with a force constant of 10.0 kcal/mol/Å$^2$. The error analyses were estimated using four sequential simulations of 0.2 ns each.

**Analysis.** Trajectory snapshots were saved every picosecond (i.e. every 1,000 steps) and analysed using either the the molecular visualisation program VMD 1.9[37] or CHARMM[38].

**Inhibiting TCPTP by *p*NPP phosphatase assay.** The inhibition of TCPTP was determined by using the EnzoLyte Colorimetric *p*NPP Protein Phosphatase Assay kit (Anaspec, San Jose, CA). The recombinant human TCPTP protein (ab42575) was purchased from Abcam Inc (Cambridge, MA). Lupeol, betulin, and betulinic acid were purchased from Sigma-Aldrich (Castle Hill, NSW). Lupenone was purchased from Faces Biochemical Co Ltd (Wuhan, P R China). Briefly, TCPTP was incubated in different concentrations of compounds for 10 min in assay buffer at 25 °C, and then the reaction was initiated by adding the *p*NPP reagent and stopped by NaOH after 30 min at 25 °C. All readings were calibrated on the negative control wells without enzymes. The TCPTP inhibition potency of the lupane triterpenes was determined by $IC_{50}$, calculated using the GraphPad Prism 5 program (GraphPad Software Inc, La Jolla, CA). In addition, both the inhibition of TCPTP and PTP1B (ab42572, Abcam Inc, Cambridge, MA) were performed with the control drug compound 3 (Merck, Frenchs Forest, NSW), a reported allosteric PTP1B inhibitor. The PTP1B assay process was the same as the TCPTP assay mentioned above.

**PTP1B inhibition kinetics assay.** The PTP1B-catalysed hydrolyses in the presence of betulin and betulinic acid were assayed at 25 °C, and the *p*NPP Protein Phosphatase Assay kit is described above. The reaction mixture consisted of six different concentrations of *p*NPP (1.0, 2.0, 4.0, 8.0, 16.0, and 20.0 mM) and was used as a PTP1B substrate with different concentrations of lupeol, betulin, and betulinic acid. The Lupeol group was used as a control group. The absorbance at 405 nm was detected by a spectraMAX 384 microplate spectrophotometer twice every minute for a total of 15 min. Michaelis-Menten constant ($K_m$) and maximum velocity ($V_{max}$) of PTP1B were determined via Lineweaver-Burk plots using the GraphPad Prism 5 program (GraphPad Software Inc, La Jolla, CA).

**Cell culture and reagents.** Mouse hypothalamic cell line (mHypoE-46) neurons were grown in monolayer in Dulbecco's modified Eagle medium (DMEM) (Sigma D5796, Castle Hill, NSW) with 10% fetal bovine serum (FBS) (SAFC Biosciences Inc, Lenexa, KS) and 1% penicillin/streptomycin. They were maintained at 37 °C with 5% $CO_2$. Prior to treatment, the cell culture medium was replaced with DMEM containing 1% penicillin/streptomycin for 4 h. Murine TNFα was obtained from Sigma-Aldrich (Castle Hill, NSW). Lupeol and betulinic acid were dissolved in Dimethyl sulfoxide (DMSO), then diluted in sterile water, and mixed with serum free cell culture medium. The DMSO concentration was controlled below 0.15%. The final concentrations of lupeol and betulinic acid in the cell culture medium were 28 μM (5× of the $IC_{50}$ value) and 7.5 μM (5× of the $IC_{50}$ value), respectively.

**Western blot analysis.** The method was described in our previous study with modifications[39], mHypoE-46 neurons were washed with ice-cold PBS and lysed in NP-40 lysis buffer (Invitrogen Australia Pty Ltd, Mulgrave, VIC) containing a protease inhibitor cocktail, beta-glycerophosphate and phenylmethanesulfonyl fluoride (PMSF) (Sigma, Castle Hill, NSW). Cell lysates were centrifuged at 14000 rpm for 10 min at 4 °C. The supernatants were collected and protein concentrations were determined using the DC assay (Bio-Rad Laboratories, Gladesville, NSW) according to the manufacturer's instructions. Equal amounts of protein (10 μg) were separated on 4–12% Bis-Tris gels (Bio-Rad Laboratories, Gladesville, NSW,) using SDS-PAGE. Following electrophoresis (120 V for 2 h), the proteins were transferred to polyvinylidene difluoride membranes (100 V for 1 h). Membranes were blocked in 5% bovine serum albumin (BSA), followed by incubation with the primary antibodies PTP1B (sc-1718, 1:500, Santa Cruz Biotechnology Inc, Dallas, TX) in 1% BSA overnight at 4 °C. Following washes (3 × 5 min) in Tris Buffered Saline + 0.1% Tween 20 (TBST), membranes were incubated with horseradish peroxidase conjugated secondary antibodies for 1 h at 25 °C. Blots were visualised using enhanced chemiluminescence (ECL) detection reagents (Ge Healthcare, Rydalmere, NSW). The bands corresponding to the proteins of interest were scanned and densitometrically analysed using the automatic imaging analysis system Quantity One (Bio-Rad Laboratories, Gladesville, NSW). All quantitative analyses were normalised to β-actin.

**Immunoprecipitation assay of PTP1B.** Based on the instructions of the Pierce Classic IP Kit (#26146, Thermo Fisher Scientific Inc, IL) with minor modifications[40], PTP1B was immunoprecipitated using the 25 μg PTP1B antibody (sc-1718, Santa Cruz Biotechnology Inc, Dallas, TX) for 12 h at 4 °C. Immune complexes were isolated by adding the protein G-agarose, washed three times in the phosphatase assay buffer from the EnzoLyte Colorimetric *p*NPP Protein Phosphatase Assay kit (Anaspec, San Jose, CA), and resuspended in the same buffer. Samples were analysed for the phosphatase activity using the same *p*NPP assay kit mentioned above.

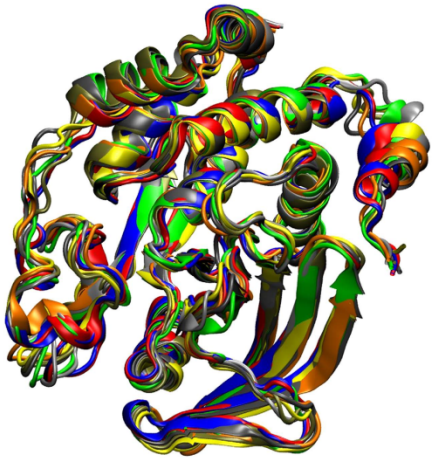

**Figure 3. Equilibrated structures of the homology model for PTP1B299.** The snapshots sampled from the molecular dynamics simulations at 10 ns (red), 15 ns (grey), 20 ns (orange), 25 ns (yellow), 30 ns (tan), 35 ns (silver), and 40 ns (green), are superimposed with the homology model using Modeller (blue).

**Statistical analysis.** Data from the western blot analysis and immunoprecipitation assays were analyzed using the SPSS 19 statistical package (SPSS, Chicago, IL). One-way analysis of variance (ANOVA) was applied followed by the *post-hoc* Tukey-Kramer honestly significant difference (HSD) test.

## Results

**Lupeol binds to PTP1B in the allosteric site.** The homology model of PTP1B in the inactive state with compound 2 (PTP1B299 w/Compound 2, see Fig. 2) was simulated for 50 ns: the first 10 ns with a harmonic restraint on the backbone atoms of the resolved crystal structure while optimising the modelled α7; and the remaining 40 ns being free molecular dynamics simulations. The snapshots sampled during the simulations are shown in Fig. 3. In general, the tertiary structures were stable for over 40 ns with the modelled α7 having greater flexibility. As expected for the relative short timescale of the free molecular dynamics simulations, no closure of the active site was observed and PTP1B remained in the inactive state.

One of the remaining problems of allosteric inhibition is to characterise the binding modes of these inhibitors and identify the key residues involved in the binding. In particular, the truncated form of PTP1B without α7 is four times less active, indicating the importance of α7 in PTP1B inhibition[16]. In addition, X-ray structures have revealed that in the presence of an allosteric inhibitor, α7 is disordered and thus the molecular details of α7 in allosteric inhibition remain unclear[16]. To determine the role of α7, molecular docking studies (blind and focused docking) were performed for PTP1B in the presence of α7 (PTP1B299) or absence of α7 (PTP1B282). These docking studies revealed similar binding modes for lupeol with the interactions for PTP1B299 being stronger. The following discussions focus mainly on PTP1B299 and note the differences between PTP1B282 and PTP1B299.

**α7 is involved in forming the allosteric binding site in PTP1B299.** The blind docking studies revealed that lupeol preferentially binds to the identified allosteric site[16] (Table S2 and Figure S1a). Subsequently, we obtained a more accurate picture of the binding modes from the focused docking at the allosteric site (Figure S1b). The molecular dynamics simulations of the docked complex showed a stable trajectory with the backbone positional root-mean-square deviations (RMSDs) of the PTP1B backbone atoms being 1.0 – 1.5 Å. Throughout the simulation, the WPD loop remained open, indicating that PTP1B was inactive and the timescale for the opening/closure of the WPD loop was beyond the current simulation timescale[41]. Considering that the structure of lupeol is mainly hydrophobic with only one polar hydroxyl group, it appears that hydrophobic interactions play a critical role in binding (Fig. 4).

*α7 helix strengthens the hydrophobic interactions between lupeol and PTP1B.* The presence of α7 creates a hydrophobic "tunnel", which surrounds lupeol and provides stronger hydrophobic interactions (Fig. 4c). This results in a tighter binding mode with the largest affinity of −10.3 kcal/mol (Table S3), compared to −7.7 kcal/mol (Table S4) in the PTP1B282 allosteric site. The hydrophobic tunnel comprised 6 non-polar amino acids located within 5 Å around lupeol including Ala189, Leu192, Phe196, Phe280, Trp291 and Leu294 (Fig. 4c, Table S5), which was significantly larger than the hydrophobic area formed by the two hydrophobic residues in PTP1B282 w/Lupeol (Phe196 and Phe280, Fig. 4d). We compared the solvent accessible surface areas (SASA) for PTP1B binding with lupeol (Table 1). Generally, reducing SASA increased the hydrophobic interactions. All of these six non-polar residues decreased SASAs in PTP1B299 w/Lupeol, indicating that a non-polar interaction was established between

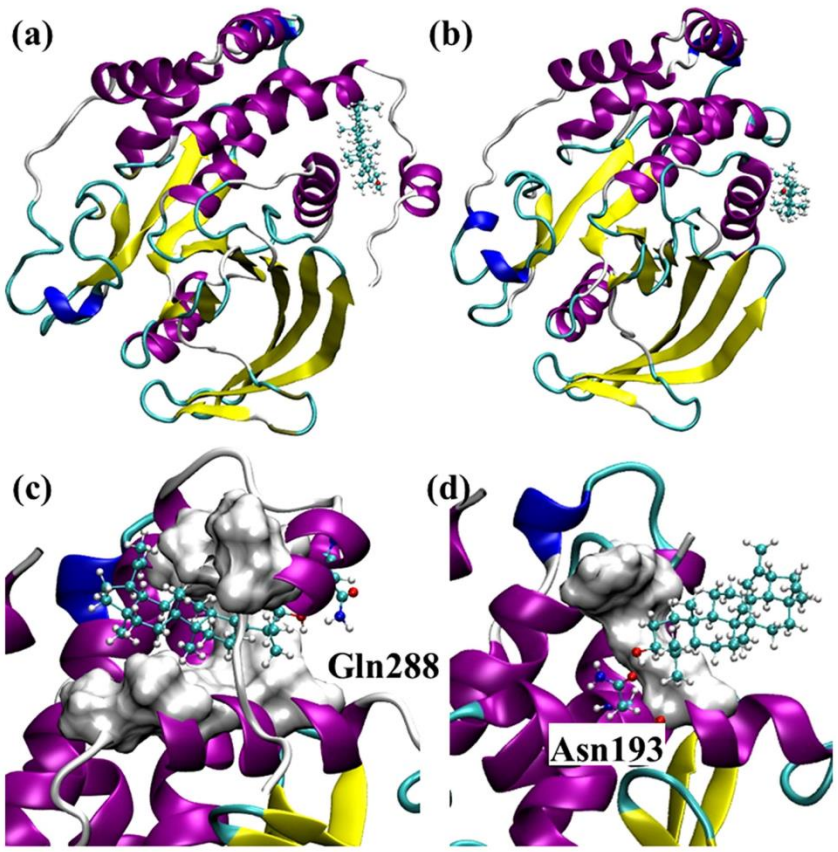


**Figure 4.** The top-ranked binding poses of lupeol to the allosteric site of PTP1B299 (**a**) and PTP1B282 (**b**). Detailed interactions revealed by the molecular dynamics simulations for lupeol and PTP1B are shown in (**c**) and (**d**). The hydrophobic residues involved in the binding in PTP1B299 (Ala189, Leu192, Phe196, Phe280, Trp291, and Leu294) are shown in Surf. The polar residue involved in the hydrogen bonding Gln288 is shown in CPK (**c**). The hydrophobic residues involved in the binding in PTP1B282 (Phe196 and Phe280) are shown in Surf while the polar residue involved in the hydrogen bonding in Asn193 is shown in CPK (**d**).

| | Ala189 | Leu192 | Phe196 | Phe280 | Trp291 | Leu294 |
|---|---|---|---|---|---|---|
| PTP1B299 | 47.6 | 29.1 | 90.7 | 83.4 | 109.3 | 138.0 |
| PTP1B299 w/Lupeol | 7.9 | 0.3 | 25.9 | 64.2 | 5.5 | 105.1 |
| PTP1B282 w/Lupeol | 50.4 | 14.9 | 50.7 | 107.4 | | |

**Table 1. Changes in solvent accessible surface area (SASA) values upon lupane triterpenes to PTP1B.** The values are the non-polar residues in the PTP1B299, PTP1B299 w/Lupeol complex, and PTP1B282 w/Lupeol complex over the trajectories of equilibrated simulations (in $Å^2$).

lupeol and these hydrophobic residues (Table 1). In particular, Leu192, Phe196 and Trp291 had respective 100-fold, 4-fold and 20-fold decreases in SASAs when they interacted with lupeol. These residues contributed significantly to the additional hydrophobic interactions. More importantly, individual mutations of Leu192Ala and Phe196Ala have been reported to significantly reduce the inhibitory effect of an allosteric inhibitor targeting the same binding pocket , indicating the prominent role of these residues in allosteric inhibition[42]. On the other hand, the SASAs of hydrophobic residues in PTP1B299 w/Lupeol were significantly lower than in PTP1B282 w/Lupeol (Table 1). This indicates that the existence of $\alpha 7$ led to a larger hydrophobic area to wrap around lupeol. In addition, we compared root-mean-square fluctuations (RMSFs) for C$\alpha$ atoms in PTP1B before and after lupeol

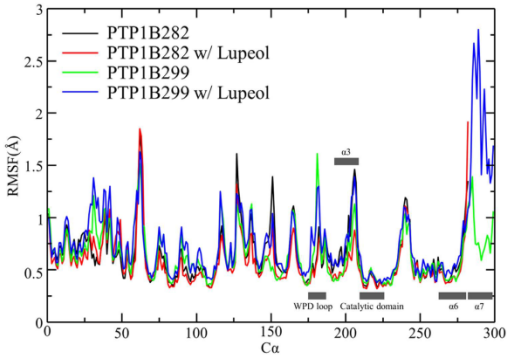


**Figure 5. Root-mean-square fluctuations (RMSF) per residue in the equilibrium molecular dynamics simulations of PTP1B282, PTP1B282 w/Lupeol, PTP1B299, and PTP1B299 w/Lupeol.** The key secondary structure elements including catalytic domain, WPD loop and allosteric site composed by α3, α6 and α7, have been labelled along X-axis.

binding. Lupeol binding increased the fluctuations of α7 (Fig. 5), which may lead to the disorder of α7. Such order to disorder transition upon binding has been proposed to play an important role in allosteric inhibition[16].

*Orientation of lupeol in the binding site changes due to the presence of α7.* Notably, although lupeol binds to the same site with or without α7, its orientation changes (Fig. 4a,b). This change is likely due to the presence of α7, which changed the preferred hydrogen bonding formation at the binding site. In PTP1B299 w/Lupeol, the residue Gln288 in α7 formed a hydrogen bond with the hydroxyl group in lupeol (Fig. 4c). However, in PTP1B282 w/ Lupeol, Asn193 formed a hydrogen bond with lupeol (Fig. 4d). Nevertheless, docking simulations suggest that both hydrophobic and hydrogen bonding interactions contributed to lupeol binding.

**Lupane triterpenes are allosteric inhibitors for PTP1B.** Lupane triterpenes share the same skeleton structure with minor differences in their polar functional groups (Fig. 2). The key functional group of lupane triterpenes is a pentacyclic triterpene displaying a non-polar characteristic, which interacts with non-polar residues in the allosteric site of PTP1B299. It is likely that the specific polar functional group of each lupane triterpene determines the diversity of the binding modes and leads to different binding affinities targeting PTP1B. In addition to lupeol, we also subjected lupenone, betulin, and betulinic acid to molecular docking (Figures S2, S3 and S4, Tables S2 and S3). To further elucidate the difference of binding modes within the lupane family, molecular dynamic simulations were performed on these compounds (Table S1) and the top-ranked docked complexes were confirmed to be stable over the duration of 100 ns (Figures S5 and 6).

*PTP1B299w/Lupeol.* α7 enhanced the hydrophobic interactions, and created a strong hydrogen bond with lupeol (Fig. 4c). The different rotamers of Gln288 in α7 formed different hydrogen bonding patterns with lupeol, with Gln288 acting as either a hydrogen bonding donor or acceptor to strengthen the interactions with lupeol. The estimated occupancy was 73% between lupeol and Gln288 during the 100 ns simulations (Fig. 7).

*PTP1B299 w/Lupenone.* The polar functional group in lupenone was a carbonyl group that formed one hydrogen bond with Lys197 in the docked complex (Fig. 6d). There was a relatively low occupancy of 33% in the molecular dynamics simulations (Fig. 7). In contrast, the hydrophobic interactions formed with the non-polar residues Ala189, Leu192, Phe196, Phe280, Trp291, and Leu294 were maintained throughout the simulations (Fig. 6d, Table S5).

*PTP1B299 w/Betulin.* Betulin had two hydroxyl groups that formed multiple hydrogen bonds in the docking studies (Fig. 6e). The molecular dynamics simulations revealed the formation of three populated hydrogen bonds between betulin and Asn193, Glu276, and Gln288. The occupancies for these hydrogen bonds were 41%, 29% and 22%, respectively (Fig. 7) with considerable fluctuations in the 100 ns simulations. The hydrophobic interactions were stable and the residues involved in the binding included Ala189, Leu192, Phe196, Phe280, Trp291, and Leu294 (Fig. 6e, Table S5).

*PTP1B299 w/Betulinic acid.* Betulinic acid contained two polar functional groups that formed three stable hydrogen bonds (Fig. 6f). The carboxyl group was close to Glu276 to form one hydrogen bond with an occupancy of 37%. Additionally, betulinic acid contained a hydroxyl group, which formed another two hydrogen bonds with Gln288 (occupancy of 58%) and Lys292 (occupancy of 37%) in the 100 ns simulations (Fig. 7). Of the four lupane triterpenes, betulinic acid formed the strongest polar interactions with PTP1B. Like the other lupane triterpenes, the strong hydrophobic interactions involved in binding were with Ala189, Leu192, Phe196, Phe280, Trp291, and Leu294 (Fig. 6f, Table S5).

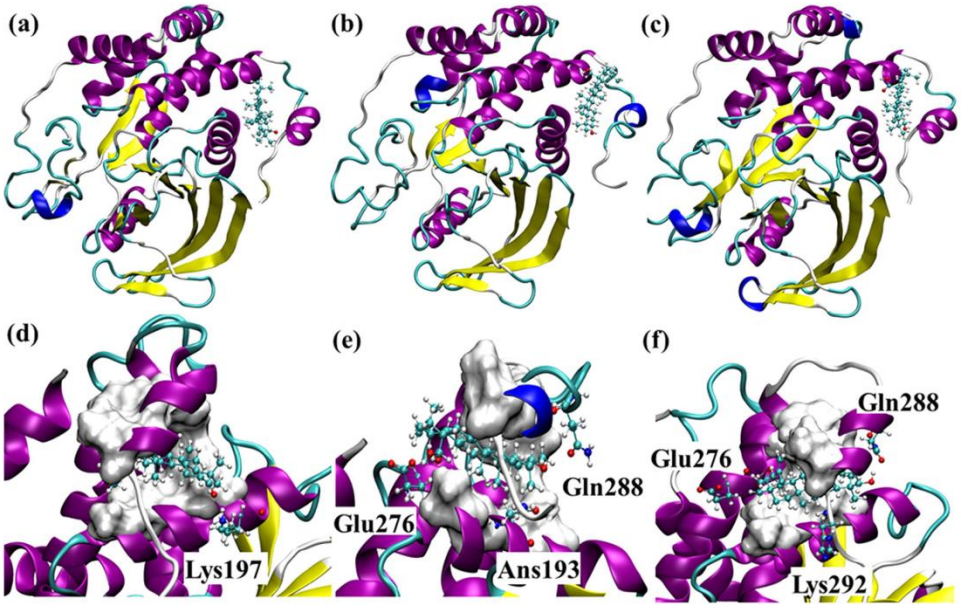


**Figure 6.** The top-ranked binding poses of lupenone (**a**), betulin (**b**), and betulinic acid (**c**) to the allosteric site of PTP1B299. The detailed interactions revealed by the molecular dynamics simulations between the ligands and PTP1B are shown in (**d–f**), respectively. The non-polar residues involved in the hydrophobic interactions with the ligands are shown in Surf. The polar residues involved in hydrogen bonding are shown in CPK.

**Binding affinities of Lupeol and Betulinic acid to PTP1B299.** The absolute binding free energies of lupeol and betulinic acid to PTP1B299 were calculated by FEP/λ-REMD. Table 2 lists the binding free energies of the two ligands examined here together with the repulsive, dispersive, electrostatic, and restrained components. The free energy of solvation is also provided. Betulinic acid had a more favourable binding than lupeol (−10.6 kcal/mol vs −12.2 kcal/mol, respectively). These binding affinities are comparable with those provided by the scoring function in AutoDock Vina (Table S3). The relative binding free energy difference of −1.6 kcal/mol compares favourably from the experimentally derived number based on $IC_{50}$ values. Experimentally, $IC_{50}$ is not a direct indicator of binding affinities for non-competitive inhibitors, which however could be converted to each other. According to the algorithm proposed by Cer *et al.*[43]. We estimated the constant of inhibition $k_i$ for lupeol and betulinic acid and then calculated the binding free energies of lupeol and betulinic acid (−7.5 kcal/mol vs −8.3 kcal/mol, respectively, Table S6). The current calculations overestimate the absolute binding free energies by 3.1 kcal/mol and 3.9 kcal/mol for lupeol and betulinic acid, respectively. However, the relative binding affinity of −0.8 kcal/mol was reproduced by binding free energy calculations reasonably well (−1.6 kcal/mol). Such calculations provide confidence that in the future, relative binding free energy calculations will be applied to help the optimisation of the lead compounds with similar binding modes.

We further examined the component contributions to the binding affinities. As expected, for both ligands, the van der Waals interactions made the dominant contributions, because the allosteric site was characterised of the hydrophobic interactions with the hydrophobic skeleton of lupane triterpenes. The difference of van der Waals components between lupeol and betulinic acid to PTP1B299 was −0.6 kcal/mol (Table 2, −11.7 kcal/mol vs −12.3 kcal/mol). However, it is worth noting that betulinic acid had a slightly favourable contribution from the electrostatic interactions compared to lupeol (Table 2). The difference of electrostatic interactions in lupeol and betulinic acid was about −1.0 kcal/mol (Table 2, 0.9 kcal/mol vs −0.1 kcal/mol). Such component analyses might provide useful information in future ligands optimisation process. For instance, the binding affinities might be enhanced by increasing the hydrophilicities of the groups at $R_1$ and $R_2$ (Fig. 2), or the compounds solubility be improved by strengthening hydrogen binding interactions by such groups. However, it is worth mentioning that one has to be cautious as such free energy components are not a state function and component analyses are pathway dependent[44]. Thus when using this information to *in silico* design new inhibitors, the (relative) binding free energy will be verified with rigorous free energy calculations.

**Lupane triterpenes selectively inhibit PTP1B activity over TCPTP.** Allosteric inhibitors are selectively characterised by the inhibition effect. We have confirmed that lupane triterpenes are PTP1B allosteric inhibitors using molecular docking and dynamics simulations. We have systematically testified the inhibitory

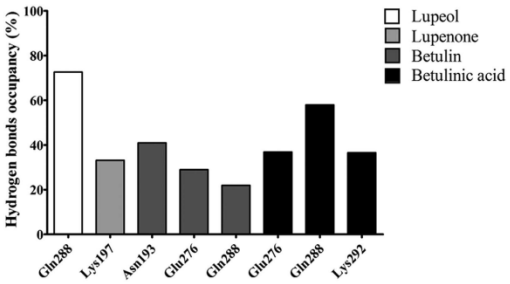


**Figure 7. The occupancy of the hydrogen bond in the 100 ns simulations of PTP1B299 w/Lupeol, PTP1B299 w/Lupenone, PTP1B299 w/Betulin, and PTP1B299 w/Betulinic acid.** A hydrogen bond is assumed to exist if the donor-acceptor distance is smaller than 3.5 Å and the donor-hydrogen-acceptor is larger than 135°. Both lupeol and lupenone perform only one hydrogen bond with PTP1B but the occupancy in lupeol is much higher than lupenone. Both betulin and betulinic acid generate multiple hydrogen bonds with PTP1B.

| | $\Delta G_b^o$ | $\Delta G_{total}$ | $\Delta G_{rep}$ | $\Delta G_{disp}$ | $\Delta G_{elec}$ | $\Delta G_{rstr}$ |
|---|---|---|---|---|---|---|
| Lupeol[a] | | $-3.8 \pm 0.4$ | $43.7 \pm 0.4$ | $-42.1 \pm 0.2$ | $-5.4 \pm 0.1$ | |
| Betulinic acid[a] | | $-9.2 \pm 0.4$ | $44.5 \pm 0.3$ | $-43.3 \pm 0.2$ | $-10.4 \pm 0.3$ | |
| Lupeol−PTP1B299[b] | $-10.6 \pm 0.6$ | $-14.4 \pm 0.6$ | $54.9 \pm 0.5$ | $-65.0 \pm 0.2$ | $-4.5 \pm 0.2$ | 0.2 |
| Betulinic acid-PTP1B299[b] | $-12.2 \pm 0.7$ | $-21.4 \pm 0.7$ | $56.0 \pm 0.6$ | $-67.1 \pm 0.2$ | $-10.5 \pm 0.2$ | 0.2 |

**Table 2. Absolute binding free energies of lupeol and betulinic acid to PTP1B.** The repulsive ($\Delta G_{rep}$), dispersive ($\Delta G_{disp}$), electrostatic ($\Delta G_{elec}$) and restraining ($\Delta G_{rstr}$) contributions sum up to the total in the FEP/λ-REMD simulations[31,32]. The error is estimated on the four sequential simulations with each of 0.2 ns for each replica. There are two separate free energy calculations, where in (a) a solvated ligand is decoupled from the aqueous solution to vacuo, and in (b) a bound ligand is decoupled from the enzyme in solution. The difference between values of (a) and (b) is the absolute binding free energy for a ligand to PTP1B ($\Delta G_b^o$).

effects of lupane triterpenes on PTP1B and TCPTP and demonstrated that lupane triterpenes specifically target PTP1B. First we applied the control drug compound 3 (Fig. 2) to both the PTP1B and TCPTP enzymes to confirm the reliability of the enzymatic assay. The $IC_{50}$ of compound 3 on PTP1B was 9.4 μM (Fig. 8a), which was similar to that of 8.0 μM reported in the literature[16]. The $IC_{50}$ of compound 3 on TCPTP was 62.7 μM (Fig. 8b), indicating that compound 3 had a 6.6-fold selectivity for PTP1B over TCPTP. The $IC_{50}$ of lupane triterpenes for TCPTP was determined and compared to the $IC_{50}$ for PTP1B as reported in the literature[21–23] (Table 3). The data indicate that lupeol, lupenone, betulin and betulinic acid are modest but promising inhibitors for PTP1B with the $IC_{50}$ being 5.6, 13.7, 15.3, and 1.5 μM, respectively. All of the lupane triterpenes had a weaker inhibitory effect on TCPTP, being 126.1 (lupeol, Fig. 8c), 91.5 (lupenone, Fig. 8d), 118.7 (betulin, Fig. 8e), and 124.2 μM (betulinic acid, Fig. 8f), respectively. In particular, lupeol and betulinic acid had a 20-fold and 80-fold selectivity for PTP1B over TCPTP, respectively.

**Lupane triterpenes inhibit PTP1B activity in an allosteric manner.** Enzyme kinetic assays have shown that lupeol and lupenone are non-competitive inhibitors for PTP1B, indicating that they target a binding site other than the active site, potentially the allosteric site[21]. We performed kinetic analysis of betulin and betulinic acid, with lupeol as a control (Fig. 9a). The modes of inhibition by betulin and betulinic acid were determined by applying the Lineweaver-Burk plot to 6 different *p*NPP and 4 different compound concentrations. As shown in Fig. 9, both betulin and betulinic acid showed a decreased $V_{max}$ value, indicating that they were not competitive inhibitors. Moreover, betulinic acid was a non-competitive inhibitor having a constant $K_m$ value with a decreased $V_{max}$ value (Fig. 9b). Betulin displayed an altered $K_m$ value and a decreased $V_{max}$ value, classified as mixed-type inhibition (Fig. 9a). None of lupane triterpenes were competitive inhibitors indicating that these compounds target an allosteric binding site.

**Lupane triterpenes attenuate PTP1B expression and activity in hypothalamic neurons.** *Activation of PTP1B by TNFα in mHypoE-46 neurons.* Neuronal PTP1B has a major role in obesity development[5]. The up-regulation of hypothalamic neuronal PTP1B expression induced by TNFα has been found in animal models[1,7,45]. In this study, we applied TNFα to induce PTP1B expression and activity in a mouse hypothalamic cell line (mHypoE-46). TNFα (20 ng/ml) had a time-course effect on PTP1B which increased PTP1B expression 1.75-fold (Figure S6), and PTP1B activity 1.5-fold (Fig. 10b) after 8 h treatment. We then investigated the cellular activity of lupane triterpenes in inhibiting PTP1B expression and activity. Lupeol and betulinic acid were chosen for the *in vitro* experiments as they showed strong potency and selectivity in inhibiting PTP1B in the enzymatic assays (Table 3).

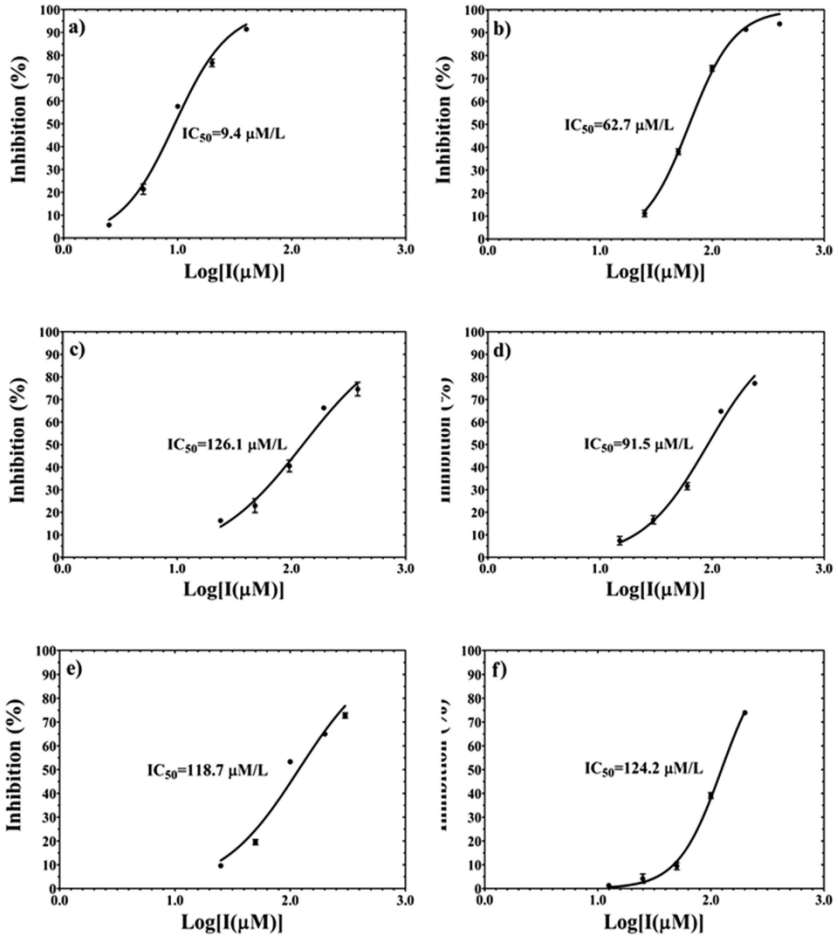


**Figure 8.** The percentage inhibition of PTP1B (**a**) and TCPTP (**b–f**) activity. Compound 3 is used as a control to validate the inhibition assay targeting PTP1B (**a**) and TCPTP (**b**). Four lupane triterpenes are tested for the inhibition potency of TCPTP: (**c**) Lupeol; (**d**) Lupenone; (**e**) Betulin; and (**f**) Betulinic acid.

| | PTP1B ($\mu$M) | TCPTP ($\mu$M) | Fold changes |
|---|---|---|---|
| Lupeol | 5.6[21] | 126.1 | 22 |
| Lupenone | 13.7[21] | 91.5 | 6 |
| Betulin | 15.3[23] | 118.7 | 7 |
| Betulinic acid | 1.5[22] | 124.2 | 81 |

**Table 3. Inhibition potency of lupane triterpenes ($IC_{50}$) targeting PTP1B and TCPTP.** The data for PTP1B are taken from refs 21–23.

*Lupeol and betulinic acid inhibit cellular PTP1B activity.* Lupeol (28 μM, 5× the $IC_{50}$ value) and betulinic acid (7.5 μM, 5× the $IC_{50}$ value) were administrated to the mHypoE-46 cell line for 10 h after treatment of TNFα for 8 h. The cells were collected for western blot and immunoprecipitation analysis. The Western blot results showed that lupeol and betulinic acid slightly decreased PTP1B protein expression (Fig. 10a). However,

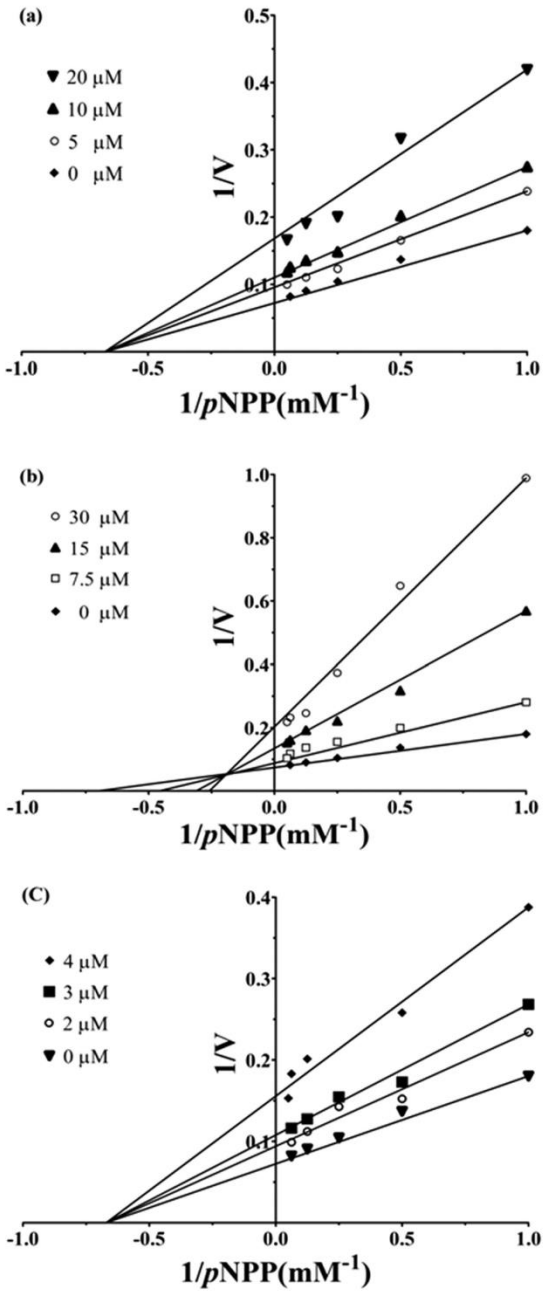


**Figure 9. PTP1B kinetics assay of lupeol, betulin, and betulinic acid indicated by Lineweaver-Burk plot.** (**a**) The concentrations of lupeol are 0 μM, 5 μM, 10 μM, and 20 μM, respectively. (**b**) The concentrations of betulin are 0 μM, 7.5 μM, 15 μM, and 30 μM, respectively. (**c**) The concentrations of betulinic acid are 0 μM, 2 μM, 3 μM, and 4 μM, respectively.

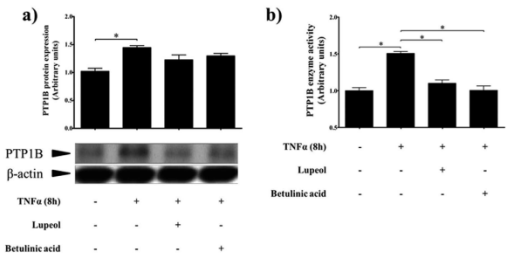


**Figure 10. Selected lupane triterpenes inhibit PTP1B protein expression and enzyme activity in mHypoE-46 neurons.** Lupane triterpenes slightly decrease TNFα-induced PTP1B protein expression (**a**), and significantly inhibit PTP1B enzyme activity (**b**). The results shown are expressed as mean ± SEM (n = 5 per group). Significance is calculated by one-way ANOVA and the *post-hoc* Tukey-Kramer HSD test. $^{*}p < 0.05$, versus control (without TNFα and lupane triterpenes treatments).

immunoprecipitation revealed that PTP1B enzyme activity was significantly inhibited by 35% (Fig. 10b). This indicates that lupeol and betulinic acid penetrated the cell membrane and reduced cellular PTP1B enzymatic activity.

## Discussion

There is compelling evidence that PTP1B is a promising therapeutic target for treating obesity and other diseases. However, it is a major challenge to develop a potent and selective PTP1B inhibitor. Only a few selective PTP1B inhibitors with acceptable pharmacological properties have been reported in the literature, such as TransTech Pharma Inc TTP814, and Ohr Pharmaceutical Inc Trodusquemine (MSI-1436)42, which are in Phase II and Phase I testing, respectively18. Recently, allosteric inhibition has become a promising alternative strategy to develop selective PTP1B inhibitors. The current study firstly predicts that lupane triterpenes bind to the PTP1B allosteric site by the application of molecular docking and molecular dynamics simulations. Enzymatic assays and neuronal cell cultures were used to demonstrate that lupane triterpenes are potential selective and allosteric inhibitors that target PTP1B. PTP1B allosteric inhibitor is featured by displaying a selective inhibitory effect on PTP1B over TCPTP. In an addition to these results, we also performed blind docking of lupane triterpenes targeting TCPTP (Figure S7, Table S7) and compared the results to those targeting PTP1B (Figure S1a, S2a, S3a and S4a). For each lupane triterpene, it is clear that only one pose among the top-ranked poses binds to the region which is equivalent to the allosteric site in PTP1B (Table S7). Thus the less-conserved PTP1B allosteric site is an ideal target for lupane triterpenes to inhibit PTP1B activity. This specificity may cause fewer side effects than the PTP1B active site inhibitors.

Previous structural and biochemical studies have unveiled the important role of α7 as a regulatory helix in the PTP1B conformational transition[16]. However, its mechanism remains unclear. Our results elucidate the contribution of α7 to the allosteric binding mode. Firstly, α7 is involved in the formation of PTP1B-ligand binding. The presence of α7 determines the orientation of lupeol (Fig. 4a,b) and RMSF data reveals a high fluctuation of α7 due to the existence of lupeol (Fig. 5). Therefore α7 directly interacts with lupeol to form the protein-ligand complex. Moreover, using blind and focused docking, we observed stronger binding affinities of lupeol in the presence of α7 (Table S3 and Table S4). SASA results indicate that the presence of α7 results in increased hydrophobic interactions as α7 provides more non-polar residues (Table 1). Lupeol contains a non-polar pentacyclic structure, which easily forms strong hydrophobic interactions with the hydrophobic "tunnel" formed by α7. In addition, experimental and computational studies on lupenone, betulin, and betulinic acid consolidate the role of α7.

Lupane triterpenes are of great interest to traditional medicine[46–48]. Lupeol has been reported to be an anti-diabetes agent[49,50], an anti-cancer agent[51], and an anti-inflammation agent[46]. Betulinic acid also shows anti-obesity activity[52], anti-HIV activity[53], and anti-cancer activity[53]. However, the exact target of lupane triterpenes remains unclear. Our Western blot and immunoprecipitation results show that lupeol and betulinic acid do not significantly decrease PTP1B protein expression in hypothalamic neurons (Fig. 10a). In contrast, PTP1B enzyme activity is significantly inhibited (Fig. 10b). Thus lupeol and betulinic acid directly inhibit PTP1B enzyme activity *in vitro*.

PTP1B is also involved in many diseases including cancer[54], inflammation[7], and diabetes[55]. Since lupane triterpenes directly target PTP1B activity, they are a potential treatment for several diseases. Betulinic acid shows higher inhibition potency as its polar functional groups form stronger hydrogen bonding interactions than lupeol, lupenone, and betulin (Fig. 7). Consistent with the $IC_{50}$ data in table 3, the results from binding free energy calculations showed that betulinic acid had a better inhibitory effect than lupeol. Their contributions of van del waal interactions were similar, therefore the electrostatic interactions mainly contributed to the slightly lower $\Delta G_b^{\circ}$ for betulinic acid (Table 2). It is encouraging to see the relative consistency between experimental results and computed data in our current work. More importantly, via investigating the structure of lupane triterpenes (Fig. 2), it is clear to notice that lupane triterpenes share a highly hydrophobic pentacyclic main structure which lead to the similarity of van del waal interactions between lupeol and betulinic acid. On the other hand, the structural difference between lupeol and betulinic acid lies in the $R_2$ group, which plays a vital role strongly increasing the inhibitory effect of betulinic acid. Since the non-polar pentacyclic structure of lupane triterpenes

is the premise for binding to the less polar allosteric site, modifying the polar functional group is a pivotal way to increase binding affinity and inhibition potency. $R_2$ (Fig. 2) is regarded as an ideal site to be modified to introduce the polar functional groups. However, such modifications need careful investigation since this will affect their pharmacokinetic properties.

## Conclusion

As an important negative regulator in controlling human energy homeostasis, PTP1B is an attractive drug target for preventing and treating obesity and its associated metabolic syndromes. We establish computational modelling for lupane triterpenes binding to PTP1B, and demonstrate that lupane triterpenes function as allosteric inhibitors targeting PTP1B. Our future work will include detailed structural characterizations of the PTP1B-lupane triterpene complex and the rational optimization of these compounds for better efficacy. Thus exploring lupane triterpenes offers the opportunity to develop novel PTP1B allosteric inhibitors with high potency, selectivity, and few side effects.

## References


1. Zabolotny, J. M. *et al.* Protein-tyrosine phosphatase 1B expression is induced by inflammation *in vivo*. *J Biol Chem* **283,** 14230–14241, doi: 10.1074/jbc.M800061200 (2008).
2. Yip, S. C., Saha, S. & Chernoff, J. PTP1B: a double agent in metabolism and oncogenesis. *Trends Biochem Sci* **35,** 442–449, doi: 10.1016/j.tibs.2010.03.004 (2010).
3. Ukkola, O. & Santaniemi, M. Protein tyrosine phosphatase 1B: a new target for the treatment of obesity and associated co-morbidities. *J Intern Med* **251,** 467–475, doi: 10.1046/j.1365-2796.2002.00992.x (2002).
4. Kelly, T., Yang, W., Chen, C. S., Reynolds, K. & He, J. Global burden of obesity in 2005 and projections to 2030. *Int J Obes (Lond)* **32,** 1431–1437, doi: 10.1038/ijo.2008.102 (2008).
5. Bence, K. K. *et al.* Neuronal PTP1B regulates body weight, adiposity and leptin action. *Nat Med* **12,** 917–924, doi: 10.1038/nm1435 (2006).
6. Schwartz, M. W., Woods, S. C., Porte, D., Jr., Seeley, R. J. & Baskin, D. G. Central nervous system control of food intake. *Nature* **404,** 661–671, doi: 10.1038/35007534 (2000).
7. Picardi, P. K. *et al.* Modulation of hypothalamic PTP1B in the TNF-alpha-induced insulin and leptin resistance. *Febs Lett* **584,** 3179–3184, doi: 10.1016/j.febslet.2010.05.064 (2010).
8. Banno, R. *et al.* PTP1B and SHP2 in POMC neurons reciprocally regulate energy balance in mice. *J Clin Invest* **120,** 720–734, doi: 10.1172/JCI39620 (2010).
9. Julien, S. G., Dube, N., Hardy, S. & Tremblay, M. L. Inside the human cancer tyrosine phosphatome. *Nat Rev Cancer* **11,** 35–49, doi: 10.1038/nrc2980 (2011).
10. Iversen, L. F. *et al.* Structure Determination of T Cell Protein-tyrosine Phosphatase. *J Biol Chem* **277,** 19982–19990, doi: 10.1074/jbc.M200567200 (2002).
11. YouTen, K. E. *et al.* Impaired bone marrow microenvironment and immune function in T cell protein tyrosine phosphatase-deficient mice. *J Exp Med* **186,** 683–693, doi: 10.1084/jem.186.5.683 (1997).
12. Simoncic, P. D., Lee-Loy, A., Barber, D. L., Tremblay, M. L. & McGlade, C. J. The T cell protein tyrosine phosphatase is a negative regulator of janus family kinases 1 and 3. *Curr Biol* **12,** 446–453, doi: 10.1016/S0960-9822(02)00697-8 (2002).
13. Zhang, S. & Zhang, Z. Y. PTP1B as a drug target: recent developments in PTP1B inhibitor discovery. *Drug Discov Today* **12,** 373–381, doi: 10.1016/j.drudis.2007.03.011 (2007).
14. Vintonyak, V. V., Antonchick, A. P., Rauh, D. & Waldmann, H. The therapeutic potential of phosphatase inhibitors. *Curr Opin Chem Biol* **13,** 272–283, doi: 10.1016/j.cbpa.2009.03.021 (2009).
15. Johnson, T. O., Ermolieff, J. & Jirousek, M. R. Protein tyrosine phosphatase 1B inhibitors for diabetes. *Nat Rev Drug Discov* **1,** 696–709, doi: 10.1038/nrd895 (2002).
16. Wiesmann, C. *et al.* Allosteric inhibition of protein tyrosine phosphatase 1B. *Nat Struct Mol Biol* **11,** 730–737, doi: 10.1038/nsmb803 (2004).
17. Jia, Z. C., Barford, D., Flint, A. J. & Tonks, N. K. Structural Basis for Phosphotyrosine Peptide Recognition by Protein-Tyrosine-Phosphatase 1b. *Science* **268,** 1754–1758, doi: 10.1126/science.7540771 (1995).
18. Osherovich, L. Inositol insulin insight. *SciBX* **4,** doi: 10.1038/scibx.2011.1 (2011).
19. Baskaran, S. K., Goswami, N., Selvaraj, S., Muthusamy, V. S. & Lakshmi, B. S. Molecular dynamics approach to probe the allosteric inhibition of PTP1B by chlorogenic and cichoric acid. *J Chem Inf Model* **52,** 2004–2012, doi: 10.1021/ci200581g (2012).
20. Shinde, R. N. & Sobhia, M. E. Binding and discerning interactions of PTP1B allosteric inhibitors: novel insights from molecular dynamics simulations. *J Mol Graph Model* **45,** 98–110, doi: 10.1016/j.jmgm.2013.08.001 (2013).
21. Na, M., Kim, B. Y., Osada, H. & Ahn, J. S. Inhibition of protein tyrosine phosphatase 1B by lupeol and lupenone isolated from Sorbus commixta. *J Enzyme Inhib Med Chem* **24,** 1056–1059, doi: 10.1080/14756360802693312 (2009).
22. Choi, J. Y. *et al.* Isolation of betulinic acid, its methyl ester and guaiane sesquiterpenoids with protein tyrosine phosphatase 1B inhibitory activity from the roots of Saussurea lappa C.B.Clarke. *Molecules* **14,** 266–272, doi: 10.3390/molecules14010266 (2009).
23. Xu, W. *et al.* Chemical Constituents of the Roots of Euphorbia micractina. *J Nat Prod* **72,** 1620–1626doi: 10.1021/np900305j (2009).
24. Sali, A. & Blundell, T. L. Comparative protein modelling by satisfaction of spatial restraints. *J Mol Biol* **234,** 779–815, doi: 10.1006/jmbi.1993.1626 (1993).
25. Trott, O. & Olson, A. J. AutoDock Vina: improving the speed and accuracy of docking with a new scoring function, efficient optimization, and multithreading. *J Comput Chem* **31,** 455–461, doi: 10.1002/jcc.21334 (2010).
26. Olsson, M. H. M., Søndergaard, C. R., Rostkowski, M. & Jensen, J. H. PROPKA3: Consistent Treatment of Internal and Surface Residues in Empirical pKa Predictions. *J Chem Theory Comput* **7,** 525–537, doi: 10.1021/ct100578z (2011).
27. Phillips, J. C. *et al.* Scalable molecular dynamics with NAMD. *J Comput Chem* **26,** 1781–1802, doi: 10.1002/jcc.20289 (2005).
28. MacKerell, A. D. *et al.* All-Atom Empirical Potential for Molecular Modeling and Dynamics Studies of Proteins†. *J Phys Chem B* **102,** 3586–3616, doi: 10.1021/jp973084f (1998).
29. Wang, J., Wolf, R. M., Caldwell, J. W., Kollman, P. A. & Case, D. A. Development and testing of a general amber force field. *J Comput Chem* **25,** 1157–1174, doi: 10.1002/jcc.20035 (2004).
30. Darden, T., York, D. & Pedersen, L. Particle Mesh Ewald - an N.Log(N) Method for Ewald Sums in Large Systems. *J Chem Phys* **98,** 10089–10092, doi: 10.1063/1.464397 (1993).
31. Jiang, W., Hodoscek, M. & Roux, B. Computation of Absolute Hydration and Binding Free Energy with Free Energy Perturbation Distributed Replica-Exchange Molecular Dynamics. *J Chem Theory Comput* **5,** 2583–2588, doi: 10.1021/Ct900223z (2009).
32. Woods, C. J., Essex, J. W. & King, M. A. The development of replica-exchange-based free-energy methods. *J Phys Chem B* **107,** 13703–13710, doi: 10.1021/jp0356620 (2003).
33. Hansen, N. & van Gunsteren, W. F. Practical Aspects of Free-Energy Calculations: A Review. *J Chem Theory Comput* **10,** 2632–2647, doi: 10.1021/ct500161f (2014).

34. Rocklin, G. J., Mobley, D. L., Dill, K. A. & Hunenberger, P. H. Calculating the binding free energies of charged species based on explicit-solvent simulations employing lattice-sum methods: An accurate correction scheme for electrostatic finite-size effects. *J Chem Phys* **139,** doi: 10.1063/1.4826261 (2013).
35. Reif, M. M. & Oostenbrink, C. Net Charge Changes in the Calculation of Relative Ligand-Binding Free Energies via Classical Atomistic Molecular Dynamics Simulation. *J Comput Chem* **35,** 227–243, doi: 10.1002/jcc.23490 (2014).
36. Payne, C. M. *et al.* Glycoside Hydrolase Processivity Is Directly Related to Oligosaccharide Binding Free Energy. *J Am Chem Soc* **135,** 18831–18839, doi: 10.1021/Ja407287f (2013).
37. Humphrey, W., Dalke, A. & Schulten, K. VMD: visual molecular dynamics. *J Mol Graph* **14,** 33–38, 27–38, doi: 10.1016/0263-7855(96)00018-5 (1996).
38. Brooks, B. R. *et al.* CHARMM: The Biomolecular Simulation Program. *J Comput Chem* **30,** 1545–1614, doi: 10.1002/jcc.21287 (2009).
39. Yu, Y. *et al.* Teasaponin Reduces Inflammation and Central Leptin Resistance in Diet-Induced Obese Male Mice. *Endocrinology* **154,** 3130–3140, doi: 10.1210/en.2013-1218 (2013).
40. Lorenz, U. Protein tyrosine phosphatase assays. *Curr Protoc Immunol Chapter: Unit-* **11,** 7, doi: 10.1002/0471142735.im1107s93 (2011).
41. Kamerlin, S. C., Rucker, R. & Boresch, S. A targeted molecular dynamics study of WPD loop movement in PTP1B. *Biochem Biophys Res Commun* **345,** 1161–1166, doi: 10.1016/j.bbrc.2006.04.181 (2006).
42. Krishnan, N. *et al.* Targeting the disordered C terminus of PTP1B with an allosteric inhibitor. *Nat Chem Biol* **10,** 558–566, doi: 10.1038/Nchembio.1528 (2014).
43. Cer, R. Z., Mudunuri, U., Stephens, R. & Lebeda, F. J. IC50-to-K-i: a web-based tool for converting IC50 to K-i values for inhibitors of enzyme activity and ligand binding. *Nucleic Acids Res* **37,** W441–W445, doi: 10.1093/nar/gkp253 (2009).
44. Mark, A. E. & Vangunsteren, W. F. Decomposition of the Free-Energy of a System in Terms of Specific Interactions - Implications for Theoretical and Experimental Studies. *J Mol Biol* **240,** 167–176, doi: 10.1006/jmbi.1994.1430 (1994).
45. Ito, Y. *et al.* TNF alpha increases hypothalamic PTP1B activity via the NF kappa B pathway in rat hypothalamic organotypic cultures. *Regul Peptides* **174,** 58–64, doi: 10.1016/j.regpep.2011.11.010 (2012).
46. Siddique, H. R. & Saleem, M. Beneficial health effects of lupeol triterpene: a review of preclinical studies. *Life Sci* **88,** 285–293, doi: 10.1016/j.lfs.2010.11.020 (2011).
47. Baltina, L. A. *et al.* Lupane triterpenes and derivatives with antiviral activity. *Bioorg Med Chem Lett* **13,** 3549–3552, doi: 10.1016/S0960-894X(03)00714-5 (2003).
48. Tolstikova, T. G., Sorokina, I. V., Tolstikov, G. A., Tolstikov, A. G. & Flekhter, O. B. Biological activity and pharmacological prospects of lupane terpenoids: I. Natural lupane derivatives. *Russ J Bioorg Chem* **32,** 37–49, doi: 10.1134/S1068162006010031 (2006).
49. Ali, H., Houghton, P. J. & Soumyanath, A. alpha-Amylase inhibitory activity of some Malaysian plants used to treat diabetes; with particular reference to Phyllanthus amarus. *J Ethnopharmacol* **107,** 449–455, doi: 10.1016/j.jep.2006.04.004 (2006).
50. Ortiz-Andrade, R. R. *et al.* alpha-Glucosidase inhibitory activity of the methanolic extract from Tournefortia hartwegiana: an anti-hyperglycemic agent. *J Ethnopharmacol* **109,** 48–53, doi: 10.1016/j.jep.2006.07.002 (2007).
51. Saleem, M. Lupeol a novel anti-inflammatory and anti-cancer dietary triterpene. *Cancer Lett* **285,** 109–115, doi: 10.1016/j.canlet.2009.04.033 (2009).
52. de Melo, C. L. *et al.* Betulinic Acid, a Natural Pentacyclic Triterpenoid, Prevents Abdominal Fat Accumulation in Mice Fed a High-Fat Diet. *J Agr Food Chem* **57,** 8776–8781, doi: 10.1021/Jf900768w (2009).
53. Yogeeswari, P. & Sriram, D. Betulinic acid and its derivatives: A review on their biological properties. *Curr Med Chem* **12,** 657–666, doi: 10.2174/0929867053202214 (2005).
54. Lessard, L., Stuible, M. & Tremblay, M. L. The two faces of PTP1B in cancer. *Bba-Proteins Proteom* **1804,** 613–619, doi: 10.1016/j.bbapap.2009.09.018 (2010).
55. Elchebly, M. *et al.* Increased insulin sensitivity and obesity resistance in mice lacking the protein tyrosine phosphatase-1B gene. *Science* **283,** 1544–1548, doi: 10.1126/science.283.5407.1544 (1999).



## Acknowledgements

The work was partly supported by the NHMRC (X.F.H.), the Chinese Scholarship Council (T.T.J.), and the University of Wollongong Small Grant Scheme (H.B.Y.). H.B.Y. is the recipient of an Australian Research Council Future Fellowship (Project number FT110100034). The authors would like to thank Ms Linda Cohen for her valuable editorial assistance.


## Author Contributions

T.T.J., H.B.Y. & X.F.H. designed research. T.T.J. & H.B.Y. conducted experiments and analyzed the data. T.T.J. and H.B.Y. wrote the main manuscript and prepared figures and tables. All the authors have reviewed the manuscript.

## Additional Information

**Supplementary information** accompanies this paper at http://www.nature.com/srep

**Competing financial interests:** The authors declare no competing financial interests.


**How to cite this article:** Jin, T. *et al.* Selective binding modes and allosteric inhibitory effects of lupane triterpenes on protein tyrosine phosphatase 1B. *Sci. Rep.* **6,** 20766; doi: 10.1038/srep20766 (2016).

**Selective binding modes and allosteric inhibitory effects of lupane triterpenes on protein tyrosine phosphatase 1B**

Tiantian Jin [a], Haibo Yu [b *] and Xu-Feng Huang [a *]

[a] Centre for Translational Neuroscience, School of Medicine, University of Wollongong, and Illawarra Health and Medical Research Institute (IHMRI), Wollongong, NSW 2522, Australia
[b] School of Chemistry, University of Wollongong, Wollongong, NSW 2522, Australia
[*] Corresponding Author: xhuang@uow.edu.au; hyu@uow.edu.au

**Table S1:** Summary of the simulated systems.

| Label | PTP1B282 | PTP1B282 w/ Compound2 | PTP1B282 w/ Lupeol | PTP1B299 | PTP1B299 w/ Compound2 | PTP1B299 w/ Lupeol | PTP1B299 w/ Lupenone | PTP1B299 w/ Betulin | PTP1B299 w/ Betulinic acid |
|---|---|---|---|---|---|---|---|---|---|
| PTP1B[a] | 282 | 282 | 282 | 299 | 299 | 299 | 299 | 299 | 299 |
| Ligand | - | Compound 2 | Lupeol | - | Compound 2 | Lupeol | Lupenone | Betulin | Betulinic acid |
| Time (ns) | 20 | 20 | 20 | 20 | 100 | 100 | 100 | 100 | 100 |

a: the number of residues included in the simulations.

**Table S2.** List of poses in blind docking of lupane triterpenes targeting PTP1B299. Only those top 20 binding modes with binding affinities less than 3.0 kcal/mol and higher than the best binding mode are listed. # indicates that the ligand binds to the proposed allosteric site.

| | Binding Affinities (kcal/mol) | | | |
|---|---|---|---|---|
| Poses | Lupeol | Lupenone | Betulin | Betulinic acid |
| 1 | -10.3# | -10.4# | -10.7# | -10.1# |
| 2 | -10.1# | -10.1# | -9.9# | -10.0# |
| 3 | -9.1# | -8.9# | -9.1# | -8.7# |
| 4 | -8.2# | -7.9# | -8.5# | -7.2 |
| 5 | -7.3 | -7.8# | -7.9# | -7.2 |
| 6 | -7.3# | -7.5 | -7.7 | -7.0# |
| 7 | -7.1 | -7.5# | -7.4# | -7.0# |
| 8 | -7.0 | -7.3# | -7.3# | -6.9 |
| 9 | -7.0 | -7.1 | -7.3 | -6.8# |
| 10 | -6.9# | -7.0 | -7.3# | -6.8 |
| 11 | -6.9 | -7.0# | -7.2 | -6.8 |
| 12 | -6.9 | -6.9 | -7.2 | -6.8 |
| 13 | -6.8 | -6.9 | -7.2 | -6.7 |
| 14 | -6.8 | -6.9 | -7.1 | -6.7 |
| 15 | -6.8# | -6.9 | -7.1 | -6.7 |
| 16 | -6.8 | -6.8 | -7.1 | -6.7 |
| 17 | -6.7 | -6.8# | -7.1 | -6.7 |
| 18 | -6.7 | -6.7 | -7.1 | -6.7 |
| 19 | -6.7# | -6.7 | -7.1 | -6.6 |
| 20 | -6.6 | | -7.0 | -6.6 |

**Table S3.** List of poses in the focused docking of lupane triterpenes targeting PTP1B299. Only those binding modes with binding affinities less than 3.0 kcal/mol and higher than the best binding mode are listed. The highest-ranking pose was subjected to further molecular dynamics simulations. These data indicate that the default scoring function in AutoDock Vina can not differentiate the four lupane triterpenes, i.e. which is a more potent inhibitor.

| | Binding Affinities (kcal/mol) | | | |
|---|---|---|---|---|
| Poses | Lupeol | Lupenone | Betulin | Betulinic acid |
| 1 | -10.3 | -10.4 | -10.7 | -10.1 |
| 2 | -10.1 | -10.1 | -10.0 | -10.0 |
| 3 | -9.1 | -8.9 | -9.8 | -8.7 |
| 4 | -7.2 | | -9.0 | -8.6 |
| 5 | -6.9 | | -7.3 | -7.0 |

**Table S4.** List of poses in the focused docking of lupane triterpenes targeting PTP1B282. Only those binding modes with binding affinities less than 3.0 kcal/mol and higher than the best binding mode are listed.

| | Binding Affinities (kcal/mol) | | | |
|---|---|---|---|---|
| Poses | Lupeol | Lupenone | Betulin | Betulinic acid |
| 1 | -7.7 | -7.8 | -7.1 | -7.5 |
| 2 | -7.2 | -7.0 | -6.8 | -7.0 |
| 3 | -7.1 | -6.9 | -6.8 | -6.8 |
| 4 | -6.8 | -6.9 | -6.6 | -6.4 |
| 5 | -6.7 | -6.8 | -6.2 | -6.3 |

**Table S5.** Average minimal distances between lupane triterpenes and non-polar residues in the allosteric binding site in PTP1B.

| | Distance (Å) | | | |
|---|---|---|---|---|
| | Lupeol | Lupenone | Betulin | Betulinic acid |
| Ala189 | 4.1 | 3.8 | 4.2 | 3.9 |
| Leu192 | 3.9 | 3.9 | 4.0 | 4.0 |
| Phe196 | 3.7 | 3.7 | 3.7 | 3.6 |
| Phe280 | 3.5 | 3.6 | 3.7 | 3.7 |
| Trp291 | 3.7 | 3.7 | 3.7 | 3.6 |
| Leu294 | 4.1 | 4.1 | 5.0 | 4.1 |

The values are the average minimal distance between the heavy atoms in non-polar residues and ligands in the PTP1B299 w/ Lupeol complex, PTP1B299 w/ Lupenone complex, PTP1B299 w/ Betulin complex, and PTP1B299 w/ Betulinic acid complex for the trajectory of 100 ns.

**Table S6.** Estimation of binging free energy based on experimental IC50 values.

| | Parameters (μM) | | | | | $\Delta G_b^\circ$ |
|---|---|---|---|---|---|---|
| | Enzyme concentration [E] | Substrate concentration [S] | Michaelis-Menten constant [$K_m$] | concentration for 50% inhibition [$IC_{50}$] | Constant of inhibition [$K_i$] | (kcal/mol) |
| Lupeol | 0.01 | 20000 | 1.54 | 5.6[1] | 5.6 | -7.5 |
| Lupenone | N/A | N/A | N/A | 13.7[1] | N/A | N/A |
| Betulin | 0.01 | 20000 | 2.8 | 15.3[2] | 15.3 | -6.8 |
| Betulinic acid | 0.01 | 20000 | 1.47 | 1.5[3] | 1.5 | -8.3 |

The $K_i$ values are calculated via the online IC50-to-Ki converter tool (http://botdb.abcc.ncifcrf.gov/toxin/kiCalES.jsp). According to the equation, for non-competitive and Uncompetitive inhibitors, When [S] >> $K_m$, $K_i$ =$IC_{50}$.

**Table S7.** List of poses in the blind docking of lupane triterpenes targeting TCPTP. Only those top 20 binding modes with binding affinities less than 3.0 kcal/mol and higher than the best binding mode are listed. * indicates that the ligand binds to the active site. # indicates that the ligand binds to the region which is equivalent to the allosteric site in PTP1B.

| | Binding Affinities (kcal/mol) | | | |
|---|---|---|---|---|
| Poses | Lupeol | Lupenone | Betulin | Betulinic acid |
| 1 | -8.2 | -8.5 | -7.9 | -8.0 |
| 2 | -8.0 | -8.0# | -7.4 | -7.7 |
| 3 | -8.0 | -8.0 | -7.4 | -7.5 |
| 4 | -7.9 | -8.0 | -7.4 | -7.5 |
| 5 | -7.9 | -7.9 | -7.4 | -7.4 |
| 6 | -7.7 | -7.8 | -7.3 | -7.4 |
| 7 | -7.7# | -7.7* | -7.3 | -7.3 |
| 8 | -7.6 | -7.7 | -7.2 | -7.3 |
| 9 | -7.6 | -7.7 | -7.1 | -7.2 |
| 10 | -7.5* | -7.7 | -7.1 | -7.2 |
| 11 | -7.5 | -7.5 | -7.0# | -7.2# |
| 12 | -7.5 | -7.5 | -7.0 | -7.1 |
| 13 | -7.4 | -7.5 | -7.0 | -7.1 |
| 14 | -7.3 | -7.5* | -7.0 | -7.1 |
| 15 | -7.3* | -7.5 | -7.0 | -7.1 |
| 16 | -7.2 | -7.4 | -6.9* | -7.0 |
| 17 | -7.2 | -7.4 | -6.8 | -7.0* |
| 18 | -7.2 | -7.3 | -6.8 | -7.0* |
| 19 | -7.2 | -7.3 | -6.8 | -7.0 |
| 20 | -7.1 | -7.2* | -6.8* | |

8

**Figure S1.** Docking poses of lupeol binding to PTP1B299. (a) Top 20 blind docking poses are listed. Poses at the proposed allosteric sites are shown in different colours with the rest in cyan. There are no poses identified which bind to the active site. (b) Top 5 focused docking poses at the proposed allosteric site (listed in Table S1).

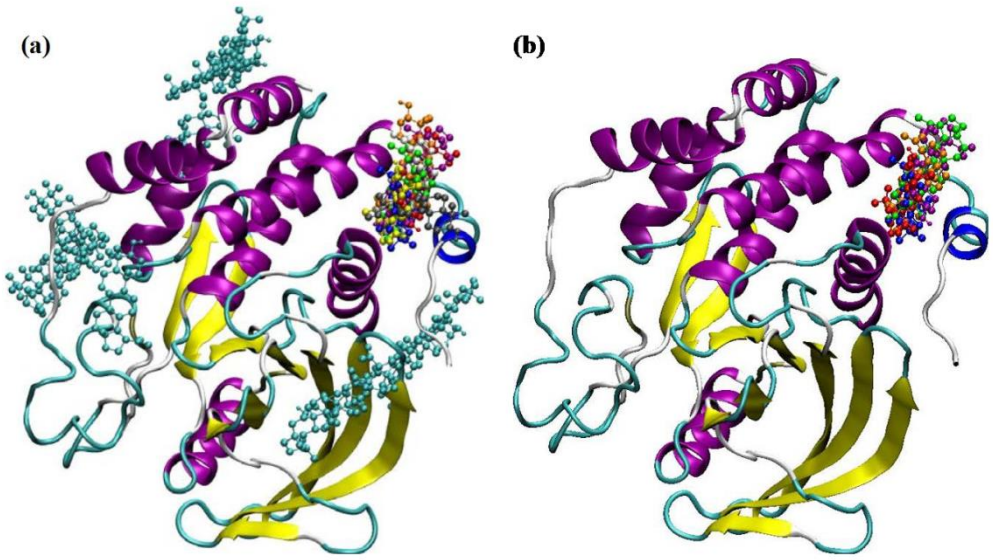

**Figure S2.** Docking poses of lupenone binding to PTP1B299. (a) Top 19 blind docking poses are listed. Poses at the proposed allosteric sites are shown in different colours with the rest in cyan. There are no poses identified which bind to the active site. (b) Top 3 focused docking poses at the proposed allosteric site (listed in Table S1).

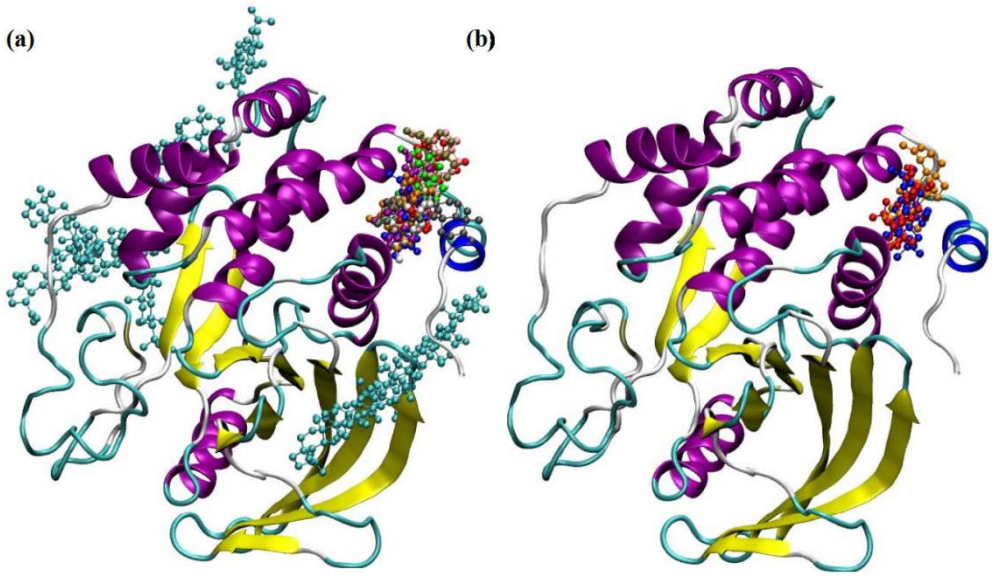

**Figure S3.** Docking poses of betulin binding to PTP1B299. (a) Top 20 blind docking poses are listed. Poses at the proposed allosteric sites are shown in different colours with the rest in cyan. There are no poses identified which bind to the active site. (b) Top 5 focused docking poses at the proposed allosteric site (listed in Table S1).

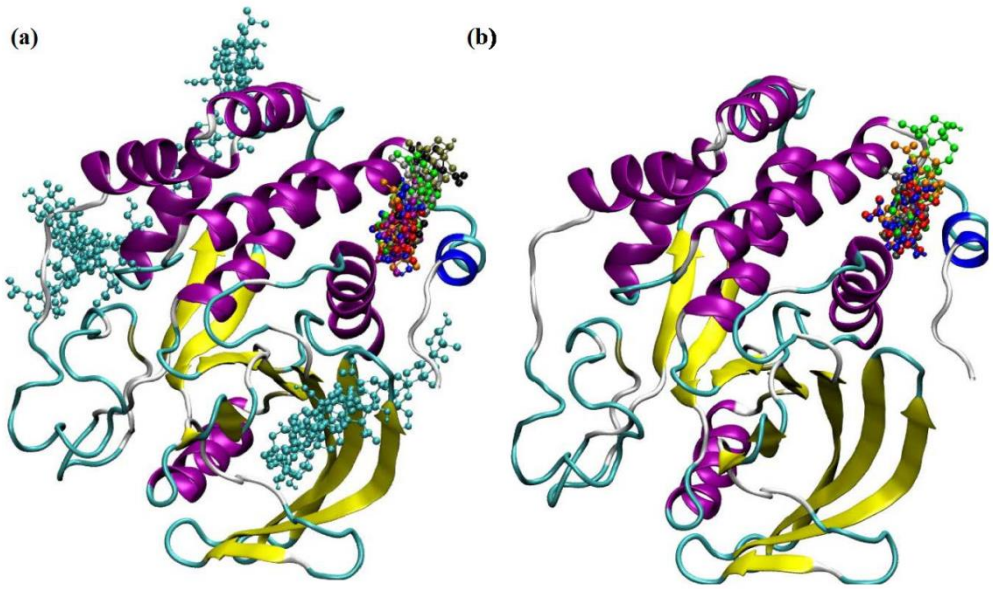

**Figure S4.** Docking poses of betulinic acid binding to PTP1B299. (a) Top 20 blind docking poses are listed. Poses at the proposed allosteric sites are shown in different colours with the rest in cyan. There are no poses identified which bind to the active site. (b) Top 5 focused docking poses at the proposed allosteric site (listed in Table S1).

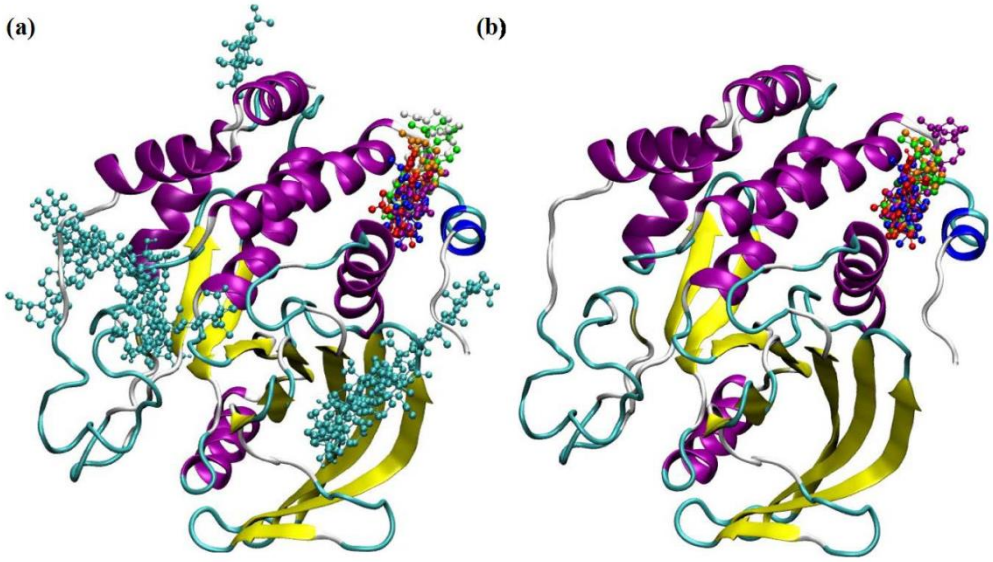

**Figure S5.** Backbone root-mean-square deviations (RMSD) in the 100 ns molecular dynamics simulations of PTP1B299 w/ Lupeol, PTP1B299 w/ Lupenone, PTP1B299 w/ Betulin, and PTP1B299 w/ Betulinic acid.

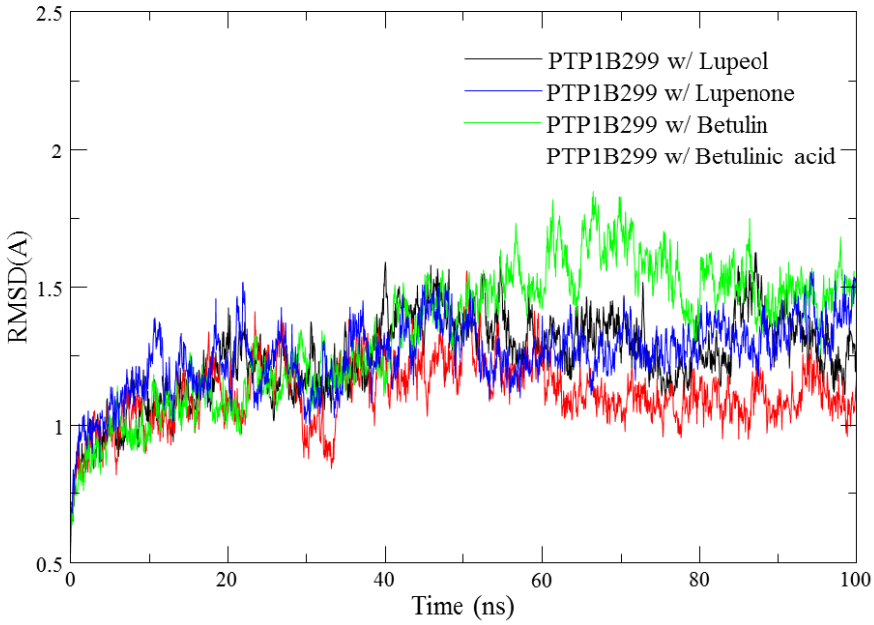


13

**Figure S6.** Time-course effects of 20ng/ml TNFα on PTP1B expression in mHypoE-46 neurons. The results shown are expressed as mean ± SEM (n=5 per group). Significance was calculated by one-way ANOVA and the *post-hoc* Tukey-Kramer HSD test. $^{*}$ $p < 0.05$, $^{**}$ $p < 0.01$ versus control (Without TNFα stimulation).

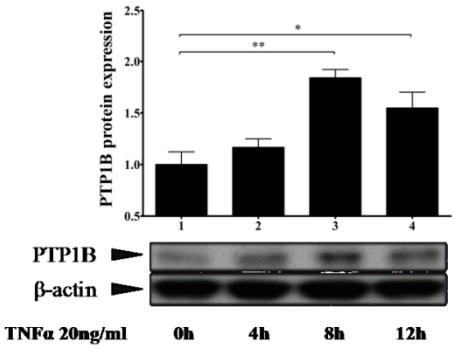

**Figure S7.** Blind docking poses of lupane triterpenes binding to TCPTP. Only those top 20 binding modes with binding affinities less than 3.0 kcal/mol and higher than the best binding mode are listed. (a) lupeol; (b) lupenone; (c) betulin; (d) betulinic acid. Those poses at the active sites and the region which is equivalent to the allosteric site of PTP1B are shown in different colours with the rest in cyan.

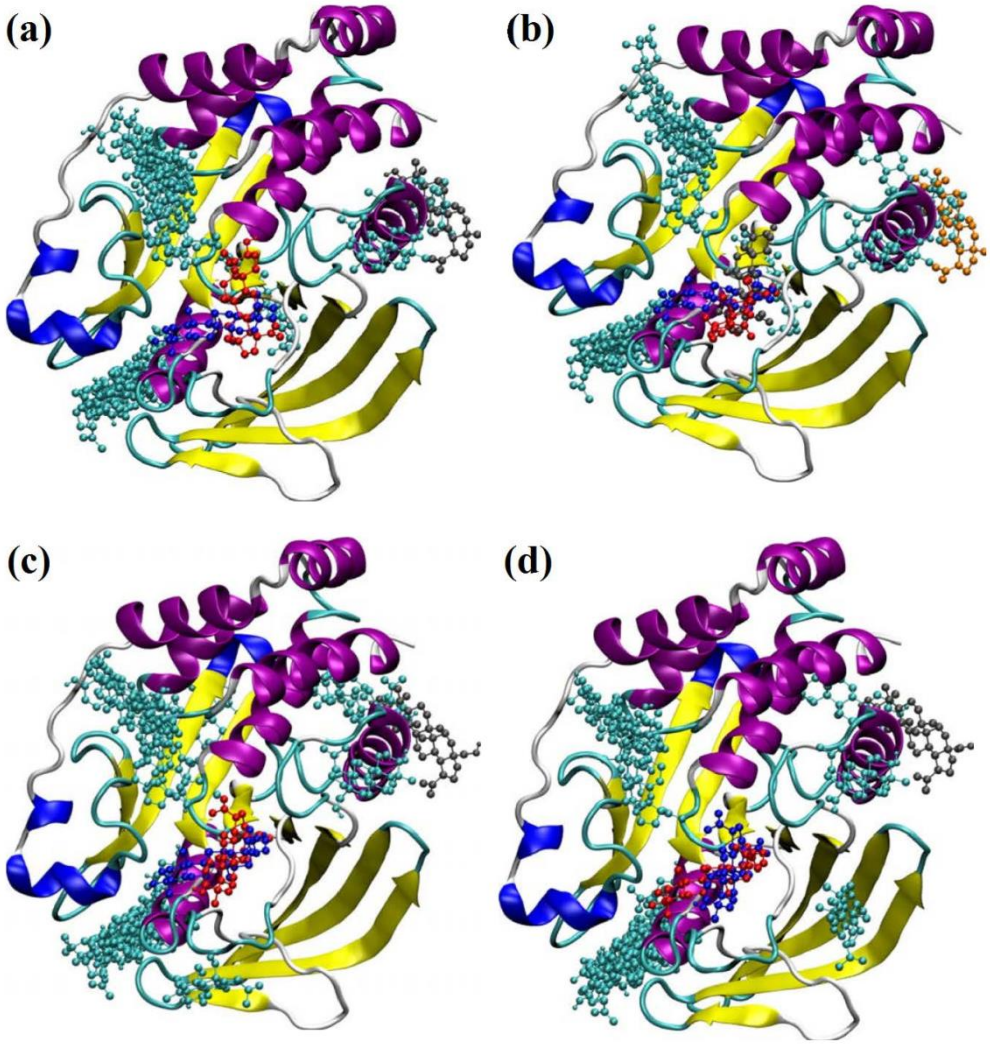

**Reference:**


1 Na, M., Kim, B. Y., Osada, H. & Ahn, J. S. Inhibition of protein tyrosine phosphatase 1B by lupeol and lupenone isolated from Sorbus commixta. *J Enzyme Inhib Med Chem* **24**, 1056-1059, doi:10.1080/14756360802693312 (2009).

2 Xu, W. *et al.* Chemical Constituents of the Roots of Euphorbia micractina. *J Nat Prod* **72**, 1620-1626, doi:10.1021/np900305j (2009).

3 Choi, J. Y. *et al.* Isolation of betulinic acid, its methyl ester and guaiane sesquiterpenoids with protein tyrosine phosphatase 1B inhibitory activity from the roots of Saussurea lappa C.B.Clarke. *Molecules* **14**, 266-272, doi:10.3390/molecules14010266 (2009).

`

# Chapter Three

---

Protein Tyrosine Phosphatase 1B mediates phencyclidine-induced BDNF reduction and neurogenesis impairment in hypothalamic neurons

Submitted to Scientific Report on 2016.7

Statement from co-authors

This is to attest that the PhD candidate, Tiantian Jin, contributed significantly to the investigation

**JIN, T.**, YU, Y. & HUANG, X.-F*. Protein Tyrosine Phosphatase 1B mediates Phencyclidine-induced BDNF reduction and neurogenesis impairment in hypothalamic neurons, Scientific reports (Submitted)

Tiantian Jin designed and performed the experimental work, analysed the data, interpreted results, and wrote the manuscript. Two co-authors are his PhD supervisors, who have provided comments on experimental design, data analysis, results interpretation, and revision of manuscripts.

Tiantian Jin:

Yinghua Yu:

Xu-Feng Huang:

`

# Protein Tyrosine Phosphatase 1B mediates phencyclidine-induced BDNF reduction and neurogenesis impairment in hypothalamic neurons

Tiantian Jin[1], Yinghua Yu[1, 2], and Xu-Feng Huang [1, 2*]

1. School of Medicine, University of Wollongong and Illawarra Health and Medical Research Institute, NSW 2522, Australia
2. Schizophrenia Research Institute, 405 Liverpool Street, Darlinghurst, New South Wales 2010 Australia

***Corresponding Author:**

Senior Professor Xu-Feng Huang, MD, PhD, MSc

School of Medicine, Faculty of Science, Medicine and Health, University of Wollongong and Illawarra Health and Medical Research Institute, Northfields Avenue, NSW2522, Australia

Tel: 61 2 42214300; Email address: xhuang@uow.edu.au

`

**Abstract:**

Protein Tyrosine Phosphatase 1B (PTP1B) inhibits BDNF-mediated signalling and attenuates leptin signalling, which can impair neurite outgrowth and synaptogenesis. On antagonizing the N-methyl-D-aspartate receptor (NMDAR), we found that the psychotomimetic drug phencyclidine (PCP) reduces neurite outgrowth and synaptogenesis with a significantly increased PTP1B in the hypothalamic neurons. We further characterised that it is NR2B, but not NR2A antagonist responsible for the increased PTP1B. Moreover, PTP1B was increased in the hypothalamic neurons of neuregulin-1 knock out mice in which the decreased hypothalamic NR2B phosphorylation was confirmed. PCP decreased neurite outgrowth and synaptogenesis via an increased PTP1B and decreased BDNF level, BDNF-mediated-Akt/GSK3β, and synaptophysin. Furthermore, leptin increases BDNF expression and promotes synaptogenesis which is also impaired by PCP-induced PTP1B. PTP1B directly inhibited JAK phosphorylation and thus attenuated leptin signalling and pSTAT3, leading to reduced BDNF. Therefore, we proposed that PTP1B-JAK2-STAT3 pathway contributed to PCP-induced BDNF reduction. Importantly, we showed that lupeol, a specific PTP1B allosteric inhibitor, significantly reduced PTP1B expression and improved antipsychotic drug's effect on BDNF, leptin signalling, neurite outgrowth and synaptogenesis, as well as prevent antipsychotic drug induced orexigenic neurotransmitter, neuropeptide Y (NPY) production.

**Key words:** PTP1B; phencyclidine; BDNF; leptin; PTP1B allosteric inhibitor

`

**Significance Statement:** This study determined hypothalamic PTP1B as a new contributor to BDNF reduction and neurogenesis impairment in phencyclidine (PCP)-mimicked schizophrenia model. BDNF reduction was broadly observed in schizophrenia patients and PCP models however the mechanism remains unclear. Here we characterised that PCP-induced PTP1B directly inhibited pJAK2 which blocked leptin signalling and downstream pSTAT3, resulting in reduction of BDNF protein and mRNA level, further attenuated BDNF-mediated Akt/GSK3β and synaptogenesis in PCP-treated model. Therefore we proposed PTP1B as a new drug target to reverse PCP-induced alterations. PTP1B allosteric inhibitor was applied which significantly restored BDNF and improved antipsychotic drug, olanzapine's treatment effect. PTP1B is an obesity related protein. Here PTP1B inhibition prevented olanzapine-induced neuropeptide Y production which caused obesity as side effects in clinical.

`

**Introduction:**

Protein Tyrosine Phosphatase 1B (PTP1B) is highly expressed in the brain tissue. Studies have shown that PTP1B influences neurite outgrowth, synaptogenesis and cognition. For example, the reduction of hippocampal PTP1B expression improves dendritic filopodia, learning and memory (Fuentes et al., 2012). An overexpression of PTP1B decreases brain derived neurotrophic factor (BDNF) and its receptor TrkB signalling; however, inhibition of PTP1B restores BDNF-mediated neurite outgrowth and synaptogenesis (Ozek et al., 2014). Krishnan etc. further demonstrated PTP1B as a negative regulator of tyrosine phosphorylation of TrkB to inhibit BDNF signalling in neurological disorder in Rett syndrome model (Krishnan et al., 2015). PTP1B is expressed in the hypothalamus, in which a neuropathology of schizophrenia has been indicated (Fannon et al., 2000, Zabolotny et al., 2002, Walker et al., 2008, Bernstein et al., 2010). Decreased BDNF expression is found in a number of mental disorders including schizophrenia (Angelucci et al., 2005, Favalli et al., 2012). Therefore it is of great interest to investigate the role of hypothalamic PTP1B in modulating BDNF-mediated neurite outgrowth and synaptogenesis in schizophrenia relevant cell models.

Previous study shows that PTP1B attenuates leptin signalling (Zabolotny et al., 2002). The adipocyte-secreted hormone leptin promotes synaptogenesis and maintains neural dendritic morphology as well as regulates energy homeostasis and facilitates learning and memory (Bariohay et al., 2005, Komori et al., 2006, Yamada et al., 2011). Leptin increases neurite outgrowth and synaptogenesis in mouse H19-7 HN neural cell lines, as well as stimulates hippocampal neurogenesis by increasing cell proliferation and differentiation (Moon et al., 2013), while memory deficits or decreased synapse density has been reported in leptin or leptin receptor deficient rodents such as *ob/ob* mice, *db/db*

`

mice and *fa/fa* rats (Li et al., 2002, Bouret et al., 2004, Pinto et al., 2004, Farr et al., 2006). Leptin stimulates BDNF expression in the dendrites of hypothalamic neurons (Liao et al., 2012). Leptin signalling is activated by Janus Kinase 2 (JAK2) phosphorylation and leads to downstream signal transducer and activator of transcription 3 **(**STAT3) expression (Bjorbaek and Kahn, 2004), which has been confirmed to benefit neurite outgrowth (Miao et al., 2006, Ng et al., 2006).

Phencyclidine (PCP), a non-competitive N-methyl-D-aspartate (NMDA) receptor antagonist, can induce schizophrenia-like behaviors in humans and rodents (Morris et al., 2005). It is known that PCP decreases neurite outgrowth and dendritic spine density both *in vitro* and *in vivo* (Hajszan et al., 2006, Adachi et al., 2013). However, the exact mechanism is still unclear. It is known that PCP decreases BDNF expression and its downstream Akt and GSK3β expression (Adachi et al., 2013). Recently, PTP1B has been revealed to inhibit BDNF signalling (Ozek et al., 2014, Krishnan et al., 2015). We hypothesize that PTP1B may be involved in PCP induced reduction of BDNF and impaired Akt and GSK3β signalling pathway. Furthermore, leptin has been revealed to stimulate NMDA-induced intracellular $Ca^{2+}$ levels and facilitates NMDA in modulating synaptic plasticity (Shanley et al., 2001). Therefore it will be interesting to investigate whether PTP1B is involved in linking NMDA hypofunction and leptin signalling in PCP-mimicked schizophrenia modelling.

In this study, PCP was administrated to primary hypothalamic neurons and hypothalamic cell line to examine if hypofunction of NMDA receptor enhance PTP1B expression, followed by investigation of NMDA receptor subunit 2A (NR2A) or NMDA receptor subunit 2B (NR2B) specific effect using their antagonists. Furthermore, PCP's effects on BNDF and its downstream signalling, synaptogenesis

`

and leptin signalling were examined. To investigate if these specific effects induced by PCP were via PTP1B, Lupeol, PTP1B allosteric inhibitor, was pretreated to prevent PCP's effects. Furthermore, co-treatment of lupeol and antipsychotics, olanzapine were applied to investigate if hypothalamic PTP1B as a potential target to improve mental disease treatment such as schizophrenia.

`

**Results:**

**PTP1B expression responds to PCP stimulation**

In a hypothalamic cell line, we observed the dose and time response effects of PTP1B expression following PCP administration. After 3 hours treatment, PCP significantly increased PTP1B (+50%) expression at dose 25μM but not 1μM (Fig.1a). After 48 hours treatment, PCP increased PTP1B in both 25μM (+60%) and 1μM (+30%) doses (Fig.1b). PCP increases PTP1B in dose and time dependent manner. In primary culture (DIV 10) of hypothalamic neurons, we treated the neurons with 25μM PCP for 3 and 48 hours. PTP1B immunoreactivity level was observed with 1.5-fold increase compared to control after 48-h treatment by quantification of MAP2-positive living cells (Fig.1c and 1d). To confirm our findings, we used RT-PCR to examine the PTP1B mRNA level. We observed similar results as there was a 2.2-fold increase in PTP1B mRNA level after 48 hours of 25μM PCP treatment (Fig.1e).

**NR2B antagonist, but not NR2A antagonist, increases PTP1B expression in the hypothalamic neurons**

PCP is a non-competitive NMDA receptor antagonist (Paoletti and Neyton, 2007). NMDA receptor consists of NR1 and NR2 subunits. NR2A and NR2B are primarily responsible for PCP induced behaviour changes in experimental animals (Anastasio et al., 2009, du Bois et al., 2012). To investigate the role of NR2A and NR2B on PTP1B regulation, specific NR2A antagonist Peaqx and NR2B antagonist ifenprodil were used to examine the changes of PTP1B expression in the hypothalamic cells. Both low dosage (5μM) and high dosage (50μM) of each two antagonists were tested for 24 and 48 hours. After 24 hours exposure, high dose of ifenprodil enhanced PTP1B protein level (1.5-fold compared to control), while low dose did not significantly increased

`

PTP1B (Fig.2a). When the incubation of ifenprodil was extended to 48 hours, low dosage group showed 1.5-fold increased PTP1B expression compared to control (Fig.2b). Similar to PCP, NR2B antagonism increases PTP1B expression in both dose and time dependent manner. However, NR2A antagonist Peaqx showed no change on PTP1B expression at neither low nor high doses or on 24 and 48 hour stimulation (Fig.2c and 2d). We suggest that NR2B antagonism is responsible for increased PTP1B expression in hypothalamic cells. We further confirmed that PCP and ifenprodil treatments reduced NR2B phosphorylation (Fig.S3).

**Neuregulin-1 (Nrg1) gene knockout leads to a decreased pNR2B, but an increased PTP1B**

Previous study showed that NR2B phosphorylation requires normal Nrg1 signalling in the prefrontal cortical neurons (Zhang et al., 2016). We found that Nrg1 knockout mice had a significantly decreased NR2B phosphorylation in the primary hypothalamic neurons (Fig.2e), which is similar to a decreased NR2B phosphorylation and NMDA receptor hypofunction reported in hippocampal neurons (Bjarnadottir et al., 2007). This suggests that Nrg1 gene mutation could lead to NR2B hypofunction. Furthermore, we found a significantly increased PTP1B immunoreactivity level by 1.7-fold in the hypothalamic neurons of Nrg1 knockout mice compared to wild type mice (Fig.2f and 2g). Furthermore, we showed that 25μM PCP did neither increase PTP1B immunoreactivity level nor decrease NR2B phosphorylation in Nrg1 knockout mice (Fig.2f and 2g).

**PCP attenuates leptin JAK2/STAT3 pathway and leptin-mediated BDNF level**

PTP1B has been reported to dephosphorylate JAK2, a kinase to activate leptin signalling STAT3 (Ahima and Flier, 2000, Zabolotny et al., 2002). We have shown in

`

above that PCP increased PTP1B. In this part of study, we examined leptin signalling pathway molecules. We used 25µM PCP to treat the hypothalamic cells for 3 hours and 48 hours, followed by100nM leptin treatment for 4 hours. Leptin alone significantly increased 1.4-fold JAK2 phosphorylation and 1.5-fold STAT3 phosphorylation (Fig.3a) which was not case in PCP co-treatment groups in neither 3 hours nor 48 hours (Fig.3a), suggesting that PCP impairs leptin signalling. We further showed that leptin increased BDNF immunoreactivity level by 45% compared to vehicle group similar to what has been reported previously (Komori et al., 2006); however, PCP co-treatment group showed that leptin was no longer able to increase BDNF (Fig.3b and 3c). To confirm these data, we also measured BDNF mRNA level after leptin treatment or leptin and PCP co-treatment for 3 and 48 hours, which showed similar findings (Fig.3d). Therefore, we showed that PCP increased PTP1B and blunted leptin-induced increases of JAK2, STAT3 and BDNF expression, which could contribute to the reduction of neurite outgrowth and synaptogenesis induced by PCP.

**PCP reduces hypothalamic neuronal BDNF expression**

After 3-h treatment, PCP (25µM) significantly (-40%) decreased BDNF expression in hypothalamic cells, but not at low dose (1µM) (Fig.4a). On the other hand, both low and high PCP doses reduced BDNF expression after 48 hour treatment (Fig.4b), indicating that PCP suppressed BDNF protein level in a dose- and time-dependent manner in the hypothalamic cells. Furthermore, primary culture of hypothalamic neurons (at DIV 10) were exposed to 25µM PCP for 48 hours showing 70% reduction of BDNF immunoreactivity level compared to control group (Fig.4c and 4d) and 50% inhibition of BDNF mRNA level (Fig.4e). Therefore, we have shown that 25µM PCP treatment

`

for 48 hours had strongest effect in BDNF expression in both hypothalamic cell line and primary cultured neurons.

**PCP reduces hypothalamic neuronal Akt/GSK3β signalling and synaptic protein**

It is known that BDNF increases the levels of the synaptic vesicle proteins synaptophysin (Tartaglia et al., 2001), in which Akt/GSK3β signalling pathway has been largely involved (Smillie et al., 2013). Since we have found that PCP increased PTP1B and reduced BDNF, we then examined if PCP may alter Akt/GSK3β signalling in the hypothalamic cells. After 3 hours of PCP treatment, both low dose and high dose of PCP reduced the $Akt^{Ser473}$ phosphorylation, while only high dose of PCP significantly reduced $GSK3\beta^{Ser9}$ phosphorylation (Fig.4f). After 48-h PCP treatment, both low and high dose of PCP reduced Akt phosphorylation (1 μM: 45%; 25 μM: 50%) and inhibited GSK3β phosphorylation (1 μM: 35%; 25 μM: 45%) (Fig.4g). Following the upregulation of PTP1B and reduction of BDNF-Akt/GSK signalling, the effect of PCP on the synaptic protein synaptophysin (SYN) as synaptogenesis marker was further examined in the primary hypothalamic neurons. Both SYN immunoreactivity and mRNA levels were significantly reduced by 50% and 50% after 25 μM PCP treatment for 48 hours (Fig.4h, 4i, and 4j). The SYN mRNA level was reduced by 40% after 3 hours of PCP treatment (Fig.4j).

**Lupeol, PTP1B allosteric inhibitor, prevents PCP-induced reduction of BDNF-Akt/GSK3β signalling and SYN expression**

Recently, PTP1B has been is revealed as a novel regulator of central BDNF signalling (Ozek et al., 2014). PTP1B inhibits BDNF–mediated signalling which is a major regulator of Akt/GSK3β signalling pathway (Kitagishi et al., 2012). To investigate whether inhibition of PTP1B could improve BDNF downstream signalling related to

`

synaptogenesis, PTP1B allosteric inhibitor Lupeol was used to examine its effects in prevention of PCP attenuated BDNF signalling in regulation of SYN. We and other group have confirmed that lupeol is PTP1B specific allosteric inhibitor (Na et al., 2009, Jin et al., 2016)**.** Based on our previous study (Jin et al., 2016), we applied 50μM lupeol to hypothalamic cells for 24 hours following 25μM PCP administration for 48 hours. Lupeol significantly prevented PCP-induced PTP1B (Fig.5a). Simultaneously, Lupeol reversed PCP-induced decrease of JAK2 phosphorylation by 3 fold (Fig.5a). Also, Lupeol prevented PCP-reduced BDNF and Akt and GSK3β phosphorylations (Fig.5a and 5b). In addition, to investigate the effect of PTP1B inhibition on the synaptogenesis, the SYN immunoreactivity was examined in MAP2-positive primary cultured hypothalamic neurons treated with 50μM lupeol for 24 hours following 25μM PCP exposure for 24 hours. Lupeol treatment performed a 1.8-fold increase of SYN immunoreactivity compared to the control group treated with PCP only (Fig.5c and Fig.5d). We showed that Lupeol's inhibition on PTP1B improved synaptogenesis.

**Lupeol facilitates olanzapine to reverse PCP-induced alterations and prevent olanzapine-induced NPY level.**

Olanzapine is known to prevent some PCP-induced behaviour changes while the mechanism is still largely unknown (Patil et al., 2007). In the present study, we investigated if olanzapine or combination of lupeol and olanzapine could prevent PCP induced over-expression of PTP1B and its related downregulation of BDNF and impairment of Akt/GSK3β pathway. 5μM olanzapine with or without 10μM and 50μM lupeol were administrated to hypothalamic cell line which had been exposed to 25μM PCP for 48 hours. PTP1B protein level was not significantly decreased by olanzapine treatment and olanzapine with low dosage of lupeol (10μM). However the co-treatment

`

of olanzapine and high dosage of lupeol (50μM) significantly inhibited PTP1B expression (Fig.6a). Olanzapine significantly increased pAkt and pGSK3β with minor improvement on pJAK2 and BDNF protein level (Fig.6b and 6c). Co-treatment of high dosage of lupeol and olanzapine further increased pJAK2, BDNF, pAkt and pGSK3β compared with olanzapine treatment (Fig.6b and 6c), suggesting lupeol improves olanzapine's effect on the enhancement of leptin signalling pJAK2, the increase of BDNF and Akt/GSK3β pathway activation. Moreover, Olanzapine has been found to induce weight gain and elevate orexigenic neurotransmitter, neuropeptide Y (NPY) mRNA level (Weston-Green et al., 2012). Here we measured effects of olanzapine and lupeol on regulating NPY level using NPY/GFP neurons. There is a 1.4-fold increase of NPY level in olanzapine treatment however the co-treatment of lupeol and olanzapine prevented olanzapine-induced NPY level (Fig.6d). Therefore, a combination therapy of olanzapine with lupeol, a PTP1B allosteric inhibitor, may offer a new strategy for the prevention and treatment of schizophrenia pathology with reduced side effects such as weight gain.

`

**Discussions**

This study showed that NMDA and NR2B receptor antagonists (PCP and ifenprodil) significantly increased PTP1B expression in the hypothalamic neurons in a dose- and time-manner. Previous study reported that PTP1B expression was decreased in an oxovanadium complex of glutamic acid suggesting possible glutamate NMDAR involvement (Lu et al., 2010). One previous study found that NMDA receptor didn't form complex with PTP1B based on a proteomic screening of NMDA receptor-adhesion protein, suggesting that NMDA receptor in suppression of PTP1B may not via direct interaction. On the other hand, the authors suggested that the undetected NMDA-PTP1B complex might be due to comigration heavy chain during immunoblotting experiments (Husi et al., 2000). Therefore the relation between NMDA receptor and PTP1B remains unclear. Further research is required to address if there is possible direct relationship between NMDAR and PTP1B. PCP is a non-competitive NMDA antagonist, which inhibits both NR2A and NR2B subunit with poor selectivity (Paoletti and Neyton, 2007). It was interesting that in the present study, we found that only application of ifenprodil, but not PEAQX, increased PTP1B expression in the hypothalamic neurons, suggesting that NR2B antagonism increased PTP1B. Furthermore, there was a negative relationship between the NR2B phosphorylation and PTP1B expression in Nrg1 KO mice which supported our finding that NR2B downregulated PTP1B. Both NR2B deficient and NRG1 gene mutation contribute to the risk of developing schizophrenia (Stefansson et al., 2002, Bjarnadottir et al., 2007). Furthermore, recent studies have showed that Nrg1-ErbB4 signalling is required for NR2B phosphorylation and TrkB interacts with ErbB4 to modulate Nrg1-induced NR2B phosphorylation (Pandya and Pillai, 2014, Zhang et al., 2016). Interestingly, PTP1B inhibits TrkB and therefore disturbs Nrg1-induced NR2B phosphorylation

`

(Pandya and Pillai, 2014), implicating a feedback loop between NR2B dephosphorylation and PTP1B increase. Here, we showed that PCP was not capable to increase PTP1B in Nrg1 KO mice. It could be because NR2B phosphorylation has been inhibited by an increased PTP1B in Nrg1 KO mice. On the other hand, Fyn appears to play an important role in facilitating NR2B phosphorylation (Bjarnadottir et al., 2007, Zhang et al., 2016). Fyn belongs to Src family which has a close link to NMDAR function and scizhophrenia (Pitcher et al., 2011). PTP1B has been revealed to physically interact Src in intact cells and modulate Src activation (Monteleone et al., 2012). It will be interesting to investigate the relation of PTP1B and Src contributing to schizophrenia and relative treatment in the future study. Overall, the findings from the present study showed that PTP1B was elevated by NMDA receptor blockade and NR2B antagonist and in Nrg1 KO mice, from which all had NR2B downregulation. Therefore, our findings indicated that PTP1B is an important mediator contributing to NMDA receptor hypofunction induced by schizophrenia mimetic drug PCP.

Leptin is known to stimulate neurite outgrowth, synaptogenesis and synaptic plasticity as well as to improve learning and memory (Li et al., 2002, Bouret et al., 2004, Pinto et al., 2004, Farr et al., 2006). Moreover, previous studies have reported that leptin exclusively improves NMDA receptor-regulated synaptic transmission including induction of long-term potentiation (Shanley et al., 2001, Harvey et al., 2005, Harvey, 2007), indicating that leptin signalling is capable of improving NMDA-mediated signalling pathway. The present study showed that NMDA receptor antagonism increased PTP1B which affected hypothalamic leptin signalling, indicating the interactions between NMDA receptor and leptin signalling pathways. Leptin signalling is featured by activated JAK2/STAT3 pathway. JAK2/STAT3 plays a key role in central nerve system involved in the regulation of synaptic plasticity (Nicolas et al.,

`

2013) (Nicolas et al., 2012), promoting nerve cell proliferation (Mangoura et al., 2000) and regulation of energy homeostasis (Villanueva and Myers, 2008). Previous study has shown that PTP1B inhibits leptin signalling through attenuating JAK2/STAT3 pathway (Zabolotny et al., 2002). We showed that NMDA receptor/NR2B antagonism increased PTP1B that could lead to a decreased hypothalamic leptin signalling including pJAK2 and pSTAT3.

A number of studies have reported that PCP decreases BDNF protein and mRNA level (Snigdha et al., 2011, Adachi et al., 2013, Katanuma et al., 2014, Zhang et al., 2016). BDNF is an important regulator of synaptic transmission and neural plasticity (Huang and Reichardt, 2001). Reduction of BDNF protein and BDNF mRNA level has been reported in the brain of schizophrenia and other mental illness (Weickert et al., 2003, Weickert et al., 2005, Favalli et al., 2012). Previous study showed that PTP1B suppresses hypothalamic BDNF and TrkB signalling (Ozek et al., 2014, Krishnan et al., 2015). In agreement with their study, the present study showed that PCP decreased BDNF-pAkt-pGSK3β signalling accompanied by an increased PTP1B. It is known that pAkt/pGSK3β improves synaptogenesis and neurite outgrowth (Kitagishi et al., 2012, Smillie et al., 2013). For example, pAkt facilitates dendritic spine protein involved in working memory formation (Emamian et al., 2004). GSK3β has abundant expression in neurons during brain development and is related to neurite outgrowth and synapse formation (Leroy and Brion, 1999). Indeed, the present study showed that blockade of NMDA receptor decreased SYN which was prevented by Lupeol. In the present study, we found that BDNF was decreased when PTP1B was increased by NMDAR blockade. In contrast, when PTP1B was inhibited by lupeol, the downregulation of BDNF expression was prevented, indicating a negative regulatory mechanism between PTP1B and BDNF. Clearly, PTP1B inhibitor lupeol was capable of preventing a

`

downregulation of BDNF via inhibiting PTP1B. These findings suggest that overexpression of PTP1B may contribute to NMDA hypofunction in reduction of synaptogenesis via lowering BDNF. While the mechanism of NMDA receptor blockade decreases BDNF is not known. One possibility is directly related to NMDAR-PSD95-Nrg1 signalling to influence BDNF or via a disinhibition effect of PTP1B on JAK2/STAT3 (Fig.7).

In this study, olanzapine alone did not prevent PCP-induced overexpression of PTP1B and reduction of leptin downstream JAK2 and BDNF. Lupeol is a PTP1B allosteric inhibitor (Na et al., 2009, Jin et al., 2016). Lupeol was able to specifically target PTP1B allosteric site to selectively inhibit PTP1B over other phosphatases including T-cell protein tyrosine phosphatase (TCPTP). TCPTP shares a 74% identical sequence in its catalytic domain with PTP1B (Iversen et al., 2002) and they have almost superimposable active sites. However TCPTP has different biological functions and signalling pathways from PTP1B as demonstrated in mouse models (You-Ten et al., 1997, Simoncic et al., 2002). In this study we found that PCP stimulated PTP1B mRNA level without affecting TCPTP mRNA level (Fig.S1), indicating the requirement to apply PTP1B inhibitor with selectivity. We showed that a combined treatment of olanzapine and lupeol, completely blocked PCP-induced PTP1B overexpression and reductions of pJAK2 and BDNF and reduced pAkt/pGSK3β signalling. Therefore, we showed that lupeol improved antipsychotic drug olanzapine's effect in the prevention of the PCP induced neuronal changes. This study suggests that PTP1B may play a significant role in psychotomimetic drug induced neuropathology and possible psychosis. PTP1B inhibition may be a new strategy to improve olanzapine's therapeutic efficacy. Furthermore, clinical studies have indicated that obesity is highly prevalent among patients with schizophrenia (Elman et al., 2006). Olanzapine and other second

`

generation of antipsychotics have been reported to increase prevalence of weight gain side-effects (Cohn et al., 2004, McEvoy et al., 2005, Haupt, 2006, Meltzer et al., 2008). Recent study has revealed the interactions between olanzapine-induced weight gain and an elevated orexigenic neurotransmitter, neuropeptide Y (NPY) mRNA level (Weston-Green et al., 2012). Hypothalamic PTP1B inhibition prevents weight gain and decrease adiposity. We further measured effects of olanzapine and lupeol on regulating NPY level using NPY/GFP neurons. We demonstrated 1.4-fold increase of NPY level in olanzapine treatment. Importantly, lupeol treatment prevented olanzapine-induced NPY level (Fig.6d). Therefore, co-treatment of PTP1B inhibitor, lupeol with olanzapine may prevent antipsychotic induced weight gain. Considering PTP1B contributes to obesity development, co-treatment of antipsychotic with PTP1B inhibitors may be a potential treatment plan.

In conclusion, this study has demonstrated that NMDA receptor blockade significantly increased PTP1B expression, which is associated with downregulation of NR2B phosphorylation. Increased PTP1B attenuated leptin signalling and leptin-mediated BDNF expression through a downregulation pJAK2/pSTAT3 signalling. Furthermore, an increased PTP1B decreased BDNF expression, and impaired BDNF-mediated pAkt/pGSK3β pathway and finally suppression of synaptophysin. When we applied a PTP1B allosteric inhibitor, lupeol significantly reduced PTP1B expression and prevented the PCP-induced alterations. Lupeol enhanced antipsychotic drug olanzapine's effect to prevent increased PTP1B and decreased BDNF expression. Therefore, PTP1B inhibition may be used as a new treatment to improve therapeutic efficacy and prevent the obesity induced by antipsychotics.

`

**Methods and Materials:**

**Primary culture of wide type and Nrg1 -/+ mouse hypothalamic neurons.** Primary hypothalamic cell cultures from hypothalamic tissues of postnatal day 0 (PN0) wild-type (WT) and Neuregulin-1 (NRG1)-knockout (KO) C57BL/6 mice were prepared based on previous literature (Hilgenberg and Smith, 2007). The procedures on animals were approved by the Animal Ethics Committee, University of Wollongong, NSW, Australia, and carried out in accordance with the Australian Code of Practice for the Care and Use of Animals for Scientific Purposes. The culture condition was adapted according to Johns Hopkins online protocol (Medicine, 2015). The culture medium was composed of NeuroBasal medium with additive B27 and extra glucose and glutamine. Neurons were plated at either a final density of $1.5\times10^5$ cells per $cm^2$ onto Poly-D-Lysine-coated coverslips for immunofluorescence imaging (G400-13, ProSciTech) or a final density of $5\times10^5$ cells per $cm^2$ into Poly-D-Lysine-coated 12-well cell culture plate for collecting protein or RNA, and maintained at 37°C with 5% $CO_2$. At DIV 10, 25μM PCP (P3209, Sigma-Aldrich) was applied to neurons for 3h and 48h. To investigate the effect of PCP on leptin signalling, 100 nM leptin (#450-31-5000, PeproTech) was applied to neurons after PCP stimulations.

**Immunofluorescence and image analysis.** For immunochemical staining, neurons were fixed with 4% paraformaldehyde in Dulbecco's PBS for 30 min at room temperature. The samples were further incubated with 100% methanol for 10 min in -20°C, and blocked with 5% donkey serum in PBST for 1 hr at 37 °C. Then, anti-PTP1B antibody (SAB1306060, Sigma-Aldrich), anti-BDNF antibody (SC-20981, Santa-Cruz), anti-SYN antibody (701503, Life Technnology) and anti-MAP2 antibody (M9942, Sigma-Aldrich) were applied overnight at 4°C. PTP1B, SYN and BDNF were

`

visualised with isotype-specific donkey anti-rabbit IgG (H+L) secondary antibody conjugated with Alexa Fluor 488. MAP2 was visualised by donkey anti-mouse IgG (H+L) secondary antibody conjugated to Alexa Fluor 594. The concentrations of antibodies were applied following manufacturer's manuals. A confocal microscope (Leica-TCS-SP5 Advanced System, Leica Microsystem) was used to obtain images. Software Image J. 10 (http://rsbweb.nih.gov/ij/download.html) was applied to quantify the immunoreactivity based on from 5 independent culture wells.

**Quantitative PCR.** Quantitative real-time PCR (qRT-PCR) was performed as previously described (Yu et al., 2013b). At DIV 10, administration of 25μM PCP (P3209, Sigma-Aldrich) was applied to neurons for 3 and 48 hours. Neurons were collected for RNA extraction via Aurum™ Total RNA Mini Kit (7326820, Bio-Rad Laboratories) and reversed to cDNA by using Applied Biosystems™ High Capacity cDNA Reverse Transcription Kit (4368814, Life Technology). Real-time PCR was then performed via SensiFAST™ SYBR No-ROX Kit (BIO-98005, Bioline). The mRNA expression levels of PTP1B (Forward: TGGCCTGACTTTGGAGTCCC; Reverse: CTCCAGTGTGCGTTTGGGTG.), SYN (Forward: GAACAAGTACCGAGAGAACAACAA; Reverse: GGTCAGTGGCCATCT TCACA.), BDNF (Forward: GGGTCACAGCGGCAGATAAA; Reverse: GCCTTTGGATA CCGGGACTT.) and TCPTP (Forward: AGAGTGGCCAAGTTTCCAG; Reverse: CACA CCATGAGCCAGAAATG.) were normalised to γ-actin (Forward: GCTAACAGAGAGAA GATGACG; Reverse: CAGATGCATACAAGGACAGC), which served as the internal control. Experiments were performed in triplicate.

`

**Mouse hypothalamic cell culture.** The mouse hypothalamic A-59 neurons (mHypoA-59 neurons, CELLutions) were grown in monolayer in Dulbecco's modified Eagle medium (DMEM) (D5796, Sigma-Aldrich) with 10% foetal bovine serum (FBS) (SFBS-F, Bovogen Biologic.Pty.Ltd) and 1% penicillin/streptomycin. Hypothalamic cells were maintained at 37°C with 5% $CO_2$. To expose the role of PCP in hypothalamic cell line, administration of 1μM PCP or 25μM PCP (P3209, Sigma-Aldrich) were applied to neurons for 3 and 48 hours. To investigate the NMDA receptor subunit involved in PTP1B expression, both 5μM and 50μM NR2A antagonist Peaqx (I2892, Sigma-Aldrich) and NR2B antagonist ifenprodil (P1999, Sigma-Aldrich) were administrated to cell line for 24 and 48 hours. To reveal the signalling pathway involved in PCP induced leptin signalling dysfunction, 100nM leptin (450-31-5000, PeproTech) was administrated to cells for 4 hours after PCP 3 and 48 hours. Prior to leptin treatment, the cell culture medium was replaced with serum free medium for 4 hours. To investigate the effect of PTP1B inhibition in hypothalamic cells, 10μM and 50μM PTP1B inhibitor Lupeol (L5632, Sigma-Aldrich) and 5μM atypical antipsychotic Olanzapine (O1141, Sigma-Aldrich) were dissolved in Dimethyl sulfoxide (DMSO), then diluted in sterile water, and mixed with serum free cell culture medium. Cells were exposed to 25μM PCP for 48 hours and replaced with serum free cell culture medium, then lupeol, olanzapine and co-treatment were applied to cells for 24 hours individually. To examine the influence of PTP1B inhibition on neurite synaptogenesis, 50μM lupeol was administrated to primary hypothalamic neurons which have been treated by 25μM PCP for 24 hours, and then co-incubated for another 24 hours. The DMSO concentration was controlled below 0.5%.

**Western blot analysis:** Detailed protocols were described in our previous study (Yu et al., 2013b), primary cultured hypothalamic neurons and mHypo neurons were washed

`

with ice-cold PBS and lysed in NP-40 lysis buffer (FNN0021, Invitrogen) containing a protease inhibitor cocktail, beta-glycerophosphate and phenylmethanesulfonyl fluoride (PMSF) (Sigma- Aldrich). Protein concentrations were determined using the DC™ Protein Assay kit (5000121, Bio-Rad Laboratories). Equal amounts of protein were separated on 4-20% Criterion™ TGX ™ Precast Gels (567-1095, Bio-Rad Laboratories) using SDS-PAGE. Following electrophoresis (120 V for 1.5 h), the proteins were transferred to polyvinylidene difluoride membranes (100 V for 1 hr). Membranes were blocked in 5% bovine serum albumin (BSA) or 5% skim milk depending on the primary antibodies used, followed by incubation with the primary antibodies anti-PTP1B (SAB1306060, Sigma-Aldrich), anti-BDNF antibody (SC-20981, Santa-Cruz), pNR2B$^{Tyr1472}$ (4208S, Cell Signalling Technology), NR2B (4207S, Cell Signalling Technology), anti-pAkt$^{Ser473}$ (D9E, Cell Signalling Technology), anti-Akt (SC8312, Cell Signalling Technology), anti-pGSK3β$^{Ser9}$ (5B3, Cell Signalling Technology), GSK3β (D75D3, Cell Signalling Technology), pJAK2$^{Tyr1007/1008}$ (C80C3, Cell Signalling Technology), JAK2 (D2E12, Cell Signalling Technology), pSTAT3$^{Tyr705}$ (D3A7, Cell Signalling Technology), STAT3 (79D7, Cell Signalling Technology) and anti-actin (MAB1501, Millipore) in 1% BSA or 1% skim milk overnight at 4°C. Following washes (3×5 min) in Tris Buffered Saline+0.1% Tween 20, membranes were incubated with respective secondary antibodies for 1 hr at 25°C. Blots were visualised using Amersham™ ECL™ Detection Reagents (RPN2106, Ge Healthcare) and exposed in dark room. The bands corresponding to the proteins of interest were scanned and analysed using the automatic imaging analysis system Quantity One (Bio-Rad Laboratories). All quantitative analyses were normalised to actin.

`

**Neuron Neuropeptide Y (NPY) detection:** The mouse hypothalamic NPY/GFP neurons (mHypoA-NPY/GFP neurons, CELLutions) were cultured in the 96-well plate in the same incubation condition as mHypoA-59 neurons. 5μM olanzapine, 50μM lupeol and co-treatment of olanzapine and lupeol were applied to neurons. After 6h treatment, discard culture medium and measure neuron NPY-bound GFP immunoactivity using FlexStation 3 (Molecular Devices). Wavelength of detection is set from 488 nm to 510 nm, cutoff at 495 nm.

**Statistical analysis:** Data from the immunofluorescence imaging, RT-PCR analysis and western blot were analysed using the SPSS 19 statistical package (SPSS, Chicago, IL). One-way analysis of variance (ANOVA) was applied in all experiments followed by the *post-hoc* Tukey-Kramer honestly significant difference (HSD) test.

**Acknowledgments:**

This work is supported by the University of Wollongong - China Scholarship Council joint scholarships.

**Authors contributions:**

T.T. J., Y.H. Y. & X.F. H. designed research. T.T. J. conducted experiments and analysed the data. T.T. J. wrote the manuscript. All the authors have reviewed the manuscript.

**Financial disclosures:**

The authors declare no competing financial interests in relation to the work described.

`

**Figure Captions:**

**Fig.1: PTP1B expression stimulated by PCP in mouse hypothalamic A-59 (mHypo) neurons and primary hypothalamic neurons.** a): 25μM PCP for 3 hours treatment significantly increased PTP1B expression in mHypo neurons. b): Both 1μM and 25μM PCP for 48 hours increased PTP1B expression (+30% and +60%) (n=6). c and d):PTP1B immunoreactivity was significantly increased in primary cultured hypothalamic neurons treated with 25μM PCP for 48 hours (n=10). e): The level of PTP1B mRNA level was significantly increased after 3 and 48 hours exposure to 25μM PCP (n=6). Mean ± SEM, Scale bar =25μm, *$p$<0.05, **$p$<0.01.

**Fig.2: PTP1B was induced by decreased pNR2B.** a): PTP1B expression was significantly increased by 50μM ifenprodil but not 5μM ifenprodil for 24h treatment (a) (n=6). b): When ifenprodil treatment was prolonged to 48h, low dosage (5μM) ifenprodil showed increased PTP1B expression as well (n=6). c and d): NR2A antagonist Peaqx did not change PTP1B expression when 5μM and 50μM dose were used for 24 and 48 hours (n=6). e): Phosphorylated NR2B was significantly lower in the Nrg1 KO hypothalamic neurons (n=6). f and g): PTP1B expression was significantly higher in Nrg1 KO mice than wild type mice and 25μM PCP had no effect on PTP1B expression in Nrg1 KO mice (n=10). Mean ± SEM, Scale bar =10μm, *$p$<0.05, **$p$<0.01.

**Fig.3: PCP reduced leptin induced elevation of BDNF, pJAK2 and pSTST3 in the hypothalamic neurons.** a): Leptin increased JAK2 and STAT3 phosphorylations,

`

which were affected by PCP examined in both 3 and 48 hours. b and c): Leptin increased BDNF protein (n=10) and mRNA (d) (n=6) level but were inhibited by PCP. Mean ± SEM, Scale bar =25 µm, *$p$<0.05, **$p$<0.01.

**Fig.4: PCP treatment reduced BDNF level and BDNF-mediated Akt/GSK3β pathway, leading to decreased synaptophysin (SYN).** PCP decreased BDNF expression in mHypo neurons in 3 (a) and 48 (b) hours (n=6). c and d): PCP decreased BDNF protein (n=10) and mRNA (e) (n=6) level in 3 and 48 hours in primary cultured hypothalamic neurons. PCP reduced Akt and GSK3β phosphorylation in both 3 (f) and 48 (g) hours in mHypo neurons (n=6). h and i): PCP significantly decreased SYN level in 48 hours (n=10). j): Both PCP 3h and 48h treatment reduced SYN mRNA (n=6). Mean ± SEM, Scale bar =10µm, *$p$<0.05, **$p$<0.01.

**Fig.5: Lupeol prevented PCP-induced changes in PTP1B, pJAK2, BDNF, pAkt, pGSK3β and synaptophysin.** a): PTP1B allosteric inhibitor lupeol reversed PCP-induced elevation of PTP1B, and down-regulation of pJAK2 and BDNF in hypothalamic neurons (n=6). b): Lupeol reversed PCP-induced reduction of pAkt and pGSK3β (n=6). c and d): Lupeol prevented SYN downregulation induced by PCP (n=10). Mean ± SEM, Scale bar =10µm, *$p$<0.05, **$p$<0.01.

**Fig.6: Lupeol improved olanzapine treatment effects and decreased olanzapine-induced NPY.** a): Olanzapine could not inhibit PCP-induced increase of PTP1B which was however prevented by a combined olanzapine and lupeol treatment (n=6). b and c):

`

A combined olanzapine and lupeol treatment showed improved efficacy to increase pJAK2, BDNF, pAkt and pGSK3β compared to olanzapine treatment (n=6). d): Olanzapine treatment showed 1.4-fold increase of NPY which was inhibited with the application of lupeol (n=10). Mean ± SEM, Scale bar =10µm, *$p$<0.05, **$p$<0.01, ***$p$<0.001.

**Fig.7: PTP1B mediates NMDA receptor/NR2B antagonism induced impairment of synaptogenesis.** NR2B dysfunction induced by PCP or Nrg1 KO stimulated PTP1B. Enhanced PTP1B directly reduced pJAK2, leading to impaired leptin signalling and decreased pSTAT3 which further inhibited BDNF level, pAkt and pGSK3β expression on synaptogenesis. Lupeol is a PTP1B allosteric inhibitor which prevented these changes and restored altered BDNF and pAkt and pGSK3β pathway to improve synaptogenesis.

`

**Reference:**


1. Fuentes F, *et al.* (2012) Protein Tyrosine Phosphatase PTP1B Is Involved in Hippocampal Synapse Formation and Learning. (Translated from English) *Plos One* 7(7) (in English).
2. Ozek C, Kanoski SE, Zhang ZY, Grill HJ, & Bence KK (2014) Protein-tyrosine Phosphatase 1B (PTP1B) Is a Novel Regulator of Central Brain-derived Neurotrophic Factor and Tropomyosin Receptor Kinase B (TrkB) Signaling. (Translated from English) *J Biol Chem* 289(46):31682-31692 (in English).
3. Krishnan N, *et al.* (2015) PTP1B inhibition suggests a therapeutic strategy for Rett syndrome. *The Journal of Clinical Investigation* 125(8):3163-3177.
4. Zabolotny JM, *et al.* (2002) PTP1B regulates leptin signal transduction in vivo. (Translated from eng) *Dev Cell* 2(4):489-495 (in eng).
5. Bernstein H-G, Keilhoff G, Steiner J, Dobrowolny H, & Bogerts B (2010) The hypothalamus in schizophrenia research: no longer a wallflower existence. *Open Neuroendocrinol J* 3:59-67.
6. Walker E, Mittal V, & Tessner K (2008) Stress and the hypothalamic pituitary adrenal axis in the developmental course of schizophrenia. (Translated from English) *Annu Rev Clin Psycho* 4:189-216 (in English).
7. Fannon D, *et al.* (2000) Third ventricle enlargement and developmental delay in first-episode psychosis: preliminary findings. (Translated from English) *Brit J Psychiat* 177:354-359 (in English).
8. Angelucci F, Brene S, & Mathe AA (2005) BDNF in schizophrenia, depression and corresponding animal models. *Mol Psychiatry* 10(4):345-352.
9. Favalli G, Li J, Belmonte-de-Abreu P, Wong AHC, & Daskalakis ZJ (2012) The role of BDNF in the pathophysiology and treatment of schizophrenia. *J Psychiatr Res* 46(1):1-11.
10. Yamada N, *et al.* (2011) Impaired CNS Leptin Action Is Implicated in Depression Associated with Obesity. *Endocrinology* 152(7):2634-2643.
11. Komori T, Morikawa Y, Nanjo K, & Senba E (2006) Induction of brain-derived neurotrophic factor by leptin in the ventromedial hypothalamus. (Translated from English) *Neuroscience* 139(3):1107-1115 (in English).
12. Bariohay B, Lebrun B, Moyse E, & Jean A (2005) Brain-Derived Neurotrophic Factor Plays a Role as an Anorexigenic Factor in the Dorsal Vagal Complex. *Endocrinology* 146(12):5612-5620.
13. Moon HS, Dincer F, & Mantzoros CS (2013) Amylin-induced downregulation of hippocampal neurogenesis is attenuated by leptin in a STAT3/AMPK/ERK-dependent manner in mice. (Translated from English) *Diabetologia* 56(3):627-634 (in English).
14. Bouret SG, Draper SJ, & Simerly RB (2004) Trophic action of leptin on hypothalamic neurons that regulate feeding. *Science* 304(5667):108-110.
15. Pinto S, *et al.* (2004) Rapid rewiring of arcuate nucleus feeding circuits by leptin. *Science* 304(5667):110-115.
16. Farr SA, Banks WA, & Morley JE (2006) Effects of leptin on memory processing. *Peptides* 27(6):1420-1425.
17. Li X-L, *et al.* (2002) Impairment of long-term potentiation and spatial memory in leptin receptor-deficient rodents. *Neuroscience* 113(3):607-615.
18. Liao G-Y, *et al.* (2012) Dendritically targeted Bdnf mRNA is essential for energy balance and response to leptin. *Nat Med* 18(4):564-571.

`

19. Bjorbaek C & Kahn BB (2004) Leptin signaling in the central nervous system and the periphery. *Recent progress in hormone research* 59:305-332.
20. Ng YP, Cheung ZH, & Ip NY (2006) STAT3 as a Downstream Mediator of Trk Signaling and Functions. *J Biol Chem* 281(23):15636-15644.
21. Miao T, *et al.* (2006) Suppressor of Cytokine Signaling-3 Suppresses the Ability of Activated Signal Transducer and Activator of Transcription-3 to Stimulate Neurite Growth in Rat Primary Sensory Neurons. *The Journal of Neuroscience* 26(37):9512-9519.
22. Morris BJ, Cochran SM, & Pratt JA (2005) PCP: from pharmacology to modelling schizophrenia. (Translated from English) *Curr Opin Pharmacol* 5(1):101-106 (in English).
23. Hajszan T, Leranth C, & Roth RH (2006) Subchronic Phencyclidine Treatment Decreases the Number of Dendritic Spine Synapses in the Rat Prefrontal Cortex. *Biol Psychiat* 60(6):639-644.
24. Adachi N, *et al.* (2013) Phencyclidine-Induced Decrease of Synaptic Connectivity via Inhibition of BDNF Secretion in Cultured Cortical Neurons. (Translated from English) *Cereb Cortex* 23(4):847-858 (in English).
25. Shanley LJ, Irving AJ, & Harvey J (2001) Leptin enhances NMDA receptor function and modulates hippocampal synaptic plasticity. *J Neurosci* 21(24):RC186.
26. Paoletti P & Neyton J (2007) NMDA receptor subunits: function and pharmacology. *Curr Opin Pharmacol* 7(1):39-47.
27. Anastasio NC, Xia Y, O'Connor ZR, & Johnson KM (2009) Differential role of N-methyl-D-aspartate receptor subunits 2A and 2B in mediating phencyclidine-induced perinatal neuronal apoptosis and behavioral deficits. *Neuroscience* 163(4):1181-1191.
28. du Bois TM, Newell KA, & Huang XF (2012) Perinatal phencyclidine treatment alters neuregulin 1/erbB4 expression and activation in later life. *Eur Neuropsychopharmacol* 22(5):356-363.
29. Zhang Q, Yu Y, & Huang X-F (2016) Olanzapine Prevents the PCP-induced Reduction in the Neurite Outgrowth of Prefrontal Cortical Neurons via NRG1. *Scientific reports* 6:19581.
30. Bjarnadottir M, *et al.* (2007) Neuregulin1 (NRG1) Signaling through Fyn Modulates NMDA Receptor Phosphorylation: Differential Synaptic Function in NRG1+/− Knock-Outs Compared with Wild-Type Mice. *The Journal of Neuroscience* 27(17):4519-4529.
31. Ahima RS & Flier JS (2000) Leptin. *Annual Review of Physiology* 62(1):413-437.
32. Tartaglia N, *et al.* (2001) Protein Synthesis-dependent and -independent Regulation of Hippocampal Synapses by Brain-derived Neurotrophic Factor. *J Biol Chem* 276(40):37585-37593.
33. Smillie KJ, Pawson J, Perkins EM, Jackson M, & Cousin MA (2013) Control of synaptic vesicle endocytosis by an extracellular signalling molecule. *Nat Commun* 4.
34. Kitagishi Y, Kobayashi M, Kikuta K, & Matsuda S (2012) Roles of PI3K/AKT/GSK3/mTOR Pathway in Cell Signaling of Mental Illnesses. *Depression Research and Treatment* 2012:8.
35. Na M, Kim BY, Osada H, & Ahn JS (2009) Inhibition of protein tyrosine phosphatase 1B by lupeol and lupenone isolated from Sorbus commixta. (Translated from eng) *J Enzyme Inhib Med Chem* 24(4):1056-1059 (in eng).

36. Jin T, Yu H, & Huang X-F (2016) Selective binding modes and allosteric inhibitory effects of lupane triterpenes on protein tyrosine phosphatase 1B. *Scientific reports* 6:20766.
37. Patil ST, *et al.* (2007) Activation of mGlu2/3 receptors as a new approach to treat schizophrenia: a randomized Phase 2 clinical trial. *Nat Med* 13(9):1102-1107.
38. Weston-Green K, Huang X-F, & Deng C (2012) Alterations to Melanocortinergic, GABAergic and Cannabinoid Neurotransmission Associated with Olanzapine-Induced Weight Gain. *Plos One* 7(3):e33548.
39. Lu L, *et al.* (2010) Inhibition protein tyrosine phosphatases by an oxovanadium glutamate complex, Na2[VO(Glu)2(CH3OH)](Glu = glutamate). *BioMetals* 23(6):1139-1147.
40. Husi H, Ward MA, Choudhary JS, Blackstock WP, & Grant SGN (2000) Proteomic analysis of NMDA receptor-adhesion protein signaling complexes. *Nat Neurosci* 3(7):661-669.
41. Stefansson H, *et al.* (2002) Neuregulin 1 and Susceptibility to Schizophrenia. *American Journal of Human Genetics* 71(4):877-892.
42. Pandya CD & Pillai A (2014) TrkB interacts with ErbB4 and regulates NRG1-induced NR2B phosphorylation in cortical neurons before synaptogenesis. *Cell Communication and Signaling* 12(1):1-11.
43. Pitcher GM, *et al.* (2011) Schizophrenia susceptibility pathway neuregulin 1-ErbB4 suppresses Src upregulation of NMDA receptors. *Nat Med* 17.
44. Monteleone MC, *et al.* (2012) ER-Bound Protein Tyrosine Phosphatase PTP1B Interacts with Src at the Plasma Membrane/Substrate Interface. *Plos One* 7(6):e38948.
45. Harvey J, Shanley L, O'Malley D, & Irving A (2005) Leptin: a potential cognitive enhancer? *Biochemical Society Transactions* 33(5):1029-1032.
46. Harvey J (2007) Leptin: a diverse regulator of neuronal function. *Journal of neurochemistry* 100(2):307-313.
47. Nicolas CS, *et al.* (2013) The role of JAK-STAT signaling within the CNS. *JAK-STAT* 2(1):e22925.
48. Nicolas Céline S, *et al.* (2012) The JAK/STAT Pathway Is Involved in Synaptic Plasticity. *Neuron* 73(2):374-390.
49. Mangoura D, Pelletiere C, Leung S, Sakellaridis N, & Wang DX (2000) Prolactin concurrently activates Src-PLD and JAK/Stat signaling pathways to induce proliferation while promoting differentiation in embryonic astrocytes. *International Journal of Developmental Neuroscience* 18(7):693-704.
50. Villanueva EC & Myers MG (2008) Leptin receptor signaling and the regulation of mammalian physiology. *International journal of obesity (2005)* 32(Suppl 7):S8-12.
51. Snigdha S, *et al.* (2011) Phencyclidine (PCP)-Induced Disruption in Cognitive Performance is Gender-Specific and Associated with a Reduction in Brain-Derived Neurotrophic Factor (BDNF) in Specific Regions of the Female Rat Brain. *Journal of Molecular Neuroscience* 43(3):337-345.
52. Katanuma Y, *et al.* (2014) Phencyclidine rapidly decreases neuronal mRNA of brain-derived neurotrophic factor. *Synapse* 68(6):257-265.
53. Huang EJ & Reichardt LF (2001) Neurotrophins: Roles in Neuronal Development and Function. *Annual review of neuroscience* 24:677-736.
54. Weickert CS, *et al.* (2003) Reduced brain-derived neurotrophic factor in prefrontal cortex of patients with schizophrenia. *Mol Psychiatry* 8(6):592-610.
55. Weickert CS, *et al.* (2005) Reductions in neurotrophin receptor mRNAs in the prefrontal cortex of patients with schizophrenia. *Mol Psychiatry* 10(7):637-650.

`

56. Emamian ES, Hall D, Birnbaum MJ, Karayiorgou M, & Gogos JA (2004) Convergent evidence for impaired AKT1-GSK3[beta] signaling in schizophrenia. *Nat Genet* 36(2):131-137.
57. Leroy K & Brion J-P (1999) Developmental expression and localization of glycogen synthase kinase-3β in rat brain. *Journal of Chemical Neuroanatomy* 16(4):279-293.
58. Iversen LF, *et al.* (2002) Structure Determination of T Cell Protein-tyrosine Phosphatase. *J Biol Chem* 277(22):19982-19990.
59. You-Ten KE, *et al.* (1997) Impaired bone marrow microenvironment and immune function in T cell protein tyrosine phosphatase-deficient mice. (Translated from eng) *J Exp Med* 186(5):683-693 (in eng).
60. Simoncic PD, Lee-Loy A, Barber DL, Tremblay ML, & McGlade CJ (2002) The T cell protein tyrosine phosphatase is a negative regulator of janus family kinases 1 and 3. (Translated from eng) *Curr Biol* 12(6):446-453 (in eng).
61. Elman I, Borsook D, & Lukas SE (2006) Food intake and reward mechanisms in patients with schizophrenia: Implications for metabolic disturbances and treatment with second-generation antipsychotic agents. (Translated from English) *Neuropsychopharmacol* 31(10):2091-2120 (in English).
62. Meltzer HY, *et al.* (2008) A randomized, double-blind comparison of clozapine and high-dose olanzapine in treatment-resistant patients with schizophrenia. (Translated from English) *J Clin Psychiatry* 69(2):274-285 (in English).
63. Haupt DW (2006) Differential metabolic effects of antipsychotic treatments. *European neuropsychopharmacology : the journal of the European College of Neuropsychopharmacology* 16:S149-S155.
64. Cohn T, Prud'homme D, Streiner D, Kameh H, & Remington G (2004) Characterizing coronary heart disease risk in chronic schizophrenia: high prevalence of the metabolic syndrome. (Translated from eng) *Can J Psychiatry* 49(11):753-760 (in eng).
65. McEvoy JP, *et al.* (2005) Prevalence of the metabolic syndrome in patients with schizophrenia: baseline results from the Clinical Antipsychotic Trials of Intervention Effectiveness (CATIE) schizophrenia trial and comparison with national estimates from NHANES III. (Translated from eng) *Schizophr Res* 80(1):19-32 (in eng).
66. Bence KK, *et al.* (2006) Neuronal PTP1B regulates body weight, adiposity and leptin action. (Translated from eng) *Nature Medicine* 12(8):917-924 (in eng).
67. Hilgenberg LGW & Smith MA (2007) Preparation of Dissociated Mouse Cortical Neuron Cultures. *Journal of Visualized Experiments : JoVE* (10):562.
68. Medicine JH (2015) Dissociated Primary Hypothalamic Neuron Culture.
69. Yu Y, *et al.* (2013) Teasaponin Reduces Inflammation and Central Leptin Resistance in Diet-Induced Obese Male Mice. *Endocrinology* 154(9):3130-3140.

`

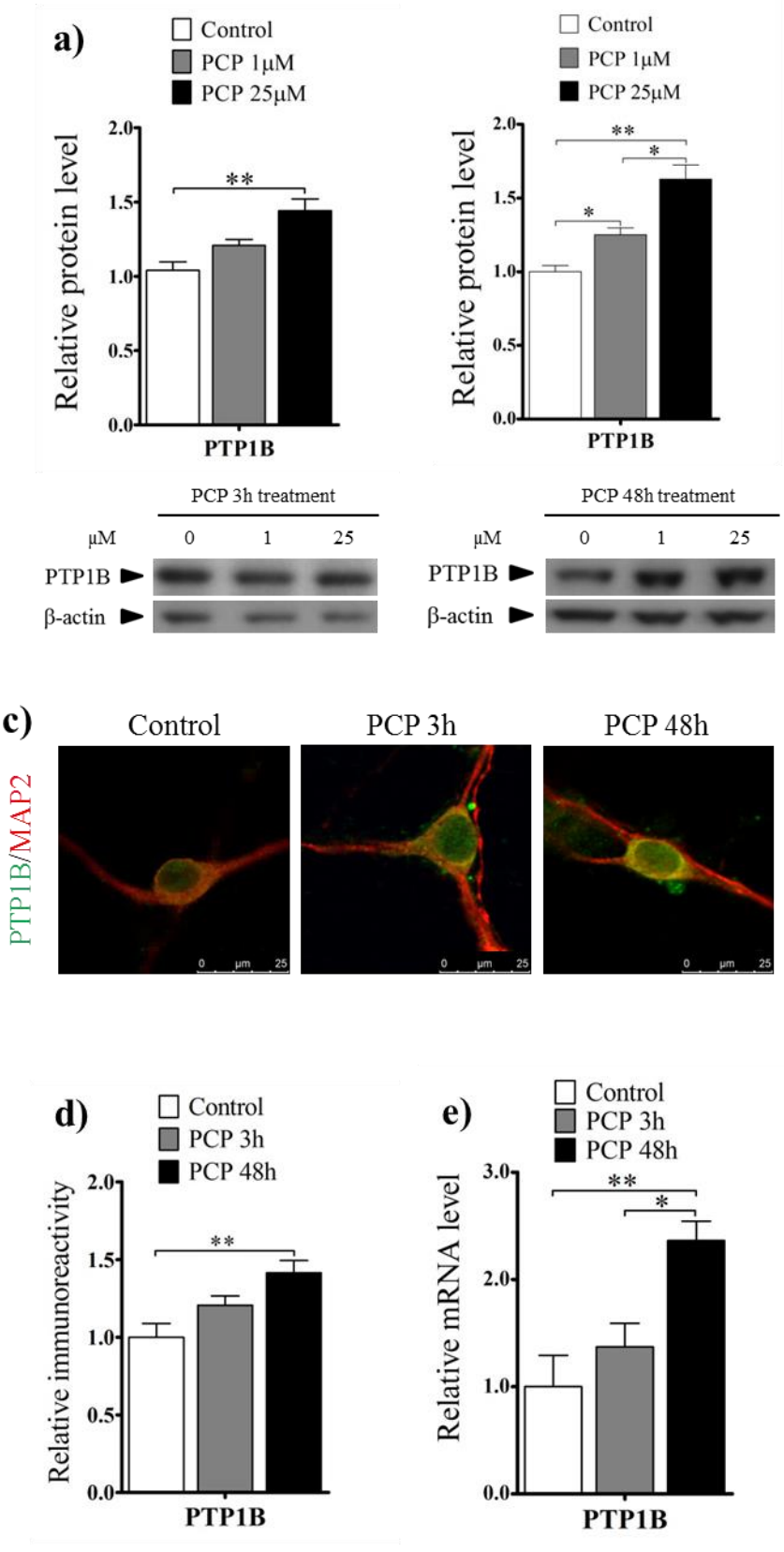
a)
Control
PCP 1μM
PCP 25μM
Relative protein level
PTP1B
PCP 3h treatment
PCP 48h treatment
μM
0
1
25
PTP1B
β-actin
c)
Control
PCP 3h
PCP 48h
PTP1B/MAP2
d)
Relative immunoreactivity
e)
Relative mRNA level

Fig.1

`

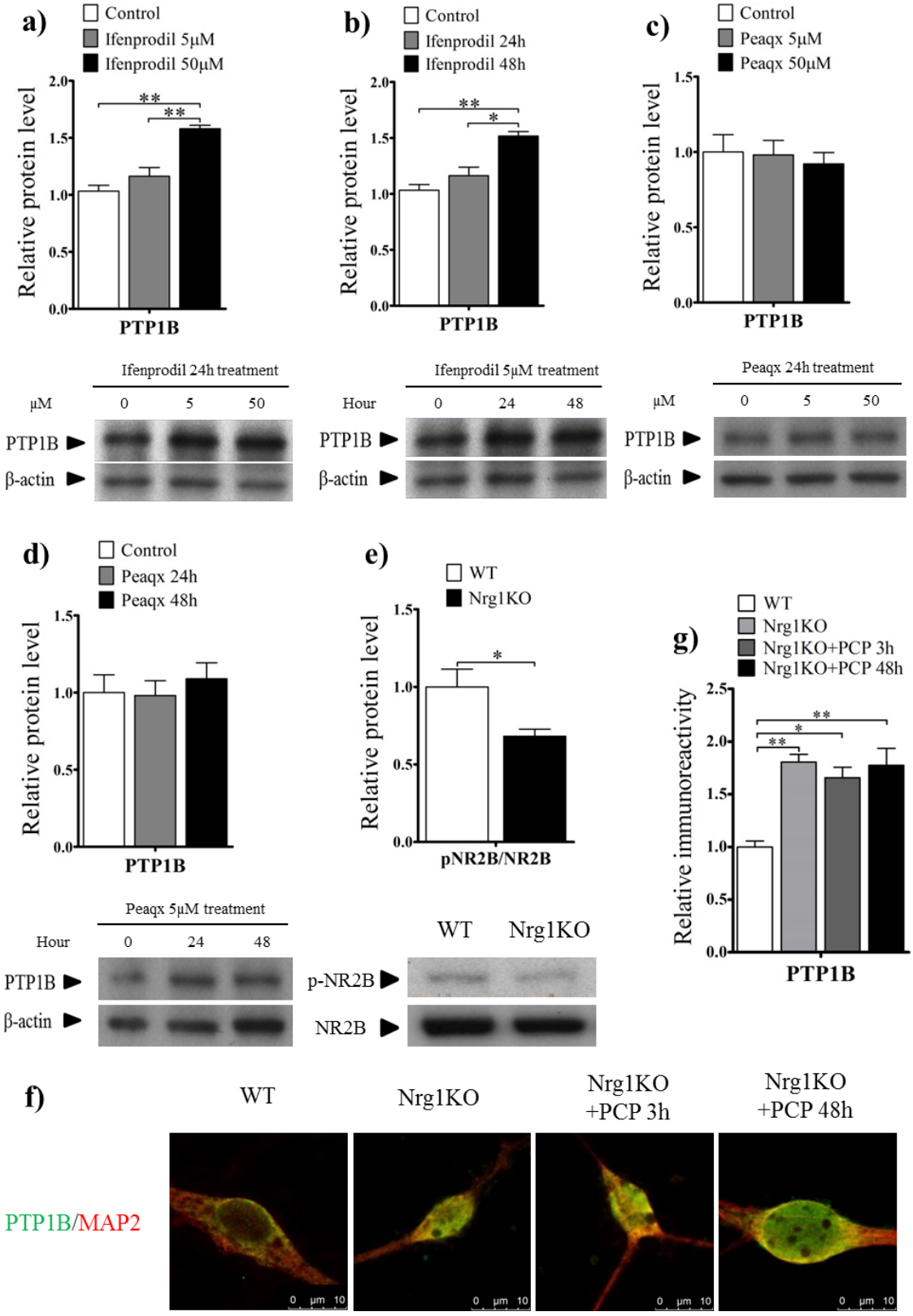
a)
Control
Ifenprodil 5μM
Ifenprodil 50μM
Relative protein level
PTP1B
b)
Control
Ifenprodil 24h
Ifenprodil 48h
Relative protein level
PTP1B
c)
Control
Peaqx 5μM
Peaqx 50μM
Relative protein level
PTP1B
Ifenprodil 24h treatment
μM
0
5
50
PTP1B
β-actin
Ifenprodil 5μM treatment
Hour
0
24
48
PTP1B
β-actin
Peaqx 24h treatment
μM
0
5
50
PTP1B
β-actin
d)
Control
Peaqx 24h
Peaqx 48h
Relative protein level
PTP1B
e)
WT
Nrg1KO
Relative protein level
pNR2B/NR2B
g)
WT
Nrg1KO
Nrg1KO+PCP 3h
Nrg1KO+PCP 48h
Relative immunoreactivity
PTP1B
Peaqx 5μM treatment
Hour
0
24
48
PTP1B
β-actin
WT
Nrg1KO
p-NR2B
NR2B
f)
WT
Nrg1KO
Nrg1KO +PCP 3h
Nrg1KO +PCP 48h
PTP1B/MAP2

Fig.2

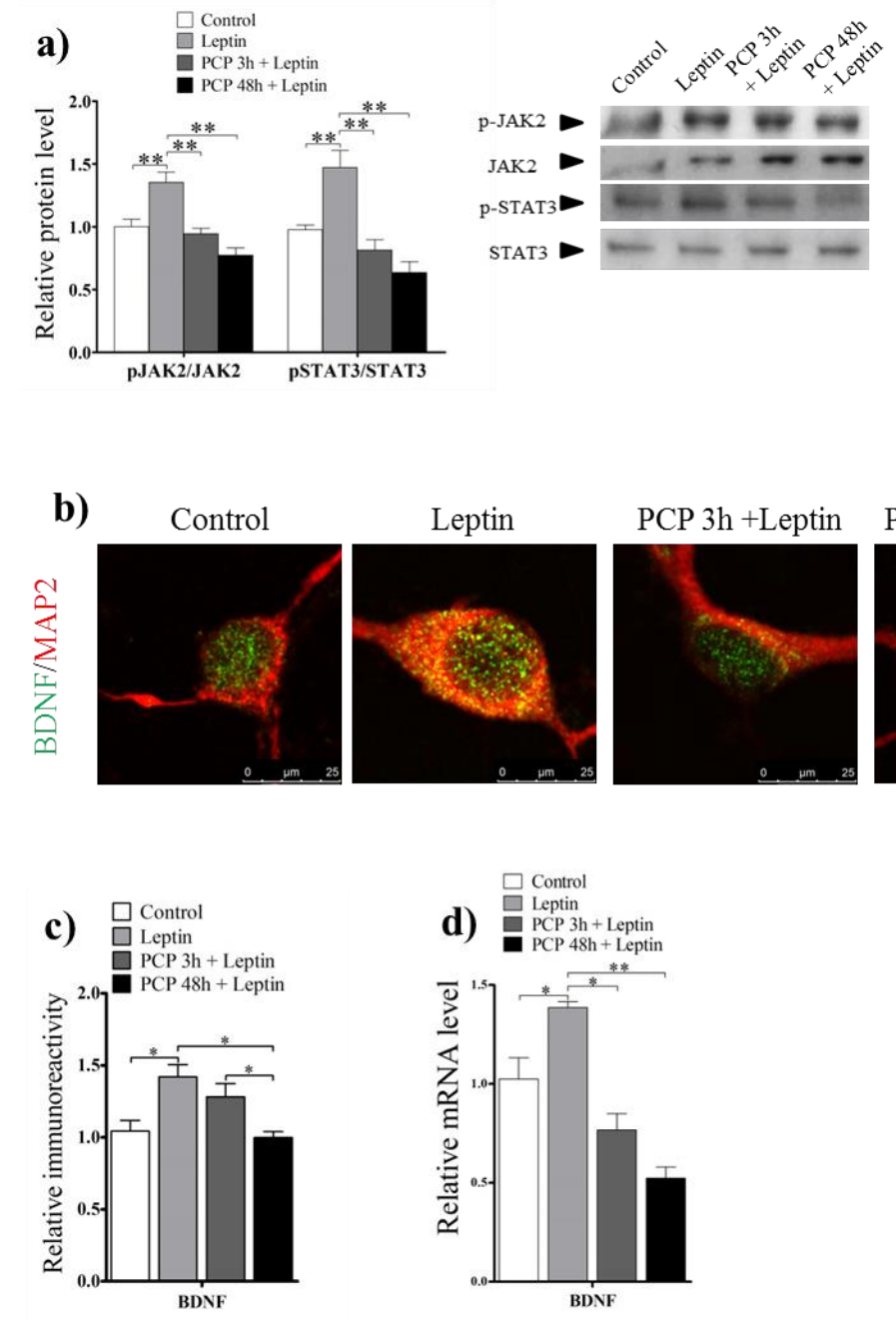
a)
Control
Leptin
PCP 3h + Leptin
PCP 48h + Leptin
Relative protein level
pJAK2/JAK2
pSTAT3/STAT3
Control
Leptin
PCP 3h + Leptin
PCP 48h + Leptin
p-JAK2
JAK2
p-STAT3
STAT3
b)
Control
Leptin
PCP 3h +Leptin
PCP 48h +Leptin
BDNF/MAP2
c)
Relative immunoreactivity
BDNF
d)
Relative mRNA level
BDNF

Fig.3

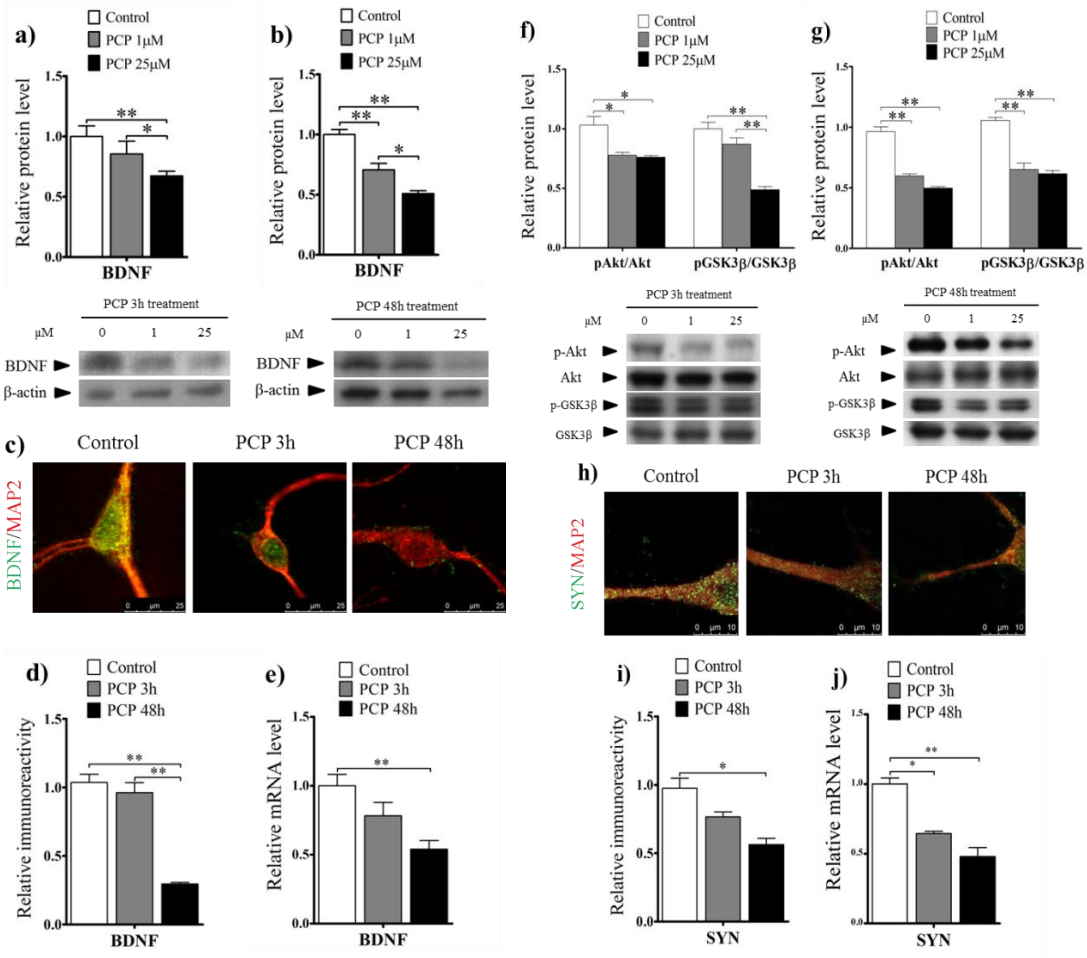
a)
Control
PCP 1μM
PCP 25μM
Relative protein level
BDNF
b)
PCP 3h treatment
PCP 48h treatment
μM
BDNF
β-actin
f)
pAkt/Akt
pGSK3β/GSK3β
g)
p-Akt
Akt
p-GSK3β
GSK3β
c)
Control
PCP 3h
PCP 48h
BDNF/MAP2
h)
SYN/MAP2
d)
Relative immunoreactivity
e)
Relative mRNA level
i)
SYN
j)

Fig.4

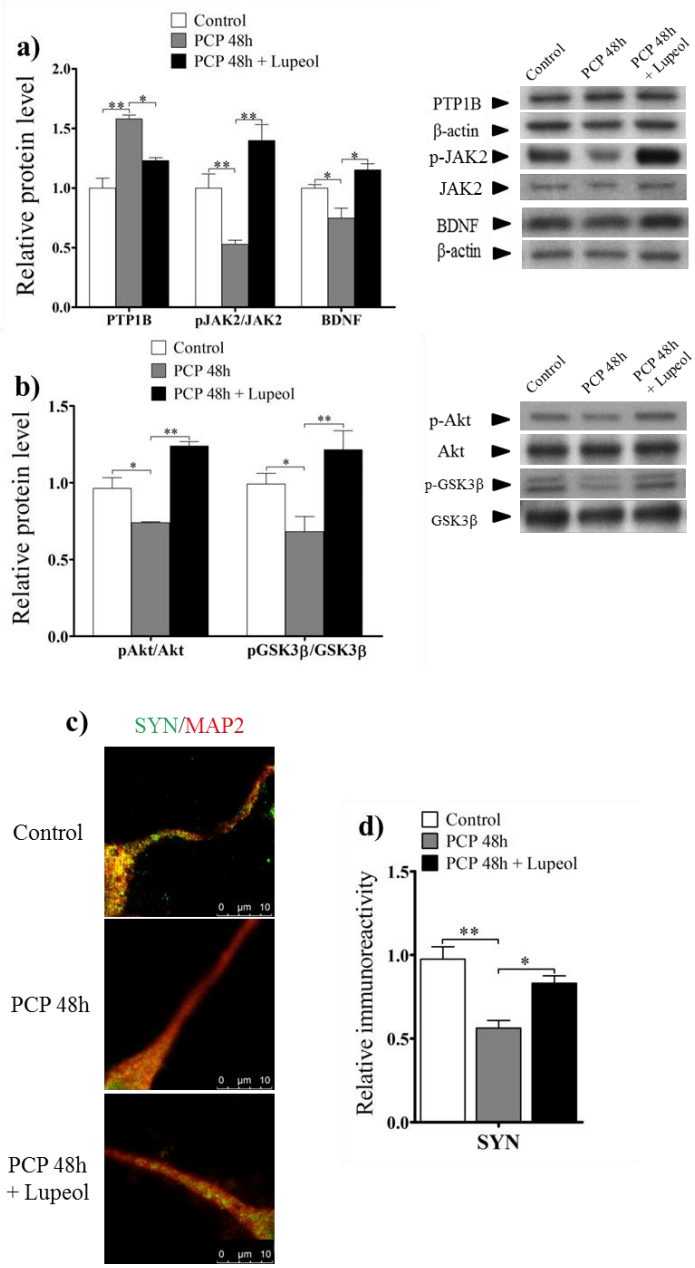
a)
Control
PCP 48h
PCP 48h + Lupeol
Relative protein level
PTP1B
pJAK2/JAK2
BDNF
Control
PCP 48h
PCP 48h + Lupeol
PTP1B
β-actin
p-JAK2
JAK2
BDNF
β-actin
b)
Control
PCP 48h
PCP 48h + Lupeol
Relative protein level
pAkt/Akt
pGSK3β/GSK3β
Control
PCP 48h
PCP 48h + Lupeol
p-Akt
Akt
p-GSK3β
GSK3β
c)
SYN/MAP2
Control
PCP 48h
PCP 48h + Lupeol
0 μm 10
d)
Control
PCP 48h
PCP 48h + Lupeol
Relative immunoreactivity
SYN

Fig.5

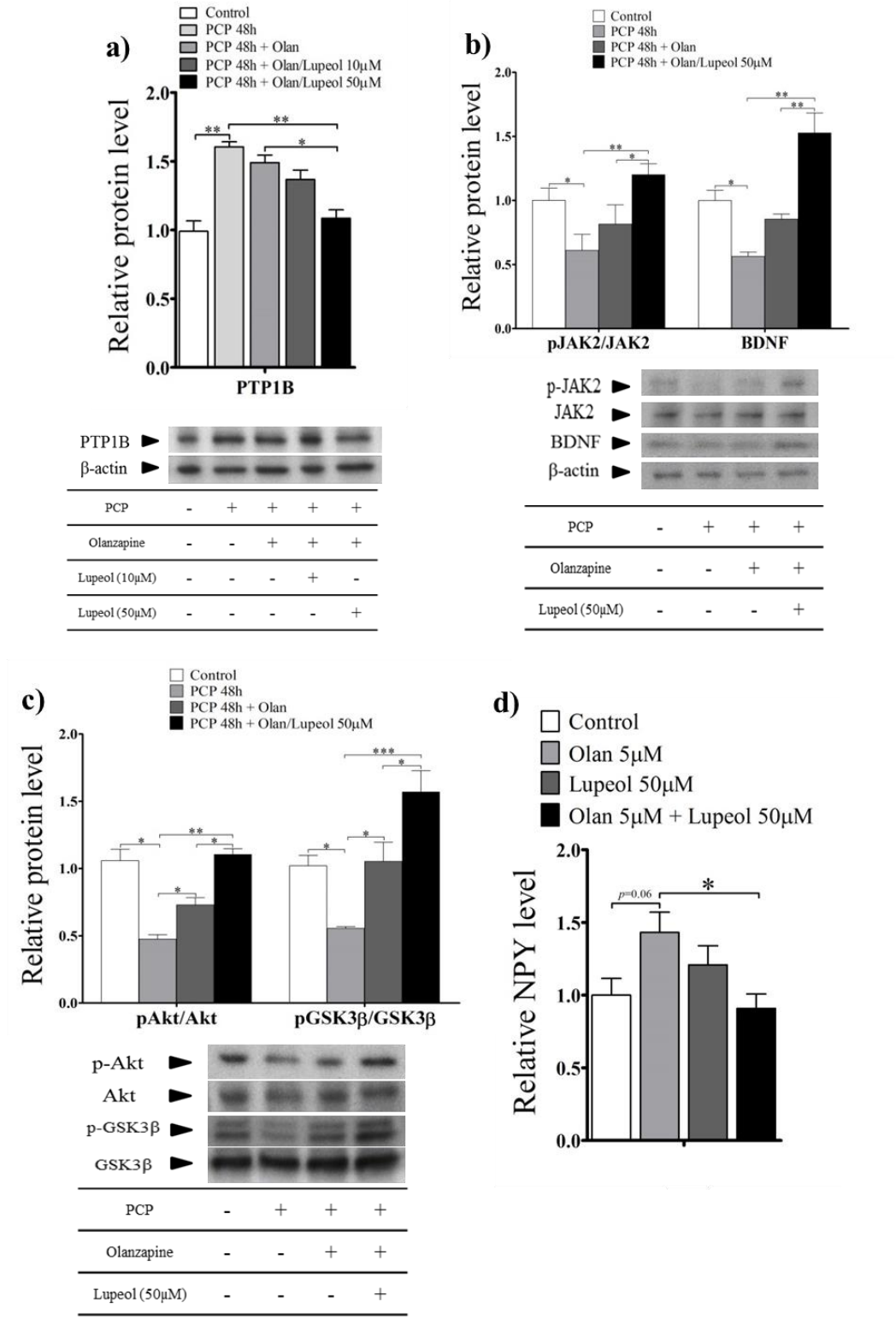
a)
Control
PCP 48h
PCP 48h + Olan
PCP 48h + Olan/Lupeol 10μM
PCP 48h + Olan/Lupeol 50μM
Relative protein level
PTP1B
PTP1B
β-actin
PCP
Olanzapine
Lupeol (10μM)
Lupeol (50μM)
b)
Control
PCP 48h
PCP 48h + Olan
PCP 48h + Olan/Lupeol 50μM
Relative protein level
pJAK2/JAK2
BDNF
p-JAK2
JAK2
BDNF
β-actin
PCP
Olanzapine
Lupeol (50μM)
c)
Control
PCP 48h
PCP 48h + Olan
PCP 48h + Olan/Lupeol 50μM
Relative protein level
pAkt/Akt
pGSK3β/GSK3β
p-Akt
Akt
p-GSK3β
GSK3β
PCP
Olanzapine
Lupeol (50μM)
d)
Control
Olan 5μM
Lupeol 50μM
Olan 5μM + Lupeol 50μM
Relative NPY level
p=0.06

Fig.6

`

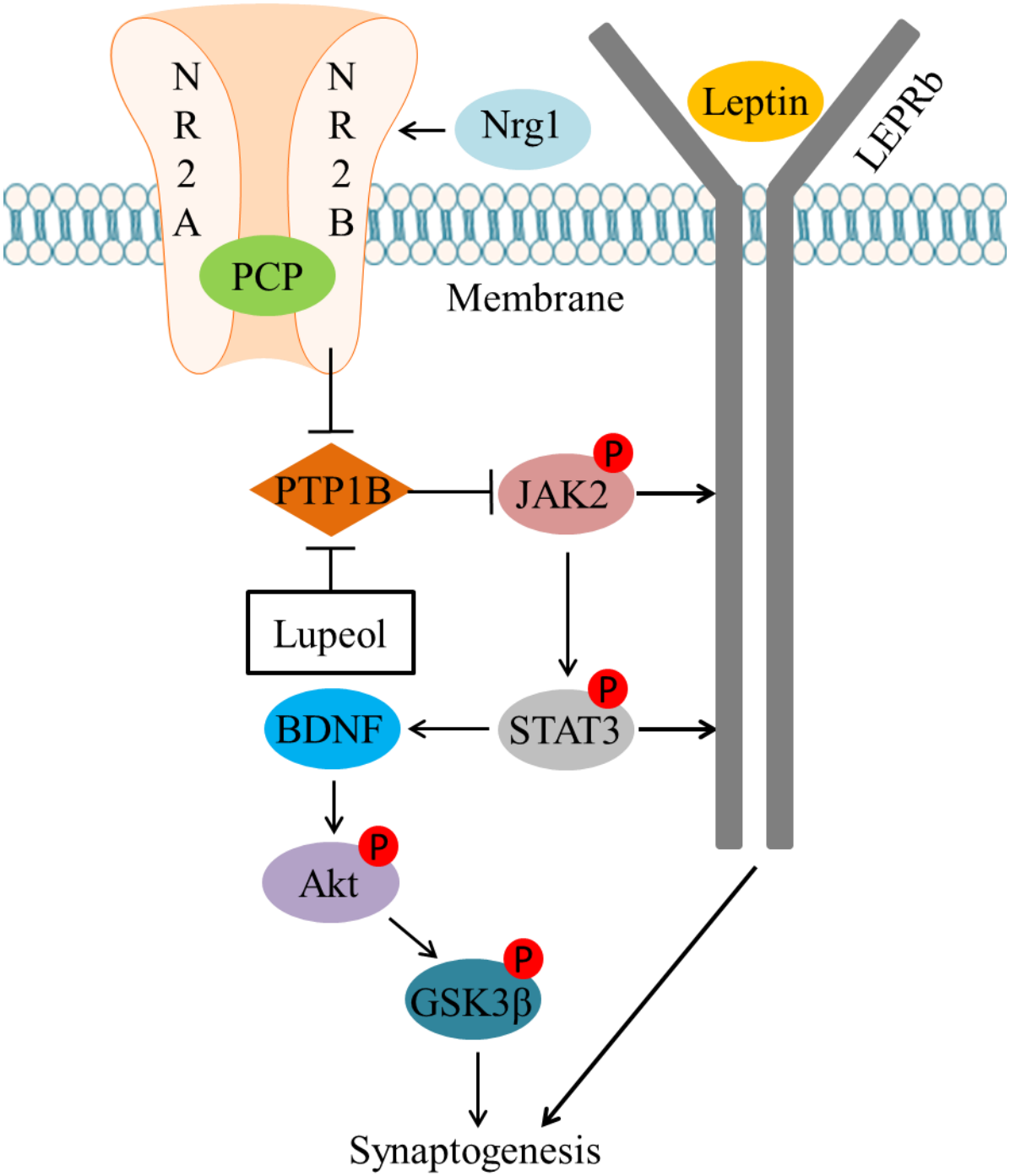
NR2A
NR2B
Nrg1
Leptin
LEPRb
PCP
Membrane
PTP1B
JAK2
P
Lupeol
BDNF
STAT3
P
Akt
P
GSK3β
P
Synaptogenesis

Fig.7

`

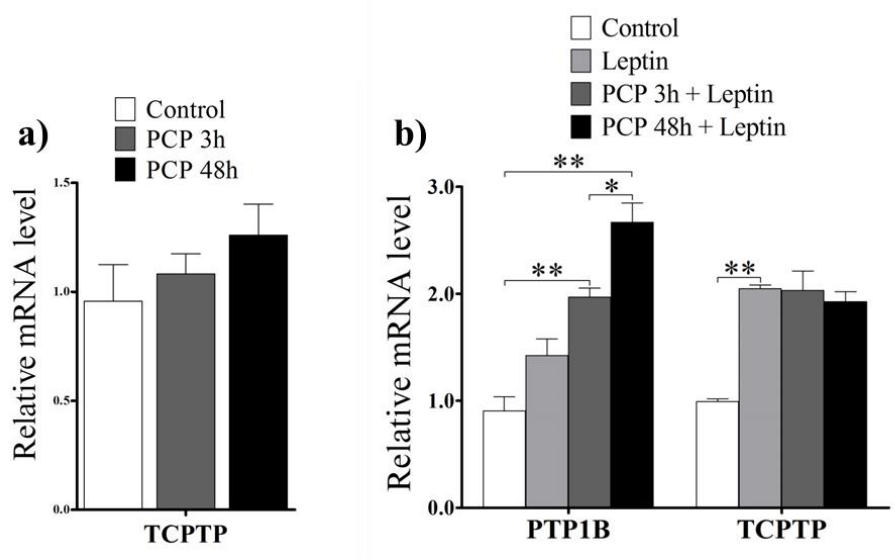


Fig.S2: PCP significantly increased PTP1B mRNA level but not TCPTP mRNA level. a: RT-PCR analysis showed that neither PCP 3-h nor 48-h treatment increased TCPTP mRNA expression (n=6). B): Both PCP 3-h and 48-h treatments increased PTP1B but not TCPTP mRNA expression following leptin stimulation (n=6). Data are presented as mean ± SEM, *$p<0.05$, **$p<0.01$.

`

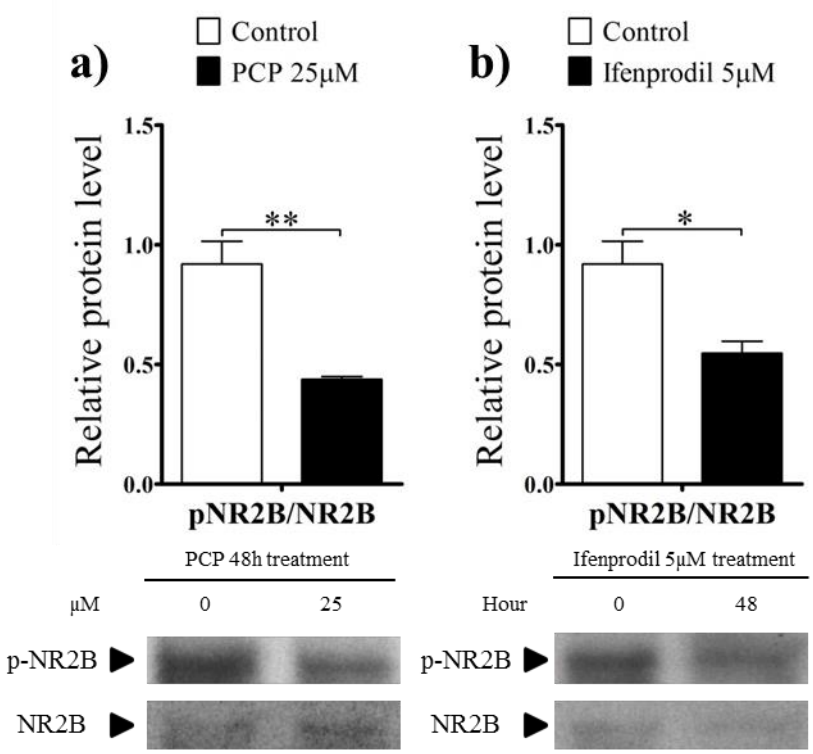


Fig.S3: a): 25 μM PCP for 48h inhibited NR2B phosphorylation. b): 5 μM Ifenprodil for 48h reduced NR2B phosphorylation. Data are presented as mean ± SEM (n=6). *p<0.05, **p<0.01.

`

# Chapter Four

---

A label-free and high-throughput separation of neuron and glial cells using an inertial microfluidic platform



Available at: http://scitation.aip.org/content/aip/journal/bmf/10/3/10.1063/1.4949770

Statement from co-authors

This is to attest that the PhD candidate, Tiantian Jin, contributed significantly to the investigation

**JIN, T.**, YAN, S., ZHANG, J., YUAN, D., HUANG, X.-F*. & LI, W*. A label-free and high-throughput separation of neuron and glial cells using an inertial microfluidic platform. Biomicrofluidics, 10, 034104.

Tiantian Jin designed and performed the experimental work, analysed the data, interpreted results, and wrote the manuscript. YAN, S., ZHANG, J. are authors of equal contributors. YUAN, D participates in data collection and analysis. X.-F* & LI, W* are supervisors, who have provided comments on experimental design, data analysis, results interpretation, and revision of manuscripts.

Tiantian Jin:

Sheng Yan:

Jun Zhang:

Dan Yuan:

Weihua Li:

Xu-Feng Huang:

# A label-free and high-throughput separation of neuron and glial cells using an inertial microfluidic platform

Tiantian Jin, Sheng Yan, Jun Zhang, Dan Yuan, Xu-Feng Huang, and Weihua Li

Citation: Biomicrofluidics **10**, 034104 (2016); doi: 10.1063/1.4949770
View online: http://dx.doi.org/10.1063/1.4949770
View Table of Contents: http://scitation.aip.org/content/aip/journal/bmf/10/3?ver=pdfcov
Published by the AIP Publishing

BIOMICROFLUIDICS **10**, 034104 (2016)

# A label-free and high-throughput separation of neuron and glial cells using an inertial microfluidic platform

Tiantian Jin,[1,a)] Sheng Yan,[2,a)] Jun Zhang,[2,a)] Dan Yuan,[2]
Xu-Feng Huang,[1,b)] and Weihua Li[2,b)]
[1]*Centre for Translational Neuroscience, School of Medicine, University of Wollongong, and Illawarra Health and Medical Research Institute (IHMRI), Wollongong, New South Wales 2522, Australia*
[2]*School of Mechanical, Materials and Mechatronic Engineering University of Wollongong, Wollongong, New South Wales 2522, Australia*

(Received 9 March 2016; accepted 3 May 2016; published online 12 May 2016)

While neurons and glial cells both play significant roles in the development and therapy of schizophrenia, their specific contributions are difficult to differentiate because the methods used to separate neurons and glial cells are ineffective and inefficient. In this study, we reported a high-throughput microfluidic platform based on the inertial microfluidic technique to rapidly and continuously separate neurons and glial cells from dissected brain tissues. The optimal working condition for an inertial biochip was investigated and evaluated by measuring its separation under different flow rates. Purified and enriched neurons in a primary neuron culture were verified by confocal immunofluorescence imaging, and neurons performed neurite growth after separation, indicating the feasibility and biocompatibility of an inertial separation. Phencyclidine disturbed the neuroplasticity and neuron metabolism in the separated and the unseparated neurons, with no significant difference. Apart from isolating the neurons, purified and enriched viable glial cells were collected simultaneously. This work demonstrates that an inertial microchip can provide a label-free, high throughput, and harmless tool to separate neurological primary cells. *Published by AIP Publishing.* [http://dx.doi.org/10.1063/1.4949770]

## I. INTRODUCTION

Schizophrenia is a globally challenging brain disorder that affects about 0.5%–1% of the general population.[1] People diagnosed with schizophrenia suffer from hallucinations, delusions, thought disorders, and cognitive deficits.[2] Previous neuropathological studies suggested that serious deficits in the neuronal processes and neuronal synaptic connectivity contribute to schizophrenia,[3] which is why the role of neurons in brain regions is of high interest in investigating cognitive and affective impairments in schizophrenia. One huge challenge is to separate neurons from complex cell mixtures dissected from brain tissues because the primary neuron culture is a widely applied experimental method for isolating neurons that closely mimics the physiological status of neurons *in vivo*. However, the traditional method makes it difficult to distinguish neurons from glial cells that normally outnumber neurons in mammalian brain tissues.[4]

The traditional method for pure neuron and pure glial cell cultures is a medium-based procedure where a NeuroBasal medium with FDU (5-Fluoro-2′-deoxyuridine) to inhibit glial cells for long term incubation is widely used.[5–7] However, this method needs long term incubation with chemical treatment, which is a huge waste of time and experimental materials. Meanwhile, Dulbecco's Modified Eagle's Medium (DMEM) is the most commonly used medium for glial cell culture or non-neuron cell culture.[5,8,9] Some studies have suggested that

[a)]T. Jin, S. Yan, and J. Zhang contributed equally to this work.
[b)]Authors to whom correspondence should be addressed. Electronic addresses: weihuali@uow.edu.au and xhuang@uow.edu.au.

DMEM may also be suitable for primary neuron culture,[10] and therefore separating neuron and glial cells by the traditional medium-based methods is difficult and inefficient.

Apart from medium-based separation methods, immune-specific separation is significant in neuron-related research. The fluorescence-activated cell sorting (FACS) and magnetically activated cell sorting (MACS) have been broadly applied in a biological laboratory for sorting cells.[11] However, labelling target cells requires several time consuming and labour intensive steps, and more importantly, applying antibodies to label cells for separation may further disturb the immunochemistry analysis on targets of interest. Microfluidic technology has increasingly become a versatile tool to control the neuronal microenvironment precisely whilst selectively probing for axons of neurons in a reproducible fashion.[12–14] Dielectrophoresis (DEP) that distinguishes cells by their dielectric properties is a label-free technique for neuronal and glial cells separation. Prasad *et al.*[15] presented a $4 \times 4$ micro-electrode array microchip to isolate and relocate individual neurons from hippocampal cells using DEP. Zhou *et al.*[16] recently described the separation of embryonic mouse hippocampal neurons from a co-culture of glial cells using multi-electrode arrays, but these devices require a low conductivity DEP buffer, which is not bio-compatible. Furthermore, these devices normally run in a batch manner and with a very limited throughput. Apart from DEP, Wu *et al.*[17] also reported on the application of viscoelasticity tuned hydrodynamic spreading on neural cell separation where the microfluidic device works in a continuous and label free manner. Their device could achieve high viability neural cell separation independent of medium dielectric properties. However, the flow rate (20 $\mu$l/h) and the throughput ($3 \times 10^4$ cells/h) are still not satisfactory, and therefore need further improvement.

There is an urgent need for a high-throughput technique that can continuously separate neurons and glial cells in a culture medium to bridge this gap for neuroscience. Inertial microfluidics is a very promising candidate due to its high throughput and simple structure, as well as being independent of the conductivity of the medium, and compatible with the cell culture medium. It has been widely used to extract blood plasma,[18,19] isolate circulating tumour cells (CTCs),[20–22] and separate leukocytes from blood.[23]

We therefore propose to use the inertial microfluidic technique to separate hypothalamic neurons and glial cells. Recent studies have revealed a hypothalamic structural abnormality and alternating neuropeptides in schizophrenia,[24–26] indicating that the hypothalamus may have a role in schizophrenia pathology and treatment. Compared with conventional protocol that isolates hypothalamic neurons at the expense of the apoptosis of glial cells using specific chemicals, this inertial microchip can simultaneously collect purified viable neurons and glial cells in a label-free, rapid, and continuous fashion, which shortens and simplifies the cell preparation process.

## II. METHODS AND MATERIALS

### A. Overall workflow

Hypothalamic tissues were dissected from postnatal one day C57BL/6 mice ($n = 6$). Brain tissues were then digested to collect cell suspensions that were then transferred into an inertial microchip for separation. Cell suspensions were collected from the outlet middle and outlet aside, respectively, and then immunostaining was performed to evaluate the separation performance. In addition, cells collected from the outlet middle were also plated into poly-D-lysine-coated coverslips in a 24-well plate in culture medium and maintained at 37 °C with 5% $CO_2$ (Fig. 1(a)).

### B. Mechanism

The inertial separation of neuron and glial cells in a serpentine channel is based on our previous study regarding differential equilibrium positions in the serpentine channel for different sized micro-particles.[27] Three inertial effects (or forces) are exerted onto micro-particles flowing in a serpentine channel: the inertial lift forces, secondary flow drag, and centrifugal force.[28] When the medium density is very close to the particles, the effect of centrifugal force is

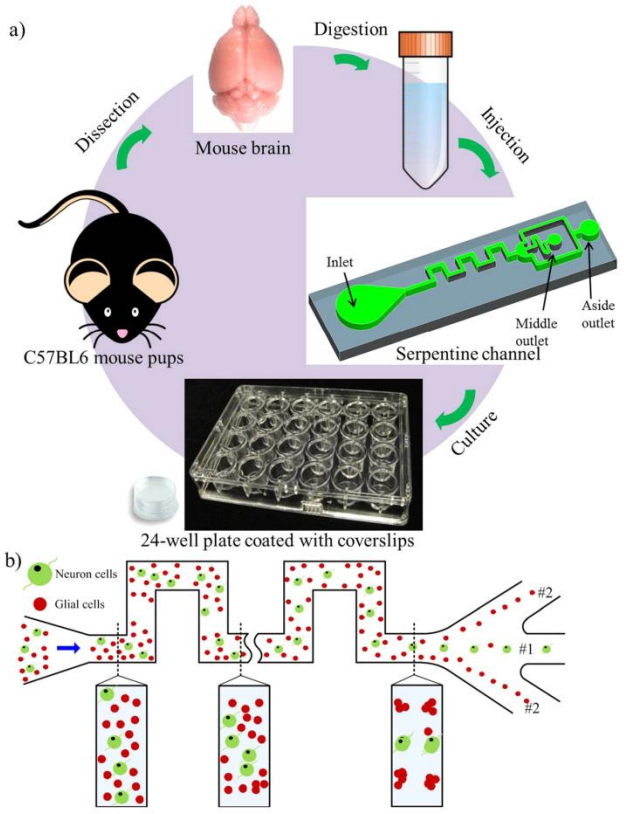


FIG. 1. (a) Overall workflow of the device, including the dissection of mouse pups, trypsinization of mouse brains, injection of cells into the inertial microchip, and culturing separated cells for various downstream immunostaining and PCP tests. (b) Schematics of inertial separation of neuron and glial cells in the inertial microchip with a symmetrical serpentine channel. Large neuron cells migrate into the outlet middle, while most of the smaller glial cells are collected in the outlet aside.

negligible because the inertial lift forces focus cells towards the two sidewalls, while secondary flow in the serpentine channel with alternating curvature pinches cells into the centre of the channel. Therefore, the final focusing position of cells is determined by the relative strength of the inertial lift forces and the secondary flow drag; large cells experiencing a much stronger secondary flow drag force are prone to migrate into the centre of the microchannel under a certain flow region, whilst small cells are mostly focused near the two sidewalls because they experience much stronger inertial lift forces than the secondary flow drag. A previous study based on human post mortem tissue indicated that the somas of neuronal cells are 4.7–22.4 $\mu$m in diameter, while the somas of glial cells are only 2.6–8.7 $\mu$m in diameter.[29] Although there is a size overlap (4.7–8.7 $\mu$m) between these two kinds of cells, there is a significant difference in size between neurons and glial cells, so by selecting a suitable flow condition, neuronal cells experience a dominant secondary flow drag and can be focused at the centre of the serpentine channel. Moreover, glial cells simultaneously experience a dominant inertial lift force and focus at the two sidewalls, and therefore neurons and glial cells can be separated efficiently by collecting the corresponding particle streams, as shown schematically in Fig. 1(b).

### C. Design and fabrication

The serpentine channel used in our experiments consists of 15 zigzag periods; the channel has a uniform 42 $\mu$m depth, and the length and width of each U-turn are 700 $\mu$m. The microchannel is 200 $\mu$m wide. A trifurcating outlet at the end of the channel is implemented at the end of the serpentine channel. Two-sided symmetrical bifurcations are combined into a single outlet to simplify the collection of two-sided streams. The microfluidic device was fabricated by the standard photolithography and soft lithography techniques.[30]

### D. Device preparation

Prior to these cell experiments, the device was rinsed with phosphate buffered saline (PBS) at 100 $\mu$l/min for 10 min using a syringe pump (Legato 100, Kd Scientific), after which the devices were sterilised through exposure to UV light for 30 min.

### E. Cell separation

Hypothalamic cell cultures were prepared according to previous literature and protocols,[5,6] and hypothalamic sections were dissected from postnatal one day C57BL/6 mice. Hypothalamic tissues were digested and triturated to suspend cells in 7 ml culture medium. A 2 ml cell suspension was kept as an inlet group for comparison, while the other 5 ml hypothalamic cell suspension was infused into the inertial microchip to perform separations under different flow rates. Separated cells were collected from the outlet middle and outlet aside, respectively, under three typical flow rates to compare the separation performance. After determining the optimal flow rate, cells separated from the optimal flow rate were used for further culture and tests. To evaluate separation performance, the purity of separation and the enrichment ratio were measured. Separation purity is defined as the ratio of the number of target cells to the total number of cells, while enrichment is defined as the concentration ratio between the target cells from the outlet to the target cells from the inlet.

### F. Mouse hypothalamic neuron culture

A culture medium was modified for neuron incubation based on the Johns Hopkins online protocol;[6] this culture medium generally consists of a NeuroBasal medium with an additive B27 and extra glucose and glutamine. Cells from inlet and outlet middle were plated into poly-D-lysine (P6407, Sigma-Aldrich) coated coverslips in a 24-well plate and maintained at 37 °C with 5% $CO_2$. To examine their rate of growth, neurons were collected after 10 days of incubation (DIV 10) for immunofluorescence and image analysis. To determine how well the cell responded to phencyclidine (PCP) stimulations, neurons at DIV 10 were administered with 25 $\mu$M PCP (P3209, Sigma-Aldrich) for 3 h and 48 h and were then collected for immunofluorescence and image analysis.

### G. Immunofluorescence and image analysis

For immunofluorescence staining, cells from the outlet middle and outlet aside, as well as further cultured neurons from the outlet middle, were fixed with 4% paraformaldehyde in Dulbecco's PBS for 30 min at room temperature. These samples were further incubated with 100% methanol for 20 min at −20 °C and then blocked with 5% goat serum in PBS for 1 h at 37 °C, and then anti-NeuN antibody (MAB377, Merck Millipore), anti-microtubule-associated protein 2 (MAP2) antibody (M9942, Sigma-Aldrich), anti-glial fibrillary acidic protein (GFAP) antibody (G9269, Sigma-Aldrich), and anti-brain derived neurotrophic factor (BDNF) antibody (SC-20981, Santa-cruz) were applied overnight at 4 °C. GFAP and BDNF were visualised with isotype-specific goat anti-rabbit IgG (H + L) secondary antibody conjugated with Alexa Fluor 488 (A11008, ThermoFisher). NeuN and MAP2 were visualised by goat anti-mouse IgG (H + L) secondary antibody conjugated to Alexa Fluor 594 (A11004, ThermoFisher). The concentrations of antibodies were applied according to the manufacturers' manuals. A confocal

microscope (Leica TCS SP5 Advanced System, Leica Microsystems) was used to obtain fluorescent images of the stained cells, while software Image J with plugin NeuriteQuant[31] was used to quantify the immunoreactivity.

### H. Statistical analysis

Data were analysed using the SPSS statistical package (SPSS.19, IBM). A two-tailed t test was applied to analyse the separation of different flow rates, variations in cell concentration between the inlet, outlet middle, and outlet aside, neuron enrichment and neuron purity from the outlet middle, glial cell enrichment and glial cell purity from the outlet aside, and neurite length and neurite branches. A one way analysis of variance (ANOVA) and the *post-hoc* Tukey-Kramer honestly significant difference (HSD) test were used to study the response of neurons to PCP stimulations. A $p$ value $<0.05$ was regarded as statistically significant. The values in Fig. 2 were expressed as mean $\pm$ SD, and the values in Figs. 3–5 were showed as mean $\pm$ SEM.

## III. RESULTS

### A. The effect of flow rates on size-based cell separation

A digested cell suspension was processed under three typical flow conditions to investigate how the flow rates affected the separation. The unprocessed cell suspension was taken as an inlet (control) group. Cells from the inlet group and two outlet groups were counted in a hemocytometer and their sizes were measured. Since the inlet group contained neuronal and glial cells, the cell size distribution was quite broad. The average cell size was 7.4 $\mu$m, with a standard deviation of 3.2 $\mu$m (Table I). Fig. 2(a) and Table I show that most neuronal (MM) and glial cells (MA) could be separated according to their size under a flow rate of 550 $\mu$l/min, a flow condition in which a distinct size threshold of ~6 $\mu$m could be interpreted. Cells that were above this threshold were prone to be collected by the outlet middle collection (Fig. 2(a), MM); their average size was $9.9 \pm 1.8$ $\mu$m (Table I). Cells below this threshold were mostly collected from the outlet aside (Fig. 2(b), MA), and they had mean sizes of $4.6 \pm 1.0$ $\mu$m (Table I). Note that a tiny part of the small cells was still inevitably collected in the outlet middle collection, indicating the possible existence of glial cells. Although a perfectly pure collection of neurons cannot be expected via this inertial microchip, a much purer neuron cell suspension could be achieved, with most glial cells depleted.

However, for the high flow rate of 750 $\mu$l/min, even though there was a distinct threshold for cell separation according to Fig. 2(a), the cell size distribution from middle collection (HM) was rather large ($8.9 \pm 2.5$ $\mu$m; Table I), indicating that more glial cells had been collected under this condition (Fig. 2(b)). Small cells tended to become defocused due to the mixing effects of secondary flow under such a high flow speed and were distributed almost uniformly along the width of the channel, and therefore a large part of glial cells were collected by the outlet middle. At a low flow rate of 350 $\mu$l/min, the cells could not be separated according to the size because the large and small cells were both focused along two sides of the channel and collected by the outlet aside (Fig. 2, Table I, LA). Cells collected by the outlet middle were those that had randomly escaped from the cell focusing streaks (Fig. 2, LM). Based on these results, a moderate flow rate of 550 $\mu$l/min was chosen to separate the neuronal and glial cells in the following tests. Cell suspensions were collected to perform immunofluorescence staining to confirm the separation effect and then incubated for 10 days to examine neuron growth and response to PCP stimulations.

### B. Enriched and purified neurons and glial cells by inertial separation

Our optimization experiments suggested that a moderate flow rate (550 $\mu$l/min) was the optimal working condition for separating cells, but for further confirmation, equal volumes (1 ml) of cells were collected from the inlet, outlet middle, and outlet aside for immunostaining immediately after separation. An anti-NeuN antibody was applied to detect neurons and an

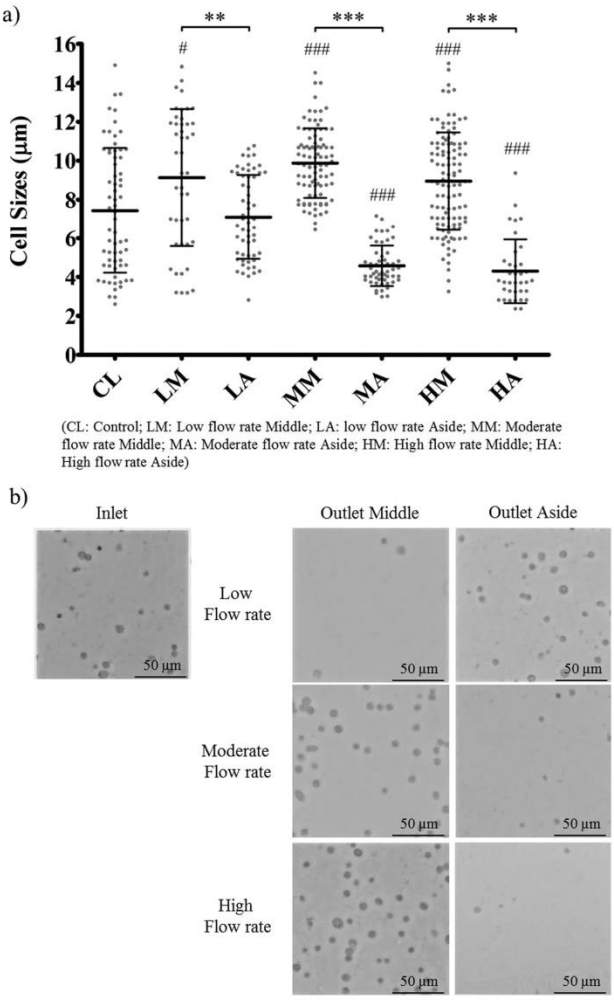


FIG. 2. Separation of neuronal and glial cells by an inertial microchip under three typical flow rates. (a) Size distribution of cells from inlet (control, CL), and two collections from outlet middle (LM, MM, and HM) and outlet aside (LA, MA, and HA) under three typical flow conditions. The first letter L, M, and H mean three different flow rates L (low, 350 $\mu$l/min), M (moderate, 550 $\mu$l/min), and H (high, 750 $\mu$l/min). The second letter M and A indicates collection positions middle and aside, respectively. Data represent mean ± SD (n = 5). A two-tailed t test was applied. # $p < 0.05$, ### $p < 0.001$ represented outlet groups versus control group; ** $p < 0.01$, *** $p < 0.001$ was used between the outlet middle and outlet aside in each flow rate group. (b) Images of cells from the inlet (control, CL), and two collections from the outlet middle and outlet aside under the three flow conditions.

anti-GFAP antibody was applied to stain astrocytes, which is the major cell type of glial cells. The immunofluorescence results confirmed that most cells in outlet middle were neurons (Fig. 3(a)), with a purity as high as 92 ± 1.5%; this was much higher than the 58 ± 5.4% in the inlet (Fig. 3(b)). In addition, the glial cells increased in purity from 36 ± 5.2% in the inlet to 81 ± 1.4% in the outlet aside (Fig. 3(c)), indicating much purer neuron and glial cells.

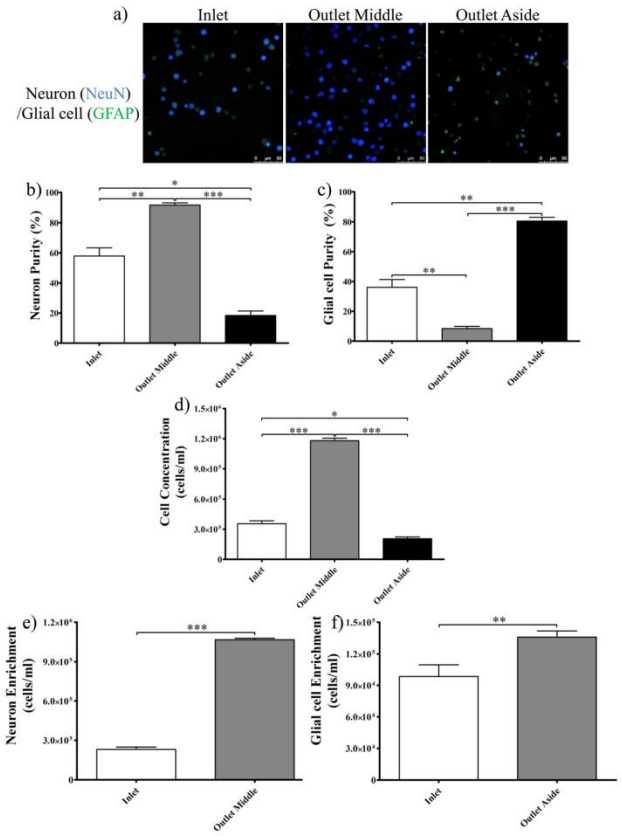


FIG. 3. Inertial separation of neuronal and glial cells at the optimal flow condition (550 $\mu$l/min). (a) Cells collected from the inlet, outlet middle, and outlet aside were stained by neuron marker NeuN (blue) and astrocyte marker GFAP (green) after separation. (b) Purity of neuronal cells in the inlet (control), outlet middle, and outlet aside. (c) Purity of glial cells in the inlet (control), outlet middle, and outlet aside. (d) Concentrations of cells in the inlet, outlet middle, and outlet aside. (e) Enrichment of concentrated neurons in the outlet middle. (f) Enrichment of glial cell astrocytes in the outlet aside. Data represent mean ± SEM (n = 5, obtained from 5 independent cultures). A two-tailed $t$ test was applied. * $p < 0.05$, ** $p < 0.01$, *** $p < 0.001$.

Furthermore, the results showed a high level of total cell concentration ($1.2 \times 10^6$ cells/ml) in the outlet middle; this is a 3.3-fold increase compared to a cell concentration of ($3.6 \times 10^5$ cells/ml) in the inlet (Fig. 3(d), indicating cell enrichment by separation. Considering the enhanced purity of neurons from the inlet to outlet middle, neurons were enriched from $2.3 \times 10^5$ cells/ml in the inlet to $1.07 \times 10^6$ cells/ml in the outlet middle (Fig. 3(e)). For glial cells, although the total cell concentration in the outlet aside ($2.1 \times 10^5$ cells/ml) is lower than the inlet (Fig. 3(d)), the glial cell astrocytes were still enriched from $9.8 \times 10^4$ cells/ml (inlet) to $1.36 \times 10^5$ cells/ml (outlet aside) due to higher purity in the outlet aside (Fig. 3(f)).

### C. Influence of inertial separation on neuron growth

The features of neurons are the growth of neurites and synaptogenesis. After microfluidic separation under a moderate flow rate, equal volumes (1 ml) of cells from the inlet (control)

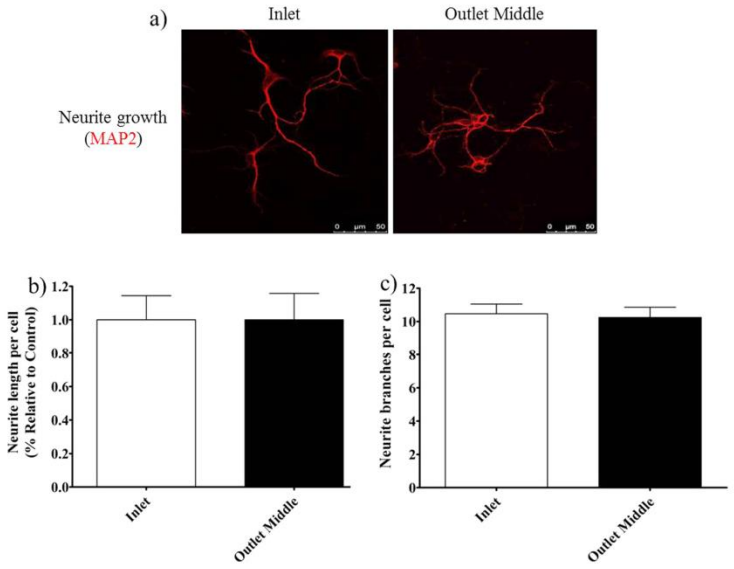


FIG. 4. Neurite growth of neuronal cells in the inlet (unprocessed) and outlet middle after inertial separation. (a) Fluorescent images of neurite growth of neurons in the inlet and outlet middle after inertial separation. Neurons collected from the inlet and outlet middle were stained by structural protein marker MAP2 (red) to label neurite synapses and dendrites. (b–c) There is no difference in the length and branches of neurites per cell in the inlet and outlet middle groups. Data represent the mean ± SEM (n = 5, obtained from 5 independent cultures). A two-tailed *t* test was applied, and there was no statistical difference between the two groups.

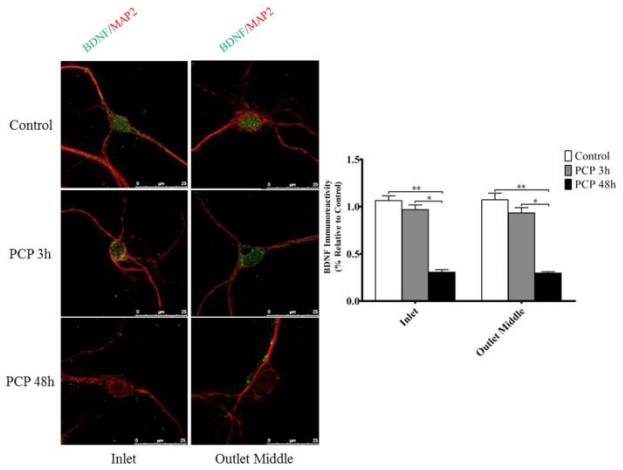


FIG. 5. BDNF expressions were inhibited in neurons from the inlet and outlet middle after treatment with PCP. There are no differences in the responses to PCP stimulations for neurons at the inlet and outlet middle. Data represent mean ± SEM (n = 5, obtained from 5 independent cultures). Significance was calculated by ANOVA and the *post-hoc* Tukey-Kramer HSD test. * $p < 0.05$, ** $p < 0.01$ versus control (without PCP).

TABLE I. List of cells' average size and standard deviation from the inlet (control) and two outlets under three different flow rates (LM: low flow rate middle; LA: low flow rate aside; MM: moderate flow rate middle; MA: moderate flow rate aside; HM: high flow rate middle; HA: high flow rate aside).

| | CL | LM | LA | MM | MA | HM | HA |
|---|---|---|---|---|---|---|---|
| Mean ($\mu$m) | 7.4 | 9.1 | 7.1 | 9.9 | 4.6 | 8.9 | 4.3 |
| SD ($\mu$m) | 3.2 | 3.5 | 2.2 | 1.8 | 1.0 | 2.5 | 1.7 |

and outlet middle were collected and incubated to investigate how inertial separation affected the growth of neurons. Since MAP2 is a neuron-specific cytoskeletal protein that can be stained to detect neuron soma, synapses, and dendrites, MAP2 antibody immunostaining was applied to the inlet group and outlet middle group at DIV 10 to characterise neuron morphology. Image J with plugin NeuriteQuant[31] was used to examine the growth and synaptogenesis of neurite by calculating its length and branches. The results confirmed that neurons from both groups generated the same neurite growth (Fig. 4(a)), and there was no statistical difference between the two groups in the length of neurites per cell (Fig. 4(b)) and their branches per cell (Fig. 4(c)). Therefore, the inertial separation of neuron cells does not have a negative influence on the growth of neurons.

### D. Influence of inertial separation on the response of neurons to PCP stimulations

To demonstrate that neurons separated from the inertial microchip could be an ideal platform for further biological studies, cells from the inlet (control) and outlet middle at DIV 10 were exposed to PCP for acute stimulations for 3 h and chronic stimulations for 48 h, respectively. PCP has been studied extensively for decades because it can mimic symptoms in patients diagnosed with schizophrenia. Previous research has confirmed that PCP can impact on the metabolism and neurochemistry of the brain regions in a time manner.[32] Immunostaining was applied to detect the expression of BDNF, an important neurotrophic factor for neuroplasticity and neuron metabolism. In the outlet middle neurons, BDNF expression decreased partly in acute treatment and then significantly reduced during chronic treatment (Fig. 5). The same results were also observed in the inlet neurons, which means that separation did not have a negative effect on the biological response of neurons to PCP stimulations; it further proves that the inertial device did not harm the neuron cells and the processed neuronal cells were healthy and functional. The total residual time of individual neurons in the serpentine channel of inertial microchip was estimated to be 15 ms, which shortened the time that neurons were exposed to shear stress, and may be why there is no negative influence on the biophysical characteristics of separated neurons for protein expressions.

## IV. DISCUSSION

Here, we developed a modified protocol using an inertial microchip to continuously separate neurons and glial cells. This proposed microfluidic platform was based on size-dependent separation. Cells collected from the outlet middle of the micro-channel were characterised as large cells (Fig. 2) with increased concentration, and we confirmed that these large cells were neurons by immunostaining (Fig. 3(a)), and therefore plated neurons from the outlet middle were enriched and purified (Figs. 3(b) and 3(e)). In the traditional medium-based method, neurons are mixed with glial cells where neurons with a low purity are used for incubation and further experiments. Our proposed method makes the primary cell culture more efficient by collecting more purified neuron samples at once, while the device can process 5 ml of cell suspension within 10 min, thus speeding up the preparation of samples. In addition, our method avoids using extra brain tissues and culture mediums that not only saves many samples but also meets the requirement of animal ethics, which suggests a minimal number of animals to be sacrificed. Moreover, separated neurons were as healthy and functional as unprocessed ones, and

there was no significant variation of in the growth and synaptogenesis of neurite caused by the inertial separation procedure (Fig. 4). Moreover, the PCP treatment of unprocessed cells from the inlet and processed cells from the outlet middle displayed the same biological responses, thus demonstrating the biocompatibility of the separation procedure. The continuity of cell separation and short residual time in the channel minimised any unexpected shear-induced effects to the neuronal phenotype. This is critical for the subsequent molecular characterisation of biological functions or gene expression of specific drug therapy. Therefore, this platform is a robust, efficient, and harmless tool for separating primary neuron cells.

Inertial separation is very important for future research into schizophrenia because applying an inertial microchip helps to separate neurons and isolate glial cells. As mentioned above, most cells from the outlet aside were small in size (Fig. 2), and further staining experiments indicated that they were mainly enriched and purified astrocyte type glial cells (Figs. 3(c) and 3(f)). Astrocytes were only examined by staining with anti-GFAP antibody because astrocyte is the major component of glial cells, although there was around 5% of unstained glial cells, including microglia and oligodendrocyte. Note also that the total number of glial cells was less than the number of neurons in the inlet sample because the mice pups were sacrificed in postnatal day 1 to ensure the health and activity of neurons. Meanwhile, the glia/neuron ratio was low in the first postnatal week, but it will increase significantly during the second and third postnatal weeks.[33] A new perspective has recently appeared suggesting that the dysfunction of glial cells due to astrocyte is also involved in the neuropathology of schizophrenia,[34] because it is the most numerous source of glial cells in mammalian brains. Various reports have revealed that altered density and genes due to expressions of astrocytes are strongly related to schizophrenia.[34] For example, astrocyte has a protein called S100B, of which there is a significant amount in schizophrenia patients,[35] which makes astrocyte a promising biomarker to predict first episode schizophrenia in the future.[36] Therefore, glial cells have become a major source to supply pathophysiological significance and possible therapeutic target. To investigate the individual contributions made by glial cells in the mechanism and treatment of schizophrenia, our advanced inertial microchip is a promising candidate for isolating glial cells from primary cell cultures.

Furthermore, the current microfluidic approaches for separating neurons and glial cells are mostly based on DEP, where cells of interest are trapped at the micro-electrodes in DEP devices, whereas the inertial microchip here can separate neurons and glial cells in a continuous manner. Compared to the fluid velocity of DEP device ($< 10\,\mu$m/s),[16] cells passed through the microchannel in the inertial microchip at $\sim$1 m/s, which significantly increased the processing speed and throughput. The throughput of our inertial microchip is $1.188 \times 10^7$ cells/h, which is a significant improvement compared to using viscoelasticity tuned hydrodynamic spreading.[17] Although the throughput of the inertial chip is slower than the FACS, the throughput capability of our proposed device can be dramatically amplified by parallelizing several microchannels in the same microchip.[19] Compared to FACS, our inertial device is label-free, which may significantly reduce the total processing time and costs.

## V. CONCLUSIONS

In this work, we have demonstrated continuous, high purity, and harmless neuronal cell separation with an inertial microchip. This inertial microchip can enrich and purify primary neuronal cells with unaltered morphology and biological function, while simultaneously purifying and enriching glial cells. We therefore anticipate that this inertial microchip will be an outstanding plugin to advance the current primary cell separation and culture method for neuroscience.

## ACKNOWLEDGMENTS

This work was supported by the University of Wollongong-China Scholarship Council joint scholarships. W.L., X.-F.H., T.J., S.Y., and J.Z. designed research. T.J., J.Z., S.Y., and D.Y. conducted experiments and analysed the data. T.J., S.Y., and J.Z. wrote the manuscript. All the authors have reviewed the manuscript. Mr. Robert Clayton, Mr. Tanju Yildirim, and the anonymous reviewers helped to polish English.

[1]R. Freedman, New Engl. J. Med. **349**(18), 1738–1749 (2003).
[2]C. A. Ross, R. L. Margolis, S. A. J. Reading, M. Pletnikov, and J. T. Coyle, Neuron **52**(1), 139–153 (2006).
[3]P. J. Harrison and S. L. Eastwood, Hippocampus **11**(5), 508–519 (2001).
[4]B. Connors, M. F. Bear, and M. Paradiso, *Neuroscience—Exploring the Brain*, 3rd ed. (Lippincott Williams & Wilkins, Philadelphia, 2006).
[5]L. G. W. Hilgenberg and M. A. Smith, J. Vis. Exp. **10**, 562 (2007).
[6]Johns Hopkins Medicine, *Dissociated Primary Hypothalamic Neuron Culture* (2015), see http://www.hopkinsmedicine.org/institute_ basic_biomedical_sciences/research_centers/metabolism_obesity_research/protocols/.
[7]G. J. Brewer, J. Neurosci. Methods **71**(2), 143–155 (1997).
[8]J. Saura, J. Neuroinflamm. **4**, 26–26 (2007).
[9]S. Schildge, C. Bohrer, K. Beck, and C. Schachtrup, J. Vis. Exp. **71**, e50079 (2013).
[10]B. A. Barres, Cold Spring Harb. Protoc. **2014**(12), 1342–1347.
[11]A. Radbruch and D. Recktenwald, Curr. Opin. Immunol. **7**(2), 270–273 (1995).
[12]G. M. Whitesides, Nature **442**(7101), 368–373 (2006).
[13]S. Takayama, E. Ostuni, P. LeDuc, K. Naruse, D. E. Ingber, and G. M. Whitesides, Chem. Biol. **10**(2), 123–130 (2003).
[14]S. Rhee, A. Taylor, D. Cribbs, C. Cotman, and N. Jeon, Biomed. Microdevices **9**(1), 15–23 (2007).
[15]S. Prasad, X. Zhang, M. Yang, Y. Ni, V. Parpura, C. S. Ozkan, and M. Ozkan, J. Neurosci. Methods **135**(1–2), 79–88 (2004).
[16]T. Zhou, S. F. Perry, Y. Ming, S. Petryna, V. Fluck, and S. Tatic-Lucic, Biomed. Microdevices **17**(3), 1–14 (2015).
[17]Z. Wu, K. Hjort, G. Wicher, and Å. Fex Svenningsen, Biomed. Microdevices **10**(5), 631–638 (2008).
[18]M. G. Lee, S. Choi, H. J. Kim, H. K. Lim, J. H. Kim, N. Huh, and J. K. Park, Appl. Phys. Lett. **98**(25), 253702 (2011).
[19]J. Zhang, S. Yan, W. Li, G. Alici, and N.-T. Nguyen, RSC Adv. **4**(63), 33149–33159 (2014).
[20]A. J. Mach, J. H. Kim, A. Arshi, S. C. Hur, and D. Di Carlo, Lab Chip **11**(17), 2827–2834 (2011).
[21]H. W. Hou, M. E. Warkiani, B. L. Khoo, Z. R. Li, R. A. Soo, D. S.-W. Tan, W.-T. Lim, J. Han, A. A. S. Bhagat, and C. T. Lim, Sci. Rep. **3**, 1259 (2013).
[22]E. Ozkumur, A. M. Shah, J. C. Ciciliano, B. L. Emmink, D. T. Miyamoto, E. Brachtel, M. Yu, P.-I. Chen, B. Morgan, and J. Trautwein, Sci. Transl. Med. **5**(179), 179ra147 (2013).
[23]L. Wu, G. Guan, H. W. Hou, A. A. S. Bhagat, and J. Han, Anal. Chem. **84**(21), 9324–9331 (2012).
[24]D. Fannon, L. Tennakoon, A. Sumich, S. O'Ceallaigh, V. Doku, X. Chitnis, J. Lowe, W. Soni, and T. Sharma, Brit. J. Psychiatr. **177**, 354–359 (2000).
[25]E. Walker, V. Mittal, and K. Tessner, Annu. Rev. Clin. Psychol. **4**, 189–216 (2008).
[26]H. Bernstein, H. Dobrowolny, and B. Bogerts, Neuropeptide Res. Trends 213–227 (2007).
[27]J. Zhang, S. Yan, R. Sluyter, W. Li, G. Alici, and N.-T. Nguyen, Sci. Rep. **4**, 4527 (2014).
[28]J. Zhang, W. Li, M. Li, G. Alici, and N.-T. Nguyen, Microfluid. Nanofluid. **17**(2), 305–316 (2014).
[29]G. Rajkowska, L. D. Selemon, and P. S. Goldman-Rakic, Arch. Gen. Psychiatry **55**(3), 215–224 (1998).
[30]D. C. Duffy, J. C. McDonald, O. J. A. Schueller, and G. M. Whitesides, Anal. Chem. **70**(23), 4974–4984 (1998).
[31]L. Dehmelt, G. Poplawski, E. Hwang, and S. Halpain, BMC Neurosci. **12**(1), 1–14 (2011).
[32]B. J. Morris, S. M. Cochran, and J. A. Pratt, Curr. Opin. Pharmacol. **5**(1), 101–106 (2005).
[33]F. Bandeira, R. Lent, and S. Herculano-Houzel, Proc. Natl. Acad. Sci. U.S.A. **106**(33), 14108–14113 (2009).
[34]H.-G. Bernstein, J. Steiner, and B. Bogerts, Expert Rev. Neurother. **9**(7), 1059–1071 (2009).
[35]M. Rothermundt, P. Falkai, G. Ponath, S. Abel, H. Burkle, M. Diedrich, G. Hetzel, M. Peters, A. Siegmund, A. Pedersen, W. Maier, J. Schramm, T. Suslow, P. Ohrmann, and V. Arolt, Mol. Psychiatr. **9**(10), 897–899 (2004).
[36]S. Yelmo-Cruz, A. L. Morera-Fumero, and P. Abreu-Gonzalez, Psychiatry Clin. Neurosci. **67**(2), 67–75 (2013).

`

# Chapter Five

## 5.1 Overall Discussion

Increasing evidence has confirmed PTP1B as a promising therapeutic target for treating obesity. However, PTP1B traditional inhibitors are targeting the PTP1B active site which is very similar to other PTPs, causing off-target effects and reduced bioavailability. Allosteric inhibition thus becomes a promising alternative strategy to develop selective PTP1B inhibitors. Previous structural and biochemical studies have unveiled the allosteric binding site, and allosteric inhibition aims to disturb PTP1B conformational transition during catalysis and therefore inhibits PTP1B activity (Wiesmann et al., 2004).

In Chapter 2, lupeol and lupane triterpenes including lupenone, betulin and betulinic acid are identified as new PTP1B allosteric inhibitors. Using molecular docking, lupane triterpenes were demonstrated to bind to the PTP1B allosteric site. The performance of molecular dynamics simulations showed the stability of the protein-ligand complex and elucidated the interactions between lupane triterpenes and the PTP1B binding site, indicating the important role of helix $\alpha 7$ and several hydrophobic residues in the binding mode. Moreover, the pentacyclic structure in lupane triterpenes is confirmed as the main contributor to allosteric binding, while the different formation of hydrogen bonds leads to variation of electrostatic forces, which explains the distinction between binding affinity and inhibitory activity among lupane triterpenes. Further enzymatic assays showed that lupane triterpenes specifically inhibited PTP1B over TCPTP. In addition, molecular docking of lupane triterpenes targeting TCPTP was applied. It appeared lupane triterpenes were not binding to TCPTP in the region which is

`

equivalent to the allosteric site in PTP1B. Thus the less-conserved PTP1B allosteric site is an ideal target for lupane triterpenes to inhibit PTP1B activity. Finally, lupane triterpenes showed significant PTP1B activity inhibition effects in neuronal cells with positive bioavailability and less toxicity.

Importantly, there was demonstrated relative consistency between computed data and experimental results in this work. For example, results from binding free energy calculations showed that betulinic acid had a better inhibitory effect than lupeol. Betulinic acid is able to form stronger hydrogen bonding interactions than lupeol and the other two lupane triterpenes, providing stronger electrostatic force, which is consistent with the experimental $IC_{50}$ data. Therefore, this computational modelling is reliable to compare the inhibitory effects between lupane triterpenes derivatives. The structural difference between lupeol and betulinic acid lies in the $R_2$ group which strongly enhance the inhibitory effect of betulinic acid. Considering that the non-polar pentacyclic structure of lupane triterpenes is the premise for binding to the less polar allosteric site, modification of the polar functional group is an alternative choice. Currently all lupane triterpenes are difficult to dissolve in water which limits drug administration, therefore further modification could be focused on increasing hydrophilicity. However, such modifications need careful investigation since this will affect their pharmacokinetic properties. As an important negative regulator modulating food intake, body weight gain and energy homeostasis, PTP1B is an attractive drug target for preventing and treating obesity and its associated metabolic syndromes including diabetes. This study provides a reliable PTP1B allosteric inhibitor discovery platform, with combined computational modelling and biological assays, to develop new PTP1B allosteric inhibitors including lupane triterpenes derivatives with enhanced potency, selectivity and bioavailability.

`

Recent studies have revealed the role of PTP1B in blocking BDNF-mediated signalling and causing impaired neurogenesis in several neurological diseases (Krishnan et al., 2015). Given the prevalence of BDNF reduction in schizophrenia patients, it is crucial to investigate whether PTP1B is involved in impaired neurogenesis in schizophrenia. In Chapter 3, PTP1B level is significantly induced in two schizophrenia-like models, PCP-treated model and NRG1 KO mouse model, both well-established models to mimic the schizophrenia symptoms in humans. PCP, as a well-recognized non-selective NMDAR antagonist, binds equally to NR2A and NR2B subunits (Paoletti and Neyton, 2007). To further investigate the mechanism of PCP induced PTP1B, NR2A specific antagonist PEAQX and NR2B specific antagonist ifenprodil were tested to stimulate PTP1B expression. Results showed that only ifenprodil treatment with reduced NR2B phosphorylation was able to increase PTP1B level. Moreover, the reduction of NR2B phosphorylation and enhanced PTP1B expression was also disclosed in Nrg1 KO mice which supported our finding that NR2B downregulated PTP1B. On the other hand, Nrg1-ErbB4 signalling is required for NR2B phosphorylation (Bjarnadottir et al., 2007). A recent study has reported that PTP1B inhibits TrkB, a crucial regulator which interacts with ErbB4 to modulate Nrg1-induced NR2B phosphorylation (Pandya and Pillai, 2014), indicating that NR2B dephosphorylation induced PTP1B which further inhibited Nrg1-induced NR2B phosphorylation as a negative feedback. Both NR2B deficient and NRG1 gene mutation are important contributors to the risk of schizophrenia (Stefansson et al., 2002, Bjarnadottir et al., 2007), and PTP1B appears to be a crucial factor in the psychopathology.

Moreover, the reduction of BDNF and BDNF-mediated Akt/GSK3β signalling leads to impaired neurogenesis and synaptogenesis, which has been demonstrated in schizophrenia patients (Weickert et al., 2003, Weickert et al., 2005, Favalli et al., 2012)

`

as well as PCP-treated models (Snigdha et al., 2011, Adachi et al., 2013, Katanuma et al., 2014, Zhang et al., 2016). However the mechanism remains unclear. This study proposes that PTP1B regulates the BDNF level and BDNF-mediated Akt/GSK3β signalling in the PCP-treated model. PTP1B has been reported to inhibit TrkB, which is the transmembrane receptor of BDNF (Ozek et al., 2014, Krishnan et al., 2015), and modulates BDNF-mediated Akt/GSK3β signalling. In Chapter 3, elevated PTP1B suppressed pAkt and pGSK3β, and inhibition of PTP1B restored Akt/GSK3β signalling and downstream synaptogenesis. Therefore, PTP1B is able to block Akt/GSK3β signalling and results in impaired neurogenesis and synaptogenesis. This study also revealed that PTP1B directly modulates BDNF level through leptin-mediated JAK2/STAT3 signalling. Leptin stimulates BDNF expression in the dendrites of hypothalamic neurons (Liao et al., 2012), as well as BDNF mRNA in the hypothalamic region (Komori et al., 2006). In Chapter 2, leptin signalling has been confirmed to be inhibited by PCP-induced PTP1B, which directly dephosphorylated JAK2 and blocked leptin-mediated JAK2/STAT3 signalling, leading to the BDNF reduction. Previous studies have suggested that leptin exclusively improves NMDA receptor-regulated synaptic transmission such as the induction of long-term potentiation (Shanley et al., 2001, Harvey et al., 2005, Harvey, 2007), indicating that leptin signalling is capable of improving the NMDA-mediated signalling pathway. The present study showed that NMDA receptor antagonism stimulated PTP1B which affected hypothalamic leptin signalling, indicating the reciprocal interactions between NMDA receptor and leptin signalling pathways. Considering the important role of leptin signalling in controlling food intake, weight gain and energy homeostasis, the disturbed leptin function in the PCP-treated model may explain the prevalence of obesity in schizophrenia patients.

`

Based on the results from Chapter 2, lupeol was identified as a PTP1B allosteric inhibitor which inhibits PTP1B with potency and selectivity over TCPTP. It is worth mentioning that in the PCP-treated model, only PTP1B was increased but not TCPTP, suggesting PTP1B selective inhibition is required for treatment. Therefore, lupeol was applied to the PCP-treated model with or without olanzapine treatment, to investigate the co-treatment effect of PTP1B inhibition and olanzapine. Olanzapine showed no effects on preventing PCP-induced overexpression of PTP1B and reduction of leptin downstream JAK2 and BDNF although BDNF-mediated Akt/GSK3β signalling was restored. However, lupeol inhibited PCP-induced PTP1B expression and the co-treatment of lupeol and olanzapine confirmed improved effects in reversing PCP-induced alterations including reduction of BDNF, Akt/GSK3β signalling, and decreased synaptophysin, mainly due to the PTP1B inhibition-related restoration of JAK2/STAT3 signalling, which stimulated BDNF expression. Importantly, a recent study has shown the interactions between olanzapine-induced weight gain and an elevated orexigenic neurotransmitter, neuropeptide Y (NPY) mRNA level (Weston-Green et al., 2012). The co-treatment of olanzapine and lupeol managed to inhibit the olanzapine-induced NPY level. Therefore, co-treatment of PTP1B inhibitor, lupeol, with olanzapine may enhance olanzapine's treatment efficacy and prevent olanzapine-induced weight gain.

Interest in glia is rising due to increasing evidence supporting the important role of dynamic neuron–glia in neurogenesis and synaptic formation. For example, astrocyte, one type of glia, modulates multiple aspects of neuron growth and synaptic function from development through to adulthood, including involvement in synapse formation, as well as uptake and recycling of neurotransmitters. Recent studies also revealed astrocytic dysfunction in several brain disorders including schizophrenia with significant cognitive impairments. Astrocyte loss has been observed in the prefrontal

`

cortex which triggered neuronal damage causing cognitive impairment in the animal model (Lima et al., 2014). Consequently, astrocyte could have an as yet unexpected role in the neuron-glia interactions in the diseased brain. An improved understanding of astrocyte biology and function offers the potential for developing novel strategies to treat neurological disorders. Despite the growing realization of the importance of the neuron-glia relationship, we are still in the early stages of understanding the physiological consequences of the bidirectional communication between neurons and glia, mainly due to the difficulty in separating neurons and glia from the cell mixture in brain tissue.

In Chapter 4, a high-throughput microfluidic platform based on an inertial microfluidic technique was established to separate neurons and glial cells from dissected brain tissue rapidly and continuously. The microfluidic platform was set up based on size-dependent separation due to the significant variation of cell diameters between neurons and glia. Larger-size cells collected from the middle outlet were characterised as neurons while smaller cells collected from the aside outlet were determined as glia. Immunostaining was applied to test the cell types and confirm the high separation effects. Collected cells were then incubated for downstream experiments. This method provided highly enriched and purified neurons and glia, compared to the traditional methods, in which glial cells are mixed with neurons, and each well for incubation only contains a limited numbers of cells of interest. Moreover, separated neurons were as healthy and functional as unprocessed neurons, and there was no significant variation in the growth and synaptogenesis of neurites caused by the inertial separation process.

Cell sorting has been broadly applied in biological studies, however live cell sorting from tissue is still a challenge. Fluorescence-activated cell sorting (FACS) and

`

magnetically-activated cell sorting (MACS) have been used for sorting cells. However, these methods require cell labelling which is a time and labour consuming step, and more importantly, application of antibodies to label cells will further interfere with the immunochemistry analysis of target proteins of interest. Microfluidic technology has been introduced to perform cell sorting studies. Dielectrophoresis (DEP)-based microfluidic devices distinguish cells by their dielectric properties as a label-free technique. However these devices normally run in a batch manner and with a very limited throughput. Apart from DEP, another study has reported the application of viscoelasticity-tuned hydrodynamic spreading to neural cell separation where the microfluidic device works in a continuous and label free manner (Wu et al., 2008). Such a device could achieve relative high viability of neural cells through separation. However, the flow rate (20 µl/h) and the throughput ($3 \times 10^4$ cells/h) are still not satisfactory, and therefore need further improvement. This study applied a label-free and high-throughput microfluidic device in which cells passed through the microchannel in an inertial microchip at ~1 m/s with significantly improved throughput of $1.188 \times 10^7$ cells/h. Although the current throughput rate is still lower than FACS, this proposed device can be further amplified by parallelizing several microchannels to increase throughput capability. Importantly, the present inertial microfluidic platform is biocompatible, elastomeric, transparent and gas-permeable, suitable for cell incubation. In future studies, this device will be designed to establish a multi-functional platform combining separating, sorting, incubation and neurite outgrowth measurement, to further investigate the neuron-glia interactions and proteins of interest. For example, a recent study has found PTP1B in microglia contributing to neuroinflammation (Song et al., 2016) and neuroinflammation is strongly linked to development of neurological disorders including schizophrenia (Meyer, 2013). Therefore, it is of great interest to

`

discover the role of PTP1B in glial cells regulating neurite outgrowth, synaptic formation and neurotransmitters function in future studies, with application of the inertial microfluidic platform.

## 5.2 Conclusion

PTP1B has been reported to impair BDNF-mediated signalling and then inhibit neurite outgrowth and synaptic formation. Moreover, PTP1B blocks leptin signalling which is known to increase BDNF and promote neurite outgrowth. Therefore PTP1B is a potential drug target to reverse abnormality of BDNF-mediated neurogenesis in neurological disorders. In this study, lupane triterpenes, a cluster of natural products, were determined as novel PTP1B allosteric inhibitors which inhibit PTP1B with strong potency and selectivity. Lupane triterpenes inhibit psychotomimetic drug-induced PTP1B and reverse PTP1B-induced BDNF reduction and neurogenesis impairment, demonstrating that lupane triterpenes are potential drug candidates for PTP1B inhibition and PTP1B-related neurological disorders.

In the present study, lupeol and other members of lupane triterpenes were demonstrated as PTP1B allosteric inhibitors. With the application of molecular modelling and biological assay, lupeol was revealed to target the PTP1B allosteric binding site to inhibit PTP1B with selectivity and potency. Through the investigation of lupeol structural properties, further structural modification was determined to discover a series of lupeol derivatives.

PTP1B is identified as a new factor contributing to the psychopathology in schizophrenia-like models. PTP1B was found significantly increased during the psychotomimetic drug (phencyclidine) treatment, resulting in the decrese of leptin

`

signalling, reduction of BDNF level, attenuation of the BDNF-mediated Akt/GSK3β pathway and neurogenesis, suggesting PTP1B as a new drug target.

Furthermore, the natural triterpene lupeol was applied to prevent PCP-induced PTP1B expression. Lupeol managed to reduce PTP1B and reversed PCP-induced schizophrenia-like alterations. Importantly, the combined treatment of lupeol and atypical antipsychotic, olanzapine, showed improved treatment efficacy and reduced side effects compared to individual olanzapine application, implicating PTP1B inhibition as a potential treatment strategy.

Finally, to investigate the role of PTP1B in specific cell types of neurons and glia in future studies, an inertial microfluidic biochip was introduced to separate neurons and glia from mouse brain tissue for primary cell culture. This microfluidic platform was a high through-put device, able to separate neurons and glia with efficiency and purity, and there was no damage to cell viability and biological functions during the process.

In conclusion, this PhD project determined natural compounds lupane triterpenes as new PTP1B allosteric inhibitors which inhibit PTP1B with high potency and selectivity. PTP1B was further confirmed as contributing to BDNF reduction and neurogenesis impairment in schizophrenia-like models, indicating PTP1B as a potential drug target. Application of lupane triterpene significantly improved therapeutic efficacy and prevented the side effects induced by antipsychotics. Finally, development of the microfluidic microchip will improve investigation of PTP1B in specific cell types in future studies.

## 5.3 Recommendations for Future Research

`

1. Further characterise the interactions between lupane triterpenes and PTP1B allosteric site. Experimental methods including NMR and mutant protein purification technologies will be applied to determine the crucial amino acids in PTP1B which contribute to the allosteric binding mode.

2. Chemical modifications of lupeol based on results and discussions in Chapter 2 and future NMR data. Apply computer-aid drug design to develop novel lupeol derivatives targeting PTP1B allosteric site with improved potency, selectivity and bioavailability.

3. Application of new lupeol derivatives on neural cell cultures to improve neurite outgrowth, synaptic function and relative signalling pathway.

4. Animal models will be applied in future studies to test the improved behaviour and cognition with the treatment of lupeol derivatives.

5. Combination of lupeol derivatives and antipsychotic olanzapine will be administrated to animal models to demonstrate improved treatment efficacy with reduced side effects such as body weight gain.

6. Microfluidics-based cell culture system will be established using new biocompatible materials and high-resolution fabrication technologies, to separate neurons and glia with purity and viability from brain sections.

7. With the new established microfluidic system, PTP1B in microglia will be examined to determine its contributions to neuroinflammation. PTP1B in astrocyte will be investigated to reveal its role contributing to impaired neurite outgrowth and neurogenesis in neurological disorders.

`

8. The microfluidic system could be further modified to establish neuron-glia co-culture system, to investigate the neuron-glia interactions in neurological disorders and reveal the role of PTP1B involved.

`

# References


ADACHI, N., NUMAKAWA, T., KUMAMARU, E., ITAMI, C., CHIBA, S., IIJIMA, Y., RICHARDS, M., KATOH-SEMBA, R. & KUNUGI, H. 2013. Phencyclidine-Induced Decrease of Synaptic Connectivity via Inhibition of BDNF Secretion in Cultured Cortical Neurons. *Cerebral Cortex,* 23**,** 847-858.

AHIMA, R. S. & FLIER, J. S. 2000. Leptin. *Annual Review of Physiology,* 62**,** 413-437.

ALLEN, N. J. 2014. Astrocyte Regulation of Synaptic Behavior. *Annual Review of Cell and Developmental Biology,* 30**,** 439-463.

ANASTASIO, N. C., XIA, Y., O'CONNOR, Z. R. & JOHNSON, K. M. 2009. Differential role of N-methyl-D-aspartate receptor subunits 2A and 2B in mediating phencyclidine-induced perinatal neuronal apoptosis and behavioral deficits. *Neuroscience,* 163**,** 1181-91.

ANDREASEN, N. 1995. Symptoms, signs, and diagnosis of schizophrenia. *The Lancet,* 346**,** 477-481.

ANGELUCCI, F., BRENE, S. & MATHE, A. A. 2005. BDNF in schizophrenia, depression and corresponding animal models. *Mol Psychiatry,* 10**,** 345-352.

BALTINA, L. A., FLEKHTER, O. B., NIGMATULLINA, L. R., BOREKO, E. I., PAVLOVA, N. I., NIKOLAEVA, S. N., SAVINOVA, O. V. & TOLSTIKOV, G. A. 2003. Lupane triterpenes and derivatives with antiviral activity. *Bioorg Med Chem Lett,* 13**,** 3549-52.

BARFORD, D., FLINT, A. J. & TONKS, N. K. 1994. Crystal structure of human protein tyrosine phosphatase 1B. *Science,* 263**,** 1397-404.

BARIOHAY, B., LEBRUN, B., MOYSE, E. & JEAN, A. 2005. Brain-Derived Neurotrophic Factor Plays a Role as an Anorexigenic Factor in the Dorsal Vagal Complex. *Endocrinology,* 146**,** 5612-5620.

BARR, A. J. 2010. Protein tyrosine phosphatases as drug targets: strategies and challenges of inhibitor development. *Future Med Chem,* 2**,** 1563-76.

BEAR MF, C. B., PARADISO M. 2006. *Neuroscience—exploring the brain, 3rd ed.,* Philadelphia, Lippincott Williams & Wilkins.

BENCE, K. K., DELIBEGOVIC, M., XUE, B., GORGUN, C. Z., HOTAMISLIGIL, G. S., NEEL, B. G. & KAHN, B. B. 2006. Neuronal PTP1B regulates body weight, adiposity and leptin action. *Nat Med,* 12**,** 917-24.

BERNSTEIN, H.-G., KEILHOFF, G., STEINER, J., DOBROWOLNY, H. & BOGERTS, B. 2010. The hypothalamus in schizophrenia research: no longer a wallflower existence. *Open Neuroendocrinol J,* 3**,** 59-67.

BJARNADOTTIR, M., MISNER, D. L., HAVERFIELD-GROSS, S., BRUUN, S., HELGASON, V. G., STEFANSSON, H., SIGMUNDSSON, A., FIRTH, D. R., NIELSEN, B., STEFANSDOTTIR, R., NOVAK, T. J., STEFANSSON, K., GURNEY, M. E. & ANDRESSON, T. 2007. Neuregulin1 (NRG1) Signaling through Fyn Modulates NMDA Receptor Phosphorylation: Differential Synaptic Function in NRG1+/− Knock-Outs Compared with Wild-Type Mice. *The Journal of Neuroscience,* 27**,** 4519-4529.

BJORBAEK, C. & KAHN, B. B. 2004. Leptin signaling in the central nervous system and the periphery. *Recent progress in hormone research,* 59**,** 305-332.

`

BOURET, S. G., DRAPER, S. J. & SIMERLY, R. B. 2004. Trophic action of leptin on hypothalamic neurons that regulate feeding. *Science,* 304**,** 108-110.

BREWER, G. J. 1997. Isolation and culture of adult rat hippocampal neurons. *Journal of Neuroscience Methods,* 71**,** 143-155.

BROOKS, B. R., BROOKS, C. L., MACKERELL, A. D., NILSSON, L., PETRELLA, R. J., ROUX, B., WON, Y., ARCHONTIS, G., BARTELS, C., BORESCH, S., CAFLISCH, A., CAVES, L., CUI, Q., DINNER, A. R., FEIG, M., FISCHER, S., GAO, J., HODOSCEK, M., IM, W., KUCZERA, K., LAZARIDIS, T., MA, J., OVCHINNIKOV, V., PACI, E., PASTOR, R. W., POST, C. B., PU, J. Z., SCHAEFER, M., TIDOR, B., VENABLE, R. M., WOODCOCK, H. L., WU, X., YANG, W., YORK, D. M. & KARPLUS, M. 2009. CHARMM: The Biomolecular Simulation Program. *Journal of Computational Chemistry,* 30**,** 1545-1614.

BROWN-SHIMER, S., JOHNSON, K. A., LAWRENCE, J. B., JOHNSON, C., BRUSKIN, A., GREEN, N. R. & HILL, D. E. 1990. Molecular cloning and chromosome mapping of the human gene encoding protein phosphotyrosyl phosphatase 1B. *Proceedings of the National Academy of Sciences,* 87**,** 5148-5152.

BUCKLEY, P. F., PILLAI, A., EVANS, D., STIREWALT, E. & MAHADIK, S. 2007. Brain Derived Neurotropic Factor in First –Episode Psychosis. *Schizophrenia Research,* 91**,** 1-5.

CHEN, D. C., WANG, J., WANG, B., YANG, S. C., ZHANG, C. X., ZHENG, Y. L., LI, Y. L., WANG, N., YANG, K. B., XIU, M. H., KOSTEN, T. R. & ZHANG, X. Y. 2009. Decreased levels of serum brain-derived neurotrophic factor in drug-naïve first-episode schizophrenia: relationship to clinical phenotypes. *Psychopharmacology,* 207**,** 375-380.

CHEN, Y.-N. P., LAMARCHE, M. J., CHAN, H. M., FEKKES, P., GARCIA-FORTANET, J., ACKER, M. G., ANTONAKOS, B., CHEN, C. H.-T., CHEN, Z. & COOKE, V. G. 2016. Allosteric inhibition of SHP2 phosphatase inhibits cancers driven by receptor tyrosine kinases. *Nature,* 535**,** 148-152.

CHENG, A., UETANI, N., SIMONCIC, P. D., CHAUBEY, V. P., LEE-LOY, A., MCGLADE, C. J., KENNEDY, B. P. & TREMBLAY, M. L. 2002. Attenuation of leptin action and regulation of obesity by protein tyrosine phosphatase 1B. *Dev Cell,* 2**,** 497-503.

CHERNOFF, J., SCHIEVELLA, A. R., JOST, C. A., ERIKSON, R. L. & NEEL, B. G. 1990. Cloning of a cDNA for a major human protein-tyrosine-phosphatase. *Proc Natl Acad Sci U S A,* 87**,** 2735-9.

CHOI, J. Y., NA, M., HYUN HWANG, I., HO LEE, S., YOUNG BAE, E., YEON KIM, B. & SEOG AHN, J. 2009. Isolation of betulinic acid, its methyl ester and guaiane sesquiterpenoids with protein tyrosine phosphatase 1B inhibitory activity from the roots of Saussurea lappa C.B.Clarke. *Molecules,* 14**,** 266-72.

COHN, T., PRUD'HOMME, D., STREINER, D., KAMEH, H. & REMINGTON, G. 2004. Characterizing coronary heart disease risk in chronic schizophrenia: high prevalence of the metabolic syndrome. *Canadian journal of psychiatry. Revue canadienne de psychiatrie,* 49**,** 753-60.

COOL, D. E., TONKS, N. K., CHARBONNEAU, H., WALSH, K. A., FISCHER, E. H. & KREBS, E. G. 1989. cDNA isolated from a human T-cell library encodes a member of the protein-tyrosine-phosphatase family. *Proc Natl Acad Sci U S A,* 86**,** 5257-61.

`

COPPARI, R., RAMADORI, G. & ELMQUIST, J. K. 2009. The role of transcriptional regulators in central control of appetite and body weight. *Nat Clin Pract End Met,* 5**,** 160-166.

DARDEN, T., YORK, D. & PEDERSEN, L. 1993. Particle Mesh Ewald - an N.Log(N) Method for Ewald Sums in Large Systems. *Journal of Chemical Physics,* 98**,** 10089-10092.

DEHMELT, L., POPLAWSKI, G., HWANG, E. & HALPAIN, S. 2011. NeuriteQuant: An open source toolkit for high content screens of neuronal Morphogenesis. *BMC Neuroscience,* 12**,** 1-14.

DU BOIS, T. M., NEWELL, K. A. & HUANG, X. F. 2012. Perinatal phencyclidine treatment alters neuregulin 1/erbB4 expression and activation in later life. *Eur Neuropsychopharmacol,* 22**,** 356-63.

DUFFY, D. C., MCDONALD, J. C., SCHUELLER, O. J. A. & WHITESIDES, G. M. 1998. Rapid prototyping of microfluidic systems in poly (dimethylsiloxane). *Analytical Chemistry,* 70**,** 4974-4984.

DURANY, N., MICHEL, T., ZÖCHLING, R., BOISSL, K. W., CRUZ-SÁNCHEZ, F. F., RIEDERER, P. & THOME, J. 2001. Brain-derived neurotrophic factor and neurotrophin 3 in schizophrenic psychoses. *Schizophrenia Research,* 52**,** 79-86.

ELMAN, I., BORSOOK, D. & LUKAS, S. E. 2006. Food intake and reward mechanisms in patients with schizophrenia: Implications for metabolic disturbances and treatment with second-generation antipsychotic agents. *Neuropsychopharmacology,* 31**,** 2091-2120.

EMAMIAN, E. S., HALL, D., BIRNBAUM, M. J., KARAYIORGOU, M. & GOGOS, J. A. 2004. Convergent evidence for impaired AKT1-GSK3[beta] signaling in schizophrenia. *Nat Genet,* 36**,** 131-137.

FANNON, D., TENNAKOON, L., SUMICH, A., O'CEALLAIGH, S., DOKU, V., CHITNIS, X., LOWE, J., SONI, W. & SHARMA, T. 2000. Third ventricle enlargement and developmental delay in first-episode psychosis: preliminary findings. *British Journal of Psychiatry,* 177**,** 354-359.

FARR, S. A., BANKS, W. A. & MORLEY, J. E. 2006. Effects of leptin on memory processing. *Peptides,* 27**,** 1420-1425.

FAVALLI, G., LI, J., BELMONTE-DE-ABREU, P., WONG, A. H. C. & DASKALAKIS, Z. J. 2012. The role of BDNF in the pathophysiology and treatment of schizophrenia. *Journal of Psychiatric Research,* 46**,** 1-11.

FRANGIONI, J. V., BEAHM, P. H., SHIFRIN, V., JOST, C. A. & NEEL, B. G. 1992. The nontransmembrane tyrosine phosphatase PTP-1B localizes to the endoplasmic reticulum via its 35 amino acid C-terminal sequence. *Cell,* 68**,** 545-60.

FRANKLE, W. G., LERMA, J. & LARUELLE, M. 2003. The synaptic hypothesis of schizophrenia. *Neuron,* 39**,** 205-216.

FUENTES, F., ZIMMER, D., ATIENZA, M., SCHOTTENFELD, J., PENKALA, I., BALE, T., BENCE, K. K. & ARREGUI, C. O. 2012. Protein Tyrosine Phosphatase PTP1B Is Involved in Hippocampal Synapse Formation and Learning. *Plos One,* 7.

GARCIA FORTANET, J., CHEN, C. H.-T., CHEN, Y.-N. P., CHEN, Z., DENG, Z., FIRESTONE, B., FEKKES, P., FODOR, M., FORTIN, P. D. & FRIDRICH, C. 2016. Allosteric Inhibition of SHP2: Identification of a Potent, Selective, and Orally Efficacious Phosphatase Inhibitor. *Journal of medicinal chemistry*.

`

HAJSZAN, T., LERANTH, C. & ROTH, R. H. 2006. Subchronic phencyclidine treatment decreases the number of dendritic spine synapses in the rat prefrontal cortex. *Biological Psychiatry,* 60**,** 639-644.

HANSEN, N. & VAN GUNSTEREN, W. F. 2014. Practical Aspects of Free-Energy Calculations: A Review. *Journal of Chemical Theory and Computation,* 10**,** 2632-2647.

HARRISON, P. J. & WEINBERGER, D. R. 2004. Schizophrenia genes, gene expression, and neuropathology: on the matter of their convergence. *Mol Psychiatry,* 10**,** 40-68.

HARVEY, J. 2007. Leptin: a diverse regulator of neuronal function. *Journal of neurochemistry,* 100**,** 307-313.

HARVEY, J., SHANLEY, L., O'MALLEY, D. & IRVING, A. 2005. Leptin: a potential cognitive enhancer? *Biochemical Society Transactions,* 33**,** 1029-1032.

HAUPT, D. W. 2006. Differential metabolic effects of antipsychotic treatments. *European neuropsychopharmacology : the journal of the European College of Neuropsychopharmacology,* 16**,** S149-S155.

HILGENBERG, L. G. W. & SMITH, M. A. 2007. Preparation of Dissociated Mouse Cortical Neuron Cultures. *Journal of Visualized Experiments : JoVE***,** 562.

HOU, H. W., WARKIANI, M. E., KHOO, B. L., LI, Z. R., SOO, R. A., TAN, D. S.-W., LIM, W.-T., HAN, J., BHAGAT, A. A. S. & LIM, C. T. 2013. Isolation and retrieval of circulating tumor cells using centrifugal forces. *Scientific reports,* 3**,** Art No. 1259.

HUANG, E. J. & REICHARDT, L. F. 2001. Neurotrophins: Roles in Neuronal Development and Function. *Annual review of neuroscience,* 24**,** 677-736.

HUMPHREY, W., DALKE, A. & SCHULTEN, K. 1996. VMD: visual molecular dynamics. *J Mol Graph,* 14**,** 33-8, 27-8.

HUSI, H., WARD, M. A., CHOUDHARY, J. S., BLACKSTOCK, W. P. & GRANT, S. G. N. 2000. Proteomic analysis of NMDA receptor-adhesion protein signaling complexes. *Nat Neurosci,* 3**,** 661-669.

IVERSEN, L. F., MØLLER, K. B., PEDERSEN, A. K., PETERS, G. H., PETERSEN, A. S., ANDERSEN, H. S., BRANNER, S., MORTENSEN, S. B. & MØLLER, N. P. H. 2002. Structure Determination of T Cell Protein-tyrosine Phosphatase. *Journal of Biological Chemistry,* 277**,** 19982-19990.

JAVITT, D. C. & ZUKIN, S. R. 1991. Recent advances in the phencyclidine model of schizophrenia. *Am J Psychiatry,* 148**,** 1301-1308.

JENTSCH, J. D. & ROTH, R. H. 1999. The neuropsychopharmacology of phencyclidine: from NMDA receptor hypofunction to the dopamine hypothesis of schizophrenia. *Neuropsychopharmacology,* 20**,** 201-225.

JIANG, W., HODOSCEK, M. & ROUX, B. 2009. Computation of Absolute Hydration and Binding Free Energy with Free Energy Perturbation Distributed Replica-Exchange Molecular Dynamics. *Journal of Chemical Theory and Computation,* 5**,** 2583-2588.

JIN, T., YU, H. & HUANG, X.-F. 2016. Selective binding modes and allosteric inhibitory effects of lupane triterpenes on protein tyrosine phosphatase 1B. *Scientific reports,* 6**,** 20766.

JOHNSON, T. O., ERMOLIEFF, J. & JIROUSEK, M. R. 2002. Protein tyrosine phosphatase 1B inhibitors for diabetes. *Nat Rev Drug Discov,* 1**,** 696-709.

JULIEN, S. G., DUBE, N., HARDY, S. & TREMBLAY, M. L. 2011. Inside the human cancer tyrosine phosphatome. *Nature Reviews Cancer,* 11**,** 35-49.

KATANUMA, Y., NUMAKAWA, T., ADACHI, N., YAMAMOTO, N., OOSHIMA, Y., ODAKA, H., INOUE, T. & KUNUGI, H. 2014. Phencyclidine rapidly decreases neuronal mRNA of brain-derived neurotrophic factor. *Synapse,* 68**,** 257-265.

KITAGISHI, Y., KOBAYASHI, M., KIKUTA, K. & MATSUDA, S. 2012. Roles of PI3K/AKT/GSK3/mTOR Pathway in Cell Signaling of Mental Illnesses. *Depression Research and Treatment,* 2012**,** 8.

KITCHEN, D. B., DECORNEZ, H., FURR, J. R. & BAJORATH, J. 2004. Docking and scoring in virtual screening for drug discovery: methods and applications. *Nat Rev Drug Discov,* 3**,** 935-949.

KOMORI, T., MORIKAWA, Y., NANJO, K. & SENBA, E. 2006. Induction of brain-derived neurotrophic factor by leptin in the ventromedial hypothalamus. *Neuroscience,* 139**,** 1107-1115.

KRISHNAN, N., KOVEAL, D., MILLER, D. H., XUE, B., AKSHINTHALA, S. D., KRAGELJ, J., JENSEN, M. R., GAUSS, C. M., PAGE, R., BLACKLEDGE, M., MUTHUSWAMY, S. K., PETI, W. & TONKS, N. K. 2014. Targeting the disordered C terminus of PTP1B with an allosteric inhibitor. *Nature Chemical Biology,* 10**,** 558-566.

KRISHNAN, N., KRISHNAN, K., CONNORS, C. R., CHOY, M. S., PAGE, R., PETI, W., VAN AELST, L., SHEA, S. D. & TONKS, N. K. 2015. PTP1B inhibition suggests a therapeutic strategy for Rett syndrome. *The Journal of Clinical Investigation,* 125**,** 3163-3177.

KUBINYI, H. 2006. Success Stories of Computer-Aided Design. *Computer Applications in Pharmaceutical Research and Development.* John Wiley & Sons, Inc.

LASZCZYK, M. N. 2009. Pentacyclic triterpenes of the lupane, oleanane and ursane group as tools in cancer therapy. *Planta Med,* 75**,** 1549-60.

LEE, J. H., REED, D. R., LI, W.-D., XU, W., JOO, E.-J., KILKER, R. L., NANTHAKUMAR, E., NORTH, M., SAKUL, H., BELL, C. & PRICE, R. A. 1999. Genome Scan for Human Obesity and Linkage to Markers in 20q13. *The American Journal of Human Genetics,* 64**,** 196-209.

LEE, M. G., CHOI, S., KIM, H. J., LIM, H. K., KIM, J. H., HUH, N. & PARK, J. K. 2011. Inertial blood plasma separation in a contraction–expansion array microchannel. *Applied Physics Letters,* 98**,** 253702.

LEMBERTAS, A. V., PÉRUSSE, L., CHAGNON, Y. C., FISLER, J. S., WARDEN, C. H., PURCELL-HUYNH, D. A., DIONNE, F. T., GAGNON, J., NADEAU, A., LUSIS, A. J. & BOUCHARD, C. 1997. Identification of an obesity quantitative trait locus on mouse chromosome 2 and evidence of linkage to body fat and insulin on the human homologous region 20q. *Journal of Clinical Investigation,* 100**,** 1240-1247.

LEROY, K. & BRION, J.-P. 1999. Developmental expression and localization of glycogen synthase kinase-3β in rat brain. *Journal of Chemical Neuroanatomy,* 16**,** 279-293.

LI, X.-L., AOU, S., OOMURA, Y., HORI, N., FUKUNAGA, K. & HORI, T. 2002. Impairment of long-term potentiation and spatial memory in leptin receptor-deficient rodents. *Neuroscience,* 113**,** 607-615.

LIAO, G.-Y., AN, J. J., GHARAMI, K., WATERHOUSE, E. G., VANEVSKI, F., JONES, K. R. & XU, B. 2012. Dendritically targeted Bdnf mRNA is essential for energy balance and response to leptin. *Nature Medicine,* 18**,** 564-571.

`

LIBY, K. T., YORE, M. M. & SPORN, M. B. 2007. Triterpenoids and rexinoids as multifunctional agents for the prevention and treatment of cancer. *Nat Rev Cancer,* 7**,** 357-69.

LIMA, A., SARDINHA, V. M., OLIVEIRA, A. F., REIS, M., MOTA, C., SILVA, M. A., MARQUES, F., CERQUEIRA, J. J., PINTO, L., SOUSA, N. & OLIVEIRA, J. F. 2014. Astrocyte pathology in the prefrontal cortex impairs the cognitive function of rats. *Molecular Psychiatry,* 19**,** 834-841.

LORENZ, U. 2011. Protein tyrosine phosphatase assays. *Curr Protoc Immunol,* Chapter 11**,** Unit 11 7.

LU, L., WANG, S., ZHU, M., LIU, Z., GUO, M., XING, S. & FU, X. 2010. Inhibition protein tyrosine phosphatases by an oxovanadium glutamate complex, Na2[VO(Glu)2(CH3OH)](Glu = glutamate). *BioMetals,* 23**,** 1139-1147.

MACH, A. J., KIM, J. H., ARSHI, A., HUR, S. C. & DI CARLO, D. 2011. Automated cellular sample preparation using a Centrifuge-on-a-Chip. *Lab on a Chip,* 11**,** 2827-2834.

MACKERELL, A. D., BASHFORD, D., BELLOTT, DUNBRACK, R. L., EVANSECK, J. D., FIELD, M. J., FISCHER, S., GAO, J., GUO, H., HA, S., JOSEPH-MCCARTHY, D., KUCHNIR, L., KUCZERA, K., LAU, F. T. K., MATTOS, C., MICHNICK, S., NGO, T., NGUYEN, D. T., PRODHOM, B., REIHER, W. E., ROUX, B., SCHLENKRICH, M., SMITH, J. C., STOTE, R., STRAUB, J., WATANABE, M., WIÓRKIEWICZ-KUCZERA, J., YIN, D. & KARPLUS, M. 1998. All-Atom Empirical Potential for Molecular Modeling and Dynamics Studies of Proteins†. *The Journal of Physical Chemistry B,* 102**,** 3586-3616.

MANGOURA, D., PELLETIERE, C., LEUNG, S., SAKELLARIDIS, N. & WANG, D. X. 2000. Prolactin concurrently activates Src-PLD and JAK/Stat signaling pathways to induce proliferation while promoting differentiation in embryonic astrocytes. *International Journal of Developmental Neuroscience,* 18**,** 693-704.

MCEVOY, J. P., MEYER, J. M., GOFF, D. C., NASRALLAH, H. A., DAVIS, S. M., SULLIVAN, L., MELTZER, H. Y., HSIAO, J., SCOTT STROUP, T. & LIEBERMAN, J. A. 2005. Prevalence of the metabolic syndrome in patients with schizophrenia: baseline results from the Clinical Antipsychotic Trials of Intervention Effectiveness (CATIE) schizophrenia trial and comparison with national estimates from NHANES III. *Schizophrenia research,* 80**,** 19-32.

MEDICINE, J. H. 2015. *Dissociated Primary Hypothalamic Neuron Culture* [Online]. Available: http://www.hopkinsmedicine.org/institute_basic_biomedical_sciences/research_centers/metabolism_obesity_research/protocols/ [Accessed 31 Jul 2015].

MEI, L. & XIONG, W. C. 2008. Neuregulin 1 in neural development, synaptic plasticity and schizophrenia. *Nat Rev Neurosci,* 9.

MELTZER, H. Y., BOBO, W. V., ROY, A., JAYATHILAKE, K., CHEN, Y., ERTUGRUL, A., ANIL YAGCIOGLU, A. E. & SMALL, J. G. 2008. A randomized, double-blind comparison of clozapine and high-dose olanzapine in treatment-resistant patients with schizophrenia. *Journal of Clinical Psychiatry,* 69**,** 274-85.

MEYER, U. 2013. Developmental neuroinflammation and schizophrenia. *Progress in Neuro-Psychopharmacology and Biological Psychiatry,* 42**,** 20-34.

MIAO, T., WU, D., ZHANG, Y., BO, X., SUBANG, M. C., WANG, P. & RICHARDSON, P. M. 2006. Suppressor of Cytokine Signaling-3 Suppresses

the Ability of Activated Signal Transducer and Activator of Transcription-3 to Stimulate Neurite Growth in Rat Primary Sensory Neurons. *The Journal of Neuroscience,* 26**,** 9512-9519.

MONTELEONE, M. C., GONZÁLEZ WUSENER, A. E., BURDISSO, J. E., CONDE, C., CÁCERES, A. & ARREGUI, C. O. 2012. ER-Bound Protein Tyrosine Phosphatase PTP1B Interacts with Src at the Plasma Membrane/Substrate Interface. *Plos One,* 7**,** e38948.

MOON, H. S., DINCER, F. & MANTZOROS, C. S. 2013. Amylin-induced downregulation of hippocampal neurogenesis is attenuated by leptin in a STAT3/AMPK/ERK-dependent manner in mice. *Diabetologia,* 56**,** 627-634.

MOREAU, R. A., WHITAKER, B. D. & HICKS, K. B. 2002. Phytosterols, phytostanols, and their conjugates in foods: structural diversity, quantitative analysis, and health-promoting uses. *Prog Lipid Res,* 41**,** 457-500.

MORRIS, B. J., COCHRAN, S. M. & PRATT, J. A. 2005. PCP: from pharmacology to modelling schizophrenia. *Current Opinion in Pharmacology,* 5**,** 101-106.

MORRIS, D. L. & RUI, L. 2009. Recent advances in understanding leptin signaling and leptin resistance. *Am J Physiol Endocrinol Metab,* 297**,** E1247-59.

MORTON, G. J. & SCHWARTZ, M. W. 2011. Leptin and the Central Nervous System Control of Glucose Metabolism. *Physiological Reviews,* 91**,** 389-411.

NA, M., KIM, B. Y., OSADA, H. & AHN, J. S. 2009. Inhibition of protein tyrosine phosphatase 1B by lupeol and lupenone isolated from Sorbus commixta. *J Enzyme Inhib Med Chem,* 24**,** 1056-9.

NG, Y. P., CHEUNG, Z. H. & IP, N. Y. 2006. STAT3 as a Downstream Mediator of Trk Signaling and Functions. *Journal of Biological Chemistry,* 281**,** 15636-15644.

NICOLAS, C. S., AMICI, M., BORTOLOTTO, Z. A., DOHERTY, A., CSABA, Z., FAFOURI, A., DOURNAUD, P., GRESSENS, P., COLLINGRIDGE, G. L. & PEINEAU, S. 2013. The role of JAK-STAT signaling within the CNS. *JAK-STAT,* 2**,** e22925.

NICOLAS, CÉLINE S., PEINEAU, S., AMICI, M., CSABA, Z., FAFOURI, A., JAVALET, C., COLLETT, VALERIE J., HILDEBRANDT, L., SEATON, G., CHOI, S.-L., SIM, S.-E., BRADLEY, C., LEE, K., ZHUO, M., KAANG, B.-K., GRESSENS, P., DOURNAUD, P., FITZJOHN, STEPHEN M., BORTOLOTTO, ZUNER A., CHO, K. & COLLINGRIDGE, GRAHAM L. 2012. The JAK/STAT Pathway Is Involved in Synaptic Plasticity. *Neuron,* 73**,** 374-390.

NOBLE, E. E., BILLINGTON, C. J., KOTZ, C. M. & WANG, C. 2011. The lighter side of BDNF. *American Journal of Physiology - Regulatory, Integrative and Comparative Physiology,* 300**,** R1053-R1069.

OLSSON, M. H. M., SØNDERGAARD, C. R., ROSTKOWSKI, M. & JENSEN, J. H. 2011. PROPKA3: Consistent Treatment of Internal and Surface Residues in Empirical pKa Predictions. *Journal of Chemical Theory and Computation,* 7**,** 525-537.

OSHEROVICH, L. 2011. Inositol insulin insight. *SciBX: Science-Business eXchange,* 4.

OVESNA, Z., VACHALKOVA, A., HORVATHOVA, K. & TOTHOVA, D. 2004. Pentacyclic triterpenoic acids: new chemoprotective compounds. Minireview. *Neoplasma,* 51**,** 327-33.

OZEK, C., KANOSKI, S. E., ZHANG, Z. Y., GRILL, H. J. & BENCE, K. K. 2014. Protein-tyrosine Phosphatase 1B (PTP1B) Is a Novel Regulator of Central

Brain-derived Neurotrophic Factor and Tropomyosin Receptor Kinase B (TrkB) Signaling. *Journal of Biological Chemistry,* 289**,** 31682-31692.

OZKUMUR, E., SHAH, A. M., CICILIANO, J. C., EMMINK, B. L., MIYAMOTO, D. T., BRACHTEL, E., YU, M., CHEN, P.-I., MORGAN, B. & TRAUTWEIN, J. 2013. Inertial focusing for tumor antigen–dependent and–independent sorting of rare circulating tumor cells. *Science Translational Medicine,* 5**,** 179ra47-179ra47.

PANDYA, C. D. & PILLAI, A. 2014. TrkB interacts with ErbB4 and regulates NRG1-induced NR2B phosphorylation in cortical neurons before synaptogenesis. *Cell Communication and Signaling,* 12**,** 1-11.

PANNIFER, A. D. B., FLINT, A. J., TONKS, N. K. & BARFORD, D. 1998. Visualization of the cysteinyl-phosphate intermediate of a protein-tyrosine phosphatase by X-ray crystallography. *Journal of Biological Chemistry,* 273**,** 10454-10462.

PAOLETTI, P. & NEYTON, J. 2007. NMDA receptor subunits: function and pharmacology. *Current Opinion in Pharmacology,* 7**,** 39-47.

PATIL, S. T., ZHANG, L., MARTENYI, F., LOWE, S. L., JACKSON, K. A., ANDREEV, B. V., AVEDISOVA, A. S., BARDENSTEIN, L. M., GUROVICH, I. Y., MOROZOVA, M. A., MOSOLOV, S. N., NEZNANOV, N. G., REZNIK, A. M., SMULEVICH, A. B., TOCHILOV, V. A., JOHNSON, B. G., MONN, J. A. & SCHOEPP, D. D. 2007. Activation of mGlu2/3 receptors as a new approach to treat schizophrenia: a randomized Phase 2 clinical trial. *Nat Med,* 13**,** 1102-7.

PAYNE, C. M., JIANG, W., SHIRTS, M. R., HIMMEL, M. E., CROWLEY, M. F. & BECKHAM, G. T. 2013. Glycoside Hydrolase Processivity Is Directly Related to Oligosaccharide Binding Free Energy. *Journal of the American Chemical Society,* 135**,** 18831-18839.

PHILLIPS, J. C., BRAUN, R., WANG, W., GUMBART, J., TAJKHORSHID, E., VILLA, E., CHIPOT, C., SKEEL, R. D., KALE, L. & SCHULTEN, K. 2005. Scalable molecular dynamics with NAMD. *J Comput Chem,* 26**,** 1781-802.

PICARDI, P. K., CARICILLI, A. M., DE ABREU, L. L. F., CARVALHEIRA, J. B. C., VELLOSO, L. A. & SAAD, M. J. A. 2010. Modulation of hypothalamic PTP1B in the TNF-alpha-induced insulin and leptin resistance. *Febs Letters,* 584**,** 3179-3184.

PINTO, S., ROSEBERRY, A. G., LIU, H., DIANO, S., SHANABROUGH, M., CAI, X., FRIEDMAN, J. M. & HORVATH, T. L. 2004. Rapid rewiring of arcuate nucleus feeding circuits by leptin. *Science,* 304**,** 110-115.

PITCHER, G. M., KALIA, L. V., NG, D., GOODFELLOW, N. M., YEE, K. T., LAMBE, E. K. & SALTER, M. W. 2011. Schizophrenia susceptibility pathway neuregulin 1-ErbB4 suppresses Src upregulation of NMDA receptors. *Nature Medicine,* 17.

RADBRUCH, A. & RECKTENWALD, D. 1995. Detection and isolation of rare cells. *Current Opinion in Immunology,* 7**,** 270-273.

REIF, M. M. & OOSTENBRINK, C. 2014. Net Charge Changes in the Calculation of Relative Ligand-Binding Free Energies via Classical Atomistic Molecular Dynamics Simulation. *Journal of Computational Chemistry,* 35**,** 227-243.

ROCKLIN, G. J., MOBLEY, D. L., DILL, K. A. & HUNENBERGER, P. H. 2013. Calculating the binding free energies of charged species based on explicit-solvent simulations employing lattice-sum methods: An accurate correction scheme for electrostatic finite-size effects. *Journal of Chemical Physics,* 139.

`

SALI, A. & BLUNDELL, T. L. 1993. Comparative protein modelling by satisfaction of spatial restraints. *J Mol Biol,* 234**,** 779-815.

SCHWARTZ, M. W. & PORTE, D., JR. 2005. Diabetes, obesity, and the brain. *Science,* 307**,** 375-9.

SCHWARTZ, M. W., WOODS, S. C., PORTE, D., JR., SEELEY, R. J. & BASKIN, D. G. 2000. Central nervous system control of food intake. *Nature,* 404**,** 661-71.

SEIFERT, G., SCHILLING, K. & STEINHAUSER, C. 2006. Astrocyte dysfunction in neurological disorders: a molecular perspective. *Nat Rev Neurosci,* 7**,** 194-206.

SHANLEY, L. J., IRVING, A. J. & HARVEY, J. 2001. Leptin enhances NMDA receptor function and modulates hippocampal synaptic plasticity. *Journal of Neuroscience,* 21**,** RC186.

SIMONCIC, P. D., LEE-LOY, A., BARBER, D. L., TREMBLAY, M. L. & MCGLADE, C. J. 2002. The T cell protein tyrosine phosphatase is a negative regulator of janus family kinases 1 and 3. *Curr Biol,* 12**,** 446-53.

SMILLIE, K. J., PAWSON, J., PERKINS, E. M., JACKSON, M. & COUSIN, M. A. 2013. Control of synaptic vesicle endocytosis by an extracellular signalling molecule. *Nat Commun,* 4.

SNIGDHA, S., NEILL, J. C., MCLEAN, S. L., SHEMAR, G. K., CRUISE, L., SHAHID, M. & HENRY, B. 2011. Phencyclidine (PCP)-Induced Disruption in Cognitive Performance is Gender-Specific and Associated with a Reduction in Brain-Derived Neurotrophic Factor (BDNF) in Specific Regions of the Female Rat Brain. *Journal of Molecular Neuroscience,* 43**,** 337-345.

SONG, G. J., JUNG, M., KIM, J.-H., PARK, H., RAHMAN, M. H., ZHANG, S., ZHANG, Z.-Y., PARK, D. H., KOOK, H., LEE, I.-K. & SUK, K. 2016. A novel role for protein tyrosine phosphatase 1B as a positive regulator of neuroinflammation. *Journal of Neuroinflammation,* 13**,** 1-14.

ST-PIERRE, J. & TREMBLAY, M. L. 2012. Modulation of leptin resistance by protein tyrosine phosphatases. *Cell Metab,* 15**,** 292-7.

STEFANSSON, H., SIGURDSSON, E., STEINTHORSDOTTIR, V., BJORNSDOTTIR, S., SIGMUNDSSON, T., GHOSH, S., BRYNJOLFSSON, J., GUNNARSDOTTIR, S., IVARSSON, O., CHOU, T. T., HJALTASON, O., BIRGISDOTTIR, B., JONSSON, H., GUDNADOTTIR, V. G., GUDMUNDSDOTTIR, E., BJORNSSON, A., INGVARSSON, B., INGASON, A., SIGFUSSON, S., HARDARDOTTIR, H., HARVEY, R. P., LAI, D., ZHOU, M., BRUNNER, D., MUTEL, V., GONZALO, A., LEMKE, G., SAINZ, J., JOHANNESSON, G., ANDRESSON, T., GUDBJARTSSON, D., MANOLESCU, A., FRIGGE, M. L., GURNEY, M. E., KONG, A., GULCHER, J. R., PETURSSON, H. & STEFANSSON, K. 2002. Neuregulin 1 and Susceptibility to Schizophrenia. *American Journal of Human Genetics,* 71**,** 877-892.

TARTAGLIA, N., DU, J., TYLER, W. J., NEALE, E., POZZO-MILLER, L. & LU, B. 2001. Protein Synthesis-dependent and -independent Regulation of Hippocampal Synapses by Brain-derived Neurotrophic Factor. *Journal of Biological Chemistry,* 276**,** 37585-37593.

TIGANIS, T. & BENNETT, A. M. 2007. Protein tyrosine phosphatase function: the substrate perspective. *Biochem J,* 402**,** 1-15.

TIGANIS, T., KEMP, B. E. & TONKS, N. K. 1999. The protein-tyrosine phosphatase TCPTP regulates epidermal growth factor receptor-mediated and phosphatidylinositol 3-kinase-dependent signaling. *J Biol Chem,* 274**,** 27768-75.

`

TOLSTIKOVA, T. G., SOROKINA, I. V., TOLSTIKOV, G. A., TOLSTIKOV, A. G. & FLEKHTER, O. B. 2006. [Biological activity and pharmacological prospects of lupane terpenoids: I. Natural lupane derivatives]. *Bioorg Khim,* 32**,** 42-55.

TONKS, N. K. 2003. PTP1B: from the sidelines to the front lines! *FEBS Lett,* 546**,** 140-8.

TROTT, O. & OLSON, A. J. 2010. AutoDock Vina: improving the speed and accuracy of docking with a new scoring function, efficient optimization, and multithreading. *J Comput Chem,* 31**,** 455-61.

TSOU, R. C. & BENCE, K. K. 2012. The Genetics of PTPN1 and Obesity: Insights from Mouse Models of Tissue-Specific PTP1B Deficiency. *Journal of Obesity,* 2012**,** 926857.

UKKOLA, O. & SANTANIEMI, M. 2002. Protein tyrosine phosphatase 1B: a new target for the treatment of obesity and associated co-morbidities. *Journal of Internal Medicine,* 251**,** 467-475.

VAN GUNSTEREN, W. F., BAKOWIES, D., BARON, R., CHANDRASEKHAR, I., CHRISTEN, M., DAURA, X., GEE, P., GEERKE, D. P., GLÄTTLI, A., HÜNENBERGER, P. H., KASTENHOLZ, M. A., OOSTENBRINK, C., SCHENK, M., TRZESNIAK, D., VAN DER VEGT, N. F. A. & YU, H. B. 2006. Biomolecular Modeling: Goals, Problems, Perspectives. *Angewandte Chemie International Edition,* 45**,** 4064-4092.

VILLANUEVA, E. C. & MYERS, M. G. 2008. Leptin receptor signaling and the regulation of mammalian physiology. *International journal of obesity (2005),* 32**,** S8-12.

WALKER, E., MITTAL, V. & TESSNER, K. 2008. Stress and the hypothalamic pituitary adrenal axis in the developmental course of schizophrenia. *Annual Review of Clinical Psychology,* 4**,** 189-216.

WANG, J., WOLF, R. M., CALDWELL, J. W., KOLLMAN, P. A. & CASE, D. A. 2004. Development and testing of a general amber force field. *Journal of Computational Chemistry,* 25**,** 1157-1174.

WARREN, G. L., ANDREWS, C. W., CAPELLI, A.-M., CLARKE, B., LALONDE, J., LAMBERT, M. H., LINDVALL, M., NEVINS, N., SEMUS, S. F., SENGER, S., TEDESCO, G., WALL, I. D., WOOLVEN, J. M., PEISHOFF, C. E. & HEAD, M. S. 2006. A Critical Assessment of Docking Programs and Scoring Functions. *Journal of medicinal chemistry,* 49**,** 5912-5931.

WEICKERT, C. S., HYDE, T. M., LIPSKA, B. K., HERMAN, M. M., WEINBERGER, D. R. & KLEINMAN, J. E. 2003. Reduced brain-derived neurotrophic factor in prefrontal cortex of patients with schizophrenia. *Mol Psychiatry,* 8**,** 592-610.

WEICKERT, C. S., LIGONS, D. L., ROMANCZYK, T., UNGARO, G., HYDE, T. M., HERMAN, M. M., WEINBERGER, D. R. & KLEINMAN, J. E. 2005. Reductions in neurotrophin receptor mRNAs in the prefrontal cortex of patients with schizophrenia. *Mol Psychiatry,* 10**,** 637-650.

WESTON-GREEN, K., HUANG, X.-F. & DENG, C. 2012. Alterations to Melanocortinergic, GABAergic and Cannabinoid Neurotransmission Associated with Olanzapine-Induced Weight Gain. *Plos One,* 7**,** e33548.

WIESMANN, C., BARR, K. J., KUNG, J., ZHU, J., ERLANSON, D. A., SHEN, W., FAHR, B. J., ZHONG, M., TAYLOR, L., RANDAL, M., MCDOWELL, R. S. & HANSEN, S. K. 2004. Allosteric inhibition of protein tyrosine phosphatase 1B. *Nat Struct Mol Biol,* 11**,** 730-7.

`

WOODS, C. J., ESSEX, J. W. & KING, M. A. 2003. The development of replica-exchange-based free-energy methods. *Journal of Physical Chemistry B,* 107**,** 13703-13710.

WU, L., GUAN, G., HOU, H. W., BHAGAT, A. A. S. & HAN, J. 2012. Separation of Leukocytes from Blood Using Spiral Channel with Trapezoid Cross-Section. *Analytical Chemistry,* 84**,** 9324-9331.

WU, Z., HJORT, K., WICHER, G. & FEX SVENNINGSEN, Å. 2008. Microfluidic high viability neural cell separation using viscoelastically tuned hydrodynamic spreading. *Biomedical microdevices,* 10**,** 631-638.

XU, W., ZHU, C., CHENG, W., FAN, X., CHEN, X., YANG, S., GUO, Y., YE, F. & SHI, J. 2009. Chemical Constituents of the Roots of Euphorbia micractina. *J Nat Prod,* 72**,** 1620-6.

YAMADA, N., KATSUURA, G., OCHI, Y., EBIHARA, K., KUSAKABE, T., HOSODA, K. & NAKAO, K. 2011. Impaired CNS Leptin Action Is Implicated in Depression Associated with Obesity. *Endocrinology,* 152**,** 2634-2643.

YIP, S. C., SAHA, S. & CHERNOFF, J. 2010. PTP1B: a double agent in metabolism and oncogenesis. *Trends in biochemical sciences,* 35**,** 442-9.

YOU-TEN, K. E., MUISE, E. S., ITIE, A., MICHALISZYN, E., WAGNER, J., JOTHY, S., LAPP, W. S. & TREMBLAY, M. L. 1997. Impaired bone marrow microenvironment and immune function in T cell protein tyrosine phosphatase-deficient mice. *J Exp Med,* 186**,** 683-93.

YU, I. C., LIN, H. Y., LIU, N. C., SPARKS, J. D., YEH, S. Y., FANG, L. Y., CHEN, L. M. & CHANG, C. S. 2013a. Neuronal Androgen Receptor Regulates Insulin Sensitivity via Suppression of Hypothalamic NF-kappa B-Mediated PTP1B Expression. *Diabetes,* 62**,** 411-423.

YU, Y., WU, Y., SZABO, A., WU, Z., WANG, H., LI, D. & HUANG, X.-F. 2013b. Teasaponin Reduces Inflammation and Central Leptin Resistance in Diet-Induced Obese Male Mice. *Endocrinology,* 154**,** 3130-3140.

ZABOLOTNY, J. M., BENCE-HANULEC, K. K., STRICKER-KRONGRAD, A., HAJ, F., WANG, Y., MINOKOSHI, Y., KIM, Y. B., ELMQUIST, J. K., TARTAGLIA, L. A., KAHN, B. B. & NEEL, B. G. 2002. PTP1B regulates leptin signal transduction in vivo. *Dev Cell,* 2**,** 489-95.

ZABOLOTNY, J. M., KIM, Y. B., WELSH, L. A., KERSHAW, E. E., NEEL, B. G. & KAHN, B. B. 2008. Protein-tyrosine phosphatase 1B expression is induced by inflammation in vivo. *J Biol Chem,* 283**,** 14230-41.

ZHANG, J., YAN, S., LI, W., ALICI, G. & NGUYEN, N.-T. 2014a. High throughput extraction of plasma using a secondary flow-aided inertial microfluidic device. *RSC Advances,* 4**,** 33149-33159.

ZHANG, J., YAN, S., SLUYTER, R., LI, W., ALICI, G. & NGUYEN, N.-T. 2014b. Inertial particle separation by differential equilibrium positions in a symmetrical serpentine micro-channel. *Scientific reports,* 4**,** 4527.

ZHANG, Q., YU, Y. & HUANG, X.-F. 2016. Olanzapine Prevents the PCP-induced Reduction in the Neurite Outgrowth of Prefrontal Cortical Neurons via NRG1. *Scientific reports,* 6**,** 19581.

ZHANG, S. & ZHANG, Z. Y. 2007. PTP1B as a drug target: recent developments in PTP1B inhibitor discovery. *Drug Discov Today,* 12**,** 373-81.

ZHANG, Z. Y. 2002. Protein tyrosine phosphatases: structure and function, substrate specificity, and inhibitor development. *Annu Rev Pharmacol Toxicol,* 42**,** 209-34.

# Appendix

## Appendix A: Copyright license for Chapter Four



**AIP PUBLISHING LLC LICENSE TERMS AND CONDITIONS**

Aug 24, 2016

This Agreement between Tiantian Jin ("You") and AIP Publishing LLC ("AIP Publishing LLC") consists of your license details and the terms and conditions provided by AIP Publishing LLC and Copyright Clearance Center.

| | |
|---|---|
| License Number | 3935330675757 |
| License date | Aug 24, 2016 |
| Licensed Content Publisher | AIP Publishing LLC |
| Licensed Content Publication | Biomicrofluidics |
| Licensed Content Title | A label-free and high-throughput separation of neuron and glial cells using an inertial microfluidic platform |
| Licensed Content Author | Tiantian Jin,Sheng Yan,Jun Zhang, et al. |
| Licensed Content Date | May 12, 2016 |
| Licensed Content Volume Number | 10 |
| Licensed Content Issue Number | 3 |
| Type of Use | Thesis/Dissertation |
| Requestor type | Author (original article) |
| Format | Electronic |
| Portion | Excerpt (> 800 words) |
| Will you be translating? | No |
| Title of your thesis / dissertation | Investigation of lupane triterpene as a novel PTP1B allosteric inhibitor for the improvement of neurite outgrowth and synaptogenesis |
| Expected completion date | Sep 2016 |
| Estimated size (number of pages) | 160 |
| Customer Tax ID | AU450578837 |
| Requestor Location | Tiantian Jin<br>14 Braeside Ave<br><br>Wollongong, NSW 2500<br>Australia<br>Attn: Tiantian Jin |
| Customer VAT ID | AU450578837 |
| Billing Type | Invoice |
| Billing Address | Tiantian Jin<br>14 Braeside Ave<br><br>Wollongong, Australia 2500<br>Attn: Tiantian Jin |
| Total | 0.00 AUD |

Terms and Conditions

AIP Publishing LLC -- Terms and Conditions: Permissions Uses

AIP Publishing hereby grants to you the non-exclusive right and license to use and/or distribute the

Material according to the use specified in your order, on a one-time basis, for the specified term, with a maximum distribution equal to the number that you have ordered. Any links or other content accompanying the Material are not the subject of this license.

1. You agree to include the following copyright and permission notice with the reproduction of the Material:"Reprinted from [FULL CITATION], with the permission of AIP Publishing." For an article, the credit line and permission notice must be printed on the first page of the article or book chapter. For photographs, covers, or tables, the notice may appear with the Material, in a footnote, or in the reference list.
2. If you have licensed reuse of a figure, photograph, cover, or table, it is your responsibility to ensure that the material is original to AIP Publishing and does not contain the copyright of another entity, and that the copyright notice of the figure, photograph, cover, or table does not indicate that it was reprinted by AIP Publishing, with permission, from another source. Under no circumstances does AIP Publishing purport or intend to grant permission to reuse material to which it does not hold appropriate rights.
   You may not alter or modify the Material in any manner. You may translate the Material into another language only if you have licensed translation rights. You may not use the Material for promotional purposes.
3. The foregoing license shall not take effect unless and until AIP Publishing or its agent, Copyright Clearance Center, receives the Payment in accordance with Copyright Clearance Center Billing and Payment Terms and Conditions, which are incorporated herein by reference.
4. AIP Publishing or Copyright Clearance Center may, within two business days of granting this license, revoke the license for any reason whatsoever, with a full refund payable to you. Should you violate the terms of this license at any time, AIP Publishing, or Copyright Clearance Center may revoke the license with no refund to you. Notice of such revocation will be made using the contact information provided by you. Failure to receive such notice will not nullify the revocation.
5. AIP Publishing makes no representations or warranties with respect to the Material. You agree to indemnify and hold harmless AIP Publishing, and their officers, directors, employees or agents from and against any and all claims arising out of your use of the Material other than as specifically authorized herein.
6. The permission granted herein is personal to you and is not transferable or assignable without the prior written permission of AIP Publishing. This license may not be amended except in a writing signed by the party to be charged.
7. If purchase orders, acknowledgments or check endorsements are issued on any forms containing terms and conditions which are inconsistent with these provisions, such inconsistent terms and conditions shall be of no force and effect. This document, including the CCC Billing and Payment Terms and Conditions, shall be the entire agreement between the parties relating to the subject matter hereof.

This Agreement shall be governed by and construed in accordance with the laws of the State of New York. Both parties hereby submit to the jurisdiction of the courts of New York County for purposes of resolving any disputes that may arise hereunder.

V1.1

**Questions? customercare@copyright.com or +1-855-239-3415 (toll free in the US) or +1-978-646-2777.**